Helical metaphase chromatid coiling is conserved

Ivona Kubalová[1+], Amanda Souza Câmara[1+], Petr Cápal[2+], Tomáš Beseda[2], Jean-Marie Rouillard[3, 4], Gina Marie Krause[1], Helena Toegelová[2], Axel Himmelbach[1], Nils Stein[1, 5], Andreas Houben[1], Jaroslav Doležel[2], Martin Mascher[1, 6]*, Hana Šimková[2]*, Veit Schubert[1]*

[1]Leibniz Institute of Plant Genetics and Crop Plant Research (IPK) Gatersleben, D-06466 Seeland, Germany

[2]Institute of Experimental Botany of the Czech Academy of Sciences, Centre of the Region Haná for Biotechnological and Agricultural Research, Šlechtitelů 31, 77900 Olomouc, Czech Republic

[3]Daicel Arbor Biosciences, Ann Arbor, MI, USA

[4]Chemical Engineering Department, University of Michigan, Ann Arbor, MI, USA

[5]Center of Integrated Breeding Research (CiBreed), Department of Crop Sciences, Georg-August-University, Von Siebold Str. 8, 37075 Göttingen, Germany

[6]German Centre for Integrative Biodiversity Research (iDiv) Halle-Jena-Leipzig, Leipzig, Germany

[+]Shared first authorship

* Corresponding authors: schubertv@ipk-gatersleben.de
mascher@ipk-gatersleben.de
simkovah@ueb.cas.cz

ORCIDs:

Ivona Kubalová	0000-0002-5673-9715
Amanda S. Câmara	0000-0002-3136-6633
Petr Cápal	0000-0002-8888-9101
Helena Toegelová	0000-0001-6983-0609
Nils Stein	0000-0003-3011-8731
Andreas Houben	0000-0003-3419-239X
Jaroslav Doležel	0000-0002-6263-0492
Martin Mascher	0000-0001-6373-6013
Hana Šimková	0000-0003-4159-7619
Veit Schubert	0000-0002-3072-0485

Summary
The higher-order organization of metaphase chromosomes has been debated for almost 140 years. Classical light and electron microscopy studies suggested that chromatids are composed of helically organized chromatin fibers (chromonemata). Non-helical models were also recently proposed. We studied chromosome organization in barley using cutting-edge approaches and obtained evidence for a helically arranged 400-nm chromatin fiber representing the chromonema within chromatid arms. The number of turns is positively correlated with arm length. Turn size and chromatin density decrease towards the telomeres. Due to their specialized functions, the helical organization of centromeres and nucleolus-organizing regions is interrupted by several thinner, straight chromatin fibers. A comparison with previously published data indicates that the helical turning of metaphase chromatid arms is a conserved feature of large eukaryotic chromosomes.

Keywords: chromatin condensation, chromonema, chromosome conformation capture sequencing (Hi-C), flow cytometric sorting, helical chromatid structure, *Hordeum vulgare*, mitotic metaphase chromosome, oligo-fluorescence in situ hybridization (oligo-FISH), polymer simulation, sister chromatid exchange (SCE), structured illumination microscopy (SIM)

Introduction
Cell growth, division, and differentiation are accompanied by drastic changes in chromatin structure to facilitate DNA replication, repair, transcription, and segregation. The most striking changes are observed during mitosis and meiosis, when the chromatin of interphase chromosome domains becomes compacted ~1000-fold to form rod-like structures. After replication, during the S phase of the cell cycle, the chromosomes consist of a pair of genetically identical chromatids (Paulson and Laemmli 1977; Marsden and Laemmli 1979; Earnshaw and Laemmli 1983; Maeshima et al. 2005). Individual chromosomes can most easily be observed during nuclear division. While some species have holocentric chromosomes (containing elongated centromeres), most eukaryotes have monocentric chromosomes characterized by a distinct primary constriction to which spindle fibers attach for proper chromatid segregation during anaphase (Musacchio and Desai, 2017; Schubert et al., 2020). Some chromosomes also harbor a nucleolus organizer region (NOR), a 45S rDNA cluster forming a secondary constriction on metaphase chromosomes (McClintock, 1934; Schöfer and Weipoltshammer, 2018). Long-standing questions about chromatin structure remain, including how DNA is compacted into rod-shaped mitotic and meiotic chromosomes, which principles govern folding, and whether such principles apply to different species.
Chromatin in interphase nuclei comprises 10-nm nucleosome fibers formed by ~147 bp of DNA wound around an octamer of nucleosome histones. The nucleosomes are connected by linker DNA like “beads-on-a-string” (Thoma et al. 1979). However, little is known about how nucleosome fibers fold into higher-order structures. Using purified 10 nm fibers, Finch and Klug (1976) observed the formation of a 30-nm chromatin fiber, the so-called solenoid. Nevertheless, its existence in native chromatin has not been confirmed, and there is growing evidence that the 30-nm fiber forms in vitro only in solutions with low salt concentrations. Several studies across various eukaryotes demonstrated that the higher-order structure of chromatin is formed by an irregularly folded 10-nm fiber (Grigoryev et al. 2016; Maeshima et al. 2010a, b, 2016, 2018, 2019; Nishino et al. 2012). The periodical arrangement of chromatin has been questioned as well. Wako et al. (2020) analyzed chromatin fibers with different levels of compactness in human metaphase

chromosomes using beam/scanning electron microscopy. Thick (30 nm) fibers were rare, excluding the possibility that they are structural units. In contrast to several existing models (Finch and Klug 1976; Manuelidis and Chen 1990), no periodical structure was found. While most researchers accept the notion that metaphase chromosomes are composed of 10 nm fibers, the higher-order organization remains obscure.

Several models have been proposed to describe the higher-order structure of metaphase chromosomes based on data obtained using a range of molecular and microscopy methods (Beseda et al. 2020). These models are categorized as helical and non-helical. Helical models assume that the chromatin in each sister chromatid at metaphase is arranged in a helix (Manton 1950; Ohnuki, 1965, 1968; Iino 1971; Bak et al. 1977; Sedat and Manuelidis 1978; Marsden and Laemmli 1979; Ris 1981; Rattner and Lin 1985; Nokkala and Nokkala 1986; Boy de la Tour and Laemmli 1988; Saitoh and Laemmli 1994; Sumner 1998; Inaga et al. 2002; Daban 2020; Gibcus et al. 2018; Schloissnig et al. 2021), whereas non-helical models suggest that chromatin is folded within the chromatids without forming a helix (Paulson and Laemmli 1977; Belmont et al. 1987, 1989; Wanner and Formanek 2000; Poirier and Marko 2002; Strukov et al. 2003; Kireeva et al. 2004; Marko 2011; Naumova et al. 2013; Chu et al. 2020).

The helical structure of chromosomes was first observed in the plant *Tradescantia virginica* L. by Baranetzky (1880) and was later supported by Ruch (1949). A similar chromatin organization called chromonema (from chromo- + Greek nēma thread; plural: chromonemata) was discovered in diverse plant species by observing native, physically, and/or chemically treated chromosomes by light microscopy (Nebel 1932a, 1939; Manton 1950; Schvartzman et al. 1978; Nokkala and Nokkala 1985). Interestingly, such chromatin coiling was not found in Drosophila (Strukov et al. 2011), and although Ohnuki et al. (1968) observed helical coiling in mitotic chromosomes of cultured human leukocytes, such a structure was not observed in mammalian cell lines by other groups (Strukov and Belmont 2009; Chu et al. 2020). Furthermore, the helical chromatin arrangement in mitotic chromatids was not observed in three human cell lines using the chromatin conformation capture (3C) methods 5C and Hi-C, which quantify the frequency of genome-wide chromatin contacts (Naumova et al. 2013). On the contrary, Hi-C data obtained from mitotic cells of chicken (Gibcus et al. 2018) and axolotl (Schloissnig et al. 2021) suggested a helical chromosome organization. After reanalyzing mitotic HeLa cell Hi-C data from Naumova et al. (2013) in more detail by deeper sequencing, Gibcus et al. (2018) confirmed the helical structure and suggested that this arrangement might be a common feature among vertebrates.

Advanced microscopy, cytology, and molecular techniques could be used to decipher the higher-order spatial (3D) chromatin organization of mitotic chromosomes at higher resolution. The use of fluorescence dyes to label specific DNA segments and proteins has led to the development of super-resolution microscopy techniques such as structured illumination microscopy (SIM), a sub-diffraction imaging method bridging the resolution gap between light and electron microscopy (Rego et al. 2012). These nanoscopic methods have been successfully used in cell biology (Fornasiero and Opazo 2015), leading to the discovery of structures within plant chromatin (Schubert,2017; Baroux and Schubert 2018; Schubert et al. 2020).

Fluorescence in situ hybridization (FISH) using oligonucleotide probes (oligo-FISH) is an efficient method for examining whole chromosomes and specific regions to investigate karyotype structure, meiotic chromosome behavior, and chromosome evolution via comparative cytogenetic mapping (Aurich-Costa et al. 2007; Han et al. 2015; Braz et al. 2018; Šimoníková et al. 2019; Xin et al. 2020; Li et al. 2021; Hoang et al. 2021). The application of super-resolution microscopy techniques in combination with oligo-FISH led to the characterization of sub-chromosomal structures (Szabo

et al. 2018). The arrangement of chromatin in sister chromatids in spontaneously occurring sister chromatid exchanges (SCEs) can be studied via the differential incorporation of DNA base analogs, such as 5-bromodeoxyuridine (BrdU) (Latt 1973) or 5-ethynyl-2′-deoxyuridine (EdU) (Schubert et al., 2011), into chromosomes during replication (Schvartzman 1987; Wilson and Thompson 2007; Schubert et al. 2016a). This method differentially labels sister chromatids (harlequin staining) and can be combined with FISH (Perry and Wolff 1974; Rachel et al. 1991; Jordan et al. 1999).

3C techniques were recently used to determine the contact probabilities of genomic loci with different distances in a linear sequence (Lieberman-Aiden et al. 2009; van Berkum et al. 2010; Kempfer and Pombo 2020; Oluwadare et al. 2019) and to uncover hierarchical chromatin organization (Oluwadare et al. 2019; Szabo et al., 2019). Using these techniques, together with polymer simulations, Gibcus et al. (2018) postulated a helical organization of late prometaphase chromosomes, comprising 200 nm thick fibers with helical turns covering 12 Mb, in chicken.

To decipher the higher-order structure of plant mitotic chromosomes, we used barley (*Hordeum vulgare* L.; 2n=14; 1C=4.88 Gb, with large chromosomes) (Doležel et al. 2018) as a model. Analysis using a combination of metaphase chromosome-derived Hi-C data, oligo-FISH, SCE detection, super-resolution microscopy, and polymer simulation revealed that sister chromatids are composed of chromatin helices of identical handedness. The helical turns cover 20–38 Mb, creating a ~400 nm thick fiber. Only centromere and NOR regions are free of the helical higher-order organization. Thus, we experimentally proved the classical model of a helical organization of somatic chromosomes for a plant species with large chromosomes.

Results

Hi-C indicates that the mitotic chromatid is organized as a helix with variable turn lengths

To analyze the organization of condensed chromosomes, we purified barley metaphase chromosomes by flow cytometric sorting, sequenced the contact pairs by Hi-C analysis, and aligned the sequences against the barley cv. Morex genome assembly version 2 (Morex v2) (Monat et al. 2019). The Hi-C contact matrix for metaphase chromosomes showed a second diagonal parallel to the main diagonal along the length of the chromosome, which faded in the vicinity of the primary and secondary constrictions and telomeres (Figures 1A, S1). The additional diagonal was unique to metaphase chromosomes and was not observed in interphase chromatin, which only showed a perpendicular diagonal indicative of the conformation described by Rabl in 1885 (Rabl, 1885) (Mascher et al. 2017).

The differences in chromatin conformation between interphase and metaphase chromosomes were also reflected by the relationship of the Hi-C contact probabilities of loci pairs and their distance in the linear genome (d) (Figures 1B, S2). The contact probabilities in interphase showed a uniform exponential decay (~d-1) from 100 kb to 100 Mb (Figures 1B, S2A, B, E). This pattern is reminiscent of the Rabl conformation observed in anaphase.

In metaphase, the distance-dependent-decay rates were more variable, and its derivative showed two regions with increased contacts, ~500 kb and 30 Mb (Figure S2C, D, E). Because mitotic chromosomes likely become compacted by chromatin loops (Gibcus et al. 2018), we suggest that the broader peak at ~500 kb arises from an arrangement of nested loops, where the largest loops (~3 Mb) appear only in metaphase, as indicated by the first peak in the contact probability ratio between metaphase and interphase (Figure S2F). The highest peak in this contact probability ratio (~30 Mb), the only one with a positive derivative, corresponds to the second diagonal in the contact matrix (Figure 1B).

Gibcus et al. (2018) proposed that this pattern reflects the arrangement of the chromatids into a helix, whose turn length corresponds to the position of the "bump" in Figure 1B. The arrangement into helical turns is schematically presented in Figure 1C, where the spatial distance between genomic loci is proportional to the contact probability. This observation suggested that the helical coiling could be observed along the chromosome axis when differentially labeled (Figure 1D). We estimated that depending on its size, a condensed barley chromosome consists of 18-23 helical turns (Figure 1E, Table S1).

A closer inspection of the metaphase contact matrix suggested that the distance between the main and secondary diagonal is variable. We analyzed turn sizes along the chromosome lengths based on Hi-C using a sliding window approach and considering only contacts spanning a moving focal point. We observed different local patterns. The characteristic bump of the contact probability shifted (Figures S3, S4; Movie 1) as the focal point moved along the chromosome. The different placements of the bump indicate that the turn length varies along the length of the chromosome.

The turn size decreased smoothly, but non-linearly, from the centromere towards the telomere, with turn sizes ranging from 20 to 38 Mb. Moreover, the turn length decreased sharply towards the primary and secondary chromosome constrictions (Figure 1E).

Oligo-FISH confirms the helical organization of mitotic chromatids

To validate the results obtained by Hi-C, we performed FISH with pooled oligonucleotide (oligo) probes. A search for unique sequences suitable for probe design by scanning Morex v1 (Beier et al. 2017; Mascher et al. 2017) with a 40 Mb window revealed a continuous region of ~157 Mb with a high density of single-copy sequences on the long arm of chromosome 5H (Figures 2A, S5). We designed FISH probes comprising pools of ~45 bp oligos to label selected parts of this region; the pooled probes were named Stork, Eagle, Ostrich, Rhea, Moa, and Flamingo. Examples of Stork and Moa probes are shown in Figure S6. Based on the Hi-C data and Morex v1, Stork and Eagle covered half helical turns, whereas Ostrich, Rhea, and Moa each represented one full helical turn. The Flamingo probe was located at the chromosome terminus, just before the subtelomeric and telomeric repeats (Figure 2B, C). The density of single-copy sequences increased towards the telomere (Figure S7), in agreement with the reported higher density of genic and single-copy sequences in distal regions (Mascher et al. 2017).

After our probe design, an improved assembly of the barley genome (Morex v2) was published (Monat et al. 2019), resulting in a change in the probe coordinates (Table S2). This had no noticeable effect on the oligo probe distribution or specificity, but the lengths of the labeled intervals changed.

The completeness of the assayed interval, located between 442 and 599 Mb in the Morex v2 5H pseudomolecule, was validated by examining a genome-wide optical map of barley cv. Morex (Mascher et al. 2021). The interval was covered by three optical map contigs (1, 55, and 17), which were concordant with the sequence (Figure S8). A single discrepancy within the interval was a missing sequence of ~403 kb around position 491 Mb, detected as unaligned ends of the optical map contigs 1 and 55. This indicates that the correct length of the DNA segment labeled by the Ostrich probe is 34.8 Mb.

Three-dimensional structured illumination microscopy (3D-SIM) of chromosomes after FISH with pooled oligo probes (Figure 2D; Movies 2, 3) showed that the chromosome diameter decreased towards the termini. This corresponded with the changes in turn size along the chromosome observed by Hi-C analysis. Once the Morex v2 assembly became available, we re-estimated the turn coverage of the probes. Stork and Eagle cover ~0.6 of a turn (in a region with a turn size of

29.6 Mb), Ostrich, Rhea, and Moa cover ~1.5 turns (in a region with a turn size of 22.5 Mb), and Flamingo covers a region of ~2.3 decreasing turns (in a region with a turn size of 8.3 Mb). Thus, the probes cover fewer turns in regions with larger turn sizes (Figure 2F, G; Table S2).

The signals of the oligo-FISH probes Stork and Eagle showed an average height of 380 nm. Although three FISH probes (Ostrich, Rhea, and Moa) represented more than one full helical turn and were labeled by fluorescence dyes delivering a different SIM resolution (laterally ~120 nm for Alexa488 and ~140 nm Atto594), the signals of all three probes had similar dimensions (Figures 2H, S9A). On average, these signals were ~460-480 nm in height. As Hi-C predicted 21 turns for chromosome 5H (Figure 1E), this corresponds to a chromosome length of 9.0–9.4 µm, which is consistent with our chromosome length measurements (Figure S9A).

Based on these observations, we call the helically arranged 400-nm chromatin fiber chromonema. A partial intermingling of smaller chromatin loops inside the chromonema was identifiable between neighboring turns of the helix (Figures 2D, S10; Movie 4). Therefore, the chromatin was arranged in lower-order loops within the chromonema, with the intertwining possibly caused by the dynamic properties of the loops. Remarkably, the orientation of the FISH signals was always identical in both chromatids, indicating that both chromonemata were turned with the same handedness (Figure S11).

We performed surface rendering of the 3D-SIM image stacks and determined the volumes of the different oligo-FISH signals and the whole chromosome 5H (Figures 2I, 6C, S9B; Movie 5). To avoid artificial flatting of chromosomes after preparation, we embedded the isolated chromosomes in polyacrylamide and imaged them by 3D-SIM after DAPI staining. These spatially preserved chromosomes showed ~1.2-fold higher volumes than chromosomes that were dried on slides for subsequent FISH (Table S3). The volume of an embedded 5H chromatid (~599 Mb) was ~24.75 µm3, corresponding to ~24.2 Mb/µm3, i.e., 1 Mb chromatin is folded into ~0.041 µm3. In the Flamingo-positive chromosome region, the Hi-C data indicated a smaller turn contact pattern (Figure 2F, G). The volume of the Flamingo signal, the only one larger than expected for a uniformly dense chromosome (Figure 2I), suggested a lower chromatin density (DNA amount per µm3). Compared to Flamingo (19.5 Mb/µm3), the regions of the Stork (32.0 Mb/µm3), Eagle (34.3 Mb/µm3), Ostrich (38.2 Mb/µm3), Rhea (34.0 Mb/µm3), and Moa (32.0 Mb/µm3) probes were ~1.7 times more condensed. Thus, the terminal Flamingo region was characterized by lower chromatin density and smaller turn size. The flexibility of the chromatin arrangement at the chromosome ends was also visible after FISH with subtelomeric and telomeric probes. Their positions varied at the chromosomal termini, and the subtelomeres showed ring-like shapes, as described by Schubert et al. (2016a) (Figure 2E; Movie 6).

In short, these cytological observations suggest that both metaphase sister chromatids are formed by a ~400 nm thick chromatin fiber arranged as a helix of identical handedness with decreasing turn size towards the telomeres. The chromosome ends are less compact, possibly allowing for higher chromatin fiber flexibility than in interstitial arm regions.

Analysis of SCEs confirms the helical 400 nm chromonema structure

The harlequin staining pattern after differential labeling of sister chromatids with base analogs is caused by SCEs and allows chromatin segment exchanges even smaller than the width of a chromatid to be detected. Based on this observation, metaphase chromatids were previously proposed to be formed by a chromatin helix in onion (Schvartzman and Cortés 1977; Schvartzman et al. 1978). We applied the same approach to confirm the spatial chromatin organization of mitotic barley chromosomes.

The extension of the exchanged chromatid segments differed in height and width. The measurements were done parallel and perpendicular to the chromatid axis (Figure 3). Although both dimensions were affected by the degree of chromosome condensation, all exchanged regions shared the following patterns. The height never dropped below 300 nm, the minimum size that may be exchanged. The maximum height was restricted by the chromosome arm length. Importantly, the height of the exchanged part never exceeded 300–550 nm before the exchanged part spanned the full chromatid width (Figure 3B). These findings agree with the helical chromatin arrangement determined by Hi-C and oligo-FISH.

We then combined SCE detection and FISH with the Stork, Eagle, Rhea, and Flamingo oligo-probes to relate the exchanged chromatid segments to the FISH-painted regions. As shown in Figure 4 and Movies 7 and 8, both 5H homologs contained a small SCE segment close to a Rhea-positive region, and the adjacent regions not painted by FISH with the Moa and Ostrich probes. The shapes and heights (~400 nm) of the exchanged chromatid segments and FISH signals were similar and partially replaced each other. These findings further confirm the helical chromatin arrangement of metaphase chromatids.

In contrast to the remaining chromatids, no helical organization was identified in the centromeric regions and secondary constrictions (NORs). Instead, straight chromatin fibers were observed (Figure 3C).

The 400-nm chromonema consists of loops of ~80-nm chromatin fibers and shows no large cavities

In addition to the ongoing discussion about the helical versus non-helical higher-order metaphase chromosome structure, it remained an open question whether the chromatin-free 'cavities' along the entire lengths of chromatids detected in several electron microscopy investigations in plants and human (Hao et al. 1988, 1990; Hamano et al. 2014; Kuznetsova et al. 2017) reflect a real phenomenon or simply a preparation artifact. Thus, we stained barley chromosomes with DAPI to reach a 3D-SIM resolution of ~130 nm (Kubalová et al. 2021) for reliable observation of the spatial ultrastructure (Figure 5). Large cavities were never identified within complete 3D-SIM image stacks of metaphase chromosomes. Instead, we detected a network of looped ~80-nm chromatin fibers (n=36; mean 77.2±7.7). Between these fibers, chromatin-free regions no larger than ~120×220 nm were evident (Movies 9, 10). The 80-nm fibers formed the 400-nm chromonemata. At centromeres and NORs, both looped and straight ~80-nm fibers were observed. These fibers apparently represent a constriction-specific substructure of the chromonema which is not helically arranged in these regions.

Polymer modeling confirms the helical chromatid architecture

We constructed polymer models using the calculated turn sizes to reproduce the bump position in the contact probabilities of mitotic chromosome Hi-C data and the arrangement of the chromosome regions highlighted by oligo-FISH (Figure 6). The models were built with equilibrium molecular dynamics simulation based on the bottle-brush model proposed by Gibcus et al. (2018). The models were created by large side-by-side loops, whose bases followed a helical path. The large loops consisted of minor side-by-side loops that filled the space surrounding the helical path, both internal and external to it. The loops formed turns of chromatin that stacked along the chromatid axis (Figure S12D).

To compare the polymer models with the Hi-C contact probability data, we tested whether our simulation reproduced the contact probability of chicken chromosome 1 at prometaphase, as

described by Gibcus et al. (2018) (Figure S12). We simulated only five turns of the helical arrangement (with constant turn lengths) using a model of the 10-nm chromatin fiber, where each monomer represents one nucleosome.

The simulated model for chicken closely followed the experimental contact probability. To reproduce the bump that we observed in the Hi-C contact probabilities of the barley chromosomes, we set the turn length to 30 Mb and the turn height to 400 nm. However, our barley models 1–4 did not reproduce the contact probability as well as our model using the data from chicken chromosomes (Figure S12A-C). Therefore, we considered model 5 where the chromatin loops were larger, leading to a dispersed helical protein scaffold (Figure S12E). This chromatin loop arrangement followed the Hi-C data, suggesting (on average) large 3-Mb loops and small 500-kb loops (Figure S2E, F). Accordingly, we suspect that the loop arrangement differs in barley compared to other species with possible differences in the density and size of loops surrounding the helical path.

To consider a half-helical arrangement of chromatids as suggested by Chu et al. (2020), we simulated a 10-Mb region (to reduce computational costs) with coarse-grained models of the 10-nm chromatin fiber. In this model, the helical path changes the turn handedness (left to right) every half turn. The turn length was set to 2 Mb (making 10 half-turns), but instead of a lower contact probability at the half-turn distance (1 Mb), which is characteristic of helical arrangements, we observed a plateau. Sites separated in the genome sequence by half a turn length may be spatially far or close, but in the helical arrangement, they are always far apart. The irregularity of half-turn contacts broadens the bump for inter-turn contacts. We expect that other irregular structural features, such as turns with different lengths and perversions between half-turns, as suggested by Chu et al. (2020), would only broaden and not sharpen the contact probability peak for distances in the range of a turn length (Figure S13).

To achieve a model matching our cytological observations, we simulated a 600 Mb chromatid with a coarse-grained model, where each monomer represents 2 kb (Figure 6D; Movie 11). The bases of the loops were constricted to a helical arrangement, with turn lengths as calculated from Hi-C data (Figure 1E). The resulting model for chromosome 5H has seven turns in the short arm and 14 in the long arm, which fits with the estimation derived from cytogenetic observations. Regions labeled by oligo-FISH and representing successive helical turns appear as stacked layers, consistent with our cytological observations. The Stork and Eagle oligo probes (encompassing less than one turn) present signals with lower heights (corresponding to one-turn height) and do not fully occupy the width of the chromatid (depending on the viewpoint). Signals using Ostrich, Rhea, Moa, and Flaming oligo probes (encompassing more than one turn) are taller and always occupy the entire width of the chromatid. The variable turn lengths in the model reproduce the cylindrical shape of the chromosome, with a decreasing radius towards telomeres and constrictions. Replicates with different and randomly chosen loop sizes (see Materials and Methods) introduced variability into the model, where the labeled regions have slightly different shapes (Figure S14). The loop variability and flexibility should account for the expected heterogeneity of the cell population used in the Hi-C experiment (Shi and Thirumalai 2021), while the underlying main helical organization holds even for individual chromosomes, as shown by our cytological results.

Other experimentally observed features could not be reproduced by the simulated model. Subtelomeric and telomeric regions, which were mainly absent from the genome assembly, may be less dense than simulated, as indicated by volume measurements (Figures 2I, S9B). Sequences of the primary and secondary constrictions were also lacking in the genome assembly, and the less clear organization of centromeres and NORs precludes modeling of their conformations.

Discussion

Helical metaphase chromosome organization – a conserved feature?

A helical structure of plant chromosomes was previously seen in living tissues but also after physical treatments by a wide range of agents on fixed chromosomes. The coiled chromatin fiber forming chromatids (called chromonema in early publications) has been observed in plants from different families during mitosis and meiosis. The coiling of mitotic chromosomes can vary from loose and irregular to the formation of a regular compact helix. Various authors originally described two chromonemata per chromatid (Nebel 1932a, 1939; Sax 1935; Matsuura, 1935, 1938; Manton 1950). However, Ruch (1950) clarified in *Tradescantia virginica* that these observations were based on optical artifacts and postulated that only one chromatin helix was present per chromatid. Our investigations based on molecular, cytological, and super-resolution microscopy data provide independent evidence that one helically coiled 400-nm chromatin fiber forms a metaphase chromatid in barley, corresponding to the classically named chromonema in plants. Similarly, a helical chromatid organization was visualized by electron microscopy in large-genome plants including onion (Hao et al. 1990), barley (Iwano et al. 1997), and faba bean (Döbel and Schubert 1981). A helical structure was also observed in chromosomes of animals such as frog (Seto 1972), axolotl (Schloissnig et al. 2021), mouse (Sumner 1998; Rattner and Lin 1985), Chinese hamster (Ris 1981), and human (Ohnuki 1965, 1968; Utsumi 1982; Rattner and Lin 1985; Boy de la Tour and Laemmli 1988; Sumner 1991, 1998; Phengchat et al. 2019; Hayashida et al. 2021).

The available data suggest that the longer and thicker chromosomes of species with larger genomes contain more and larger chromonema turns and longer inside loops (Table 1). In human, the number of turns is positively related to chromosome length (Boy de la Tour and Laemmli 1988). If we consider the 15 turns Ohnuki (1968) observed in chromosome 1 and the chromosome size of 248.96 Mb (*Homo sapiens* GRCh38.p13 genome assembly), the average size of one turn should be 16.6 Mb. This is similar to the sizes (12 Mb and 10 Mb) determined by Gibcus et al. (2018) using Hi-C for the helical turns in chicken and human chromosomes, respectively. In contrast to the macrochromosomes of chicken, the chromatids of chicken microchromosomes, which are smaller than 12 Mb, do not form turns (Gibcus et al. 2018). The diameter of the helically coiled chromatin fiber forming mouse chromatids was estimated to be 200-300 nm (Rattner and Lin 1985). A single turn of the helically organized 28 mitotic chromosomes of the giant axolotl genome (32 Gb/1C) comprises ~35 Mb DNA (Schloissnig et al. 2021).

The number of turns was reported to vary from 16 to 46 in mitotic metaphase chromosomes and from 3 to 23 in the more condensed meiotic metaphase chromosomes in plants of the genera *Fritillaria, Osmunda, Rhoeo, Sagittaria*, *Tradescantia*, and *Trillium* (Manton 1950). We determined that each barley chromosome (522 to 675 Mb long) contains 18-23 turns of 20-38 Mb along the arms, depending on chromosome length and position. Towards the chromosomal termini, the turns become smaller and the chromatin is less densely packed. The different positions of subtelomeres and telomeres in both sister chromatids point to the flexibility of the lower-order chromatin structural organization. Using FISH on longitudinally stretched barley chromosome 1H, Valárik et al. (2004) found that telomeric sequences do not localize to the very ends of the chromosome. Ring-like subtelomeric repeat arrangements (Schubert et al., 2016a) may reflect the helical higher-order chromatin structure at the chromosome termini. The decondensation of barley telophase chromosomes starts at the chromosome ends, possibly due to lower chromatin density and higher flexibility (Wanner and Formanek 2000).

The chromosome length does not affect the average turn length within a species. We compared the contact probability of condensed chicken (Gibcus et al. 2018) and barley chromosomes, finding that the turn length differs between species but not in the same species (Figure S15). This is more obvious for chicken, whose chromosomes range from 0.6 to 196 Mb long. Only chromosomes smaller than a turn length (12 Mb) lack the characteristic bump in the contact probability diagram. A comparison between the contact probability derivatives of chicken and barley suggested that the chromatin loop arrangement within the chromonema can also differ between species but is similar between the chromosomes of the same species. Therefore, chicken shows smaller chromatin loops than barley.

The second parallel diagonal in the Hi-C contact matrix, and the respective bump in the contact probability, which relate to turn length, are key features explainable only by a helical arrangement of mitotic chromatids (Figure 1). Other arrangements modeled by polymer simulation, such as an equilibrium globule, fractal globule, and linearly compacted loops (Mirny 2011; Naumova et al. 2013), resulted in different contact patterns (Figure S13). Here, we also simulated a half-helical model, where the handedness changes every half turn, similar to the model proposed by Chu et al. (2020). However, in this case, half-turn distances are not always apart in space, and full-turn distances are not always close in space. Thus, this model had to be rejected, as the contact probability lacks the characteristic bump between half-turn and full-turn distances (Figure S13).

Using bottle-brush polymer models (Gibcus et al. 2018) and following a helical arrangement, we successfully reproduced the chicken contact probability. Our model for barley mitotic chromosomes, with a turn length of 30 Mb, correctly positioned the bump in the contact probability, confirming that the bump originates from the helical arrangement and is related to turn length. Assuming a height of 400 nm, as detected cytologically for the barley chromonema, we further approximated the model to the experimental observations. By varying the lengths of major and minor loops fitting to the experimental Hi-C data, we induced a dispersed helical scaffold (Figure S12E) and improved the contact probability. The various chromonema helix turn lengths and heights in barley and other species (Table 1) suggest a different mitotic coiling of the major chromatin loops. Due to the different minor loop sizes in these species, the major chromatin loops may attain different widths, resulting in different turn heights. The extent of these differences and how the chromonema coils remain to be elucidated.

Paulson and Laemmli (1977) suggested a 'scaffold model' based on histone-depleted human chromosomes, where a non-histone protein backbone is responsible for chromatin looping and chromosome condensation. Topoisomerase IIα and the Structural Maintenance of Chromosomes (SMC) complexes condensin I and II are components of the scaffold in *Drosophila* ([104]Sureka et al., 2018), chicken (Ohta et al. 2019), and human (Maeshima and Laemmli 2003; Fukui and Uchiyama 2007; Maeshima et al. 2018; Walther et al. 2018) and are also evident in *Arabidopsis* and barley (Kubalová et al. 2021; Municio et al. 2021). In human HeLa cells, the chromatid axes appear as isolated compaction centers rather than forming a continuous scaffold (Sun et al. 2018) and appear to consist of a helical structure that serves to organize chromatin loops into the metaphase chromatid (Phengchat et al. 2019). The network-like distribution of topoisomerase IIα that we previously identified in barley metaphase chromosomes (Kubalová et al. 2021) fits the predicted Hi-C data-based dispersed helical scaffold (Figure S12E).

Chromosome compaction by condensin II during mitosis appears to be a conserved mechanism influencing the arrangement of chromosomes in interphase nuclei (Hoencamp et al. 2021), such as the Rabl configuration (Rabl 1885) present in barley (Jasencakova et al. 2001; this work). Further studies on the localization and quantification of scaffold proteins may allow a functional model of

condensed barley chromosomes to be established, including lower-level chromatin organization. We propose that the helical arrangement is evolutionarily conserved in large (>12 Mb) metaphase chromosomes of plants and animals.

The chromatid helix turning direction is random

In the oligo-FISH-labeled regions of both mitotic barley 5H chromatids, we always observed the turning of the chromonema in identical directions. Sister chromatids of human HeLa chromosomes have predominantly opposite (mirrored) helical handedness (Boy de la Tour and Laemmli 1988). Because sister chromatids start to separate at the beginning of prophase (Nagasaka et al. 2016), the turning direction must already be determined after replication during the G2 phase, but it seems to be unrelated to the left-handedness of chromatin fibers, as reported for the salamander *Necturus* (Williams et al. 1986). Based on investigations of *Drosophila* polytene chromosomes, Sorsa (1986) suggested that the size and accumulation of chromomeric loops cause the chromonema to bend and form a helix.

In the plant genera *Trillium*, *Rhoeo*, *Osmunda*, and *Vicia*, the turning direction can change at the centromere and in different regions along the arms, suggesting that no uniform control mechanism functions throughout the whole chromosome. The ratio of left-handed to right-handed turning appears to be random. Only in certain *Tradescantia* genotypes does an excess of right-handed segments point to specific genetic control (Nebel 1932a, b; Sax and Humphrey 1934; Sax 1935; Nebel and Ruttle 1936a, b; Manton 1950; Manton and Smiles 1943). In short, it appears that the higher-order helical turning direction of chromonemata is flexible rather than strictly determined.

Why is the chromatid helix interrupted by straight and less condensed chromatin at centromeres and NORs?

Using super-resolution microscopy, we detected thinner, straight chromatin fibers at the monocentromeres and secondary constrictions of barley lacking the helical chromonema organization. This finding is in line with the observations achieved by scanning electron, helium ion, and classical light microscopy in barley (Seto 1972; Iwano et al. 1997; Wanner et al. 1991; Wanner and Formanek, 2000; Schroeder-Reiter and Wanner 2009; Schroeder-Reiter et al. 2012; Sartsanga et al. 2021), faba bean (Maruyama 1983; Schroeder-Reiter and Wanner 2009), frog (Seto 1972), Indian muntjac (Rattner 1987), wallaby, and human (Utsumi 1982; Schroeder-Reiter and Wanner 2009). The 200–300 nm chromonema of mouse, consisting of a coiled 100 nm sub-fiber, appears straight in the centromere region (Rattner and Lin 1985, 1987). Even at elongated pea centromeres (Neumann et al. 2012) and along holocentric chromosomes of the grass *Luzula nivea*, parallel chromatin fibers are evident (Schroeder-Reiter and Wanner 2009).

DNA-specific dyes stain primary and secondary constrictions less strongly than chromosome arms, which may reflect a lower chromatin density. Electron microscopy revealed that the amount of looped chromatin fibers and 'knobby' chromatin, abundantly visible along the chromosome arms, is reduced in barley centromeres, displaying less DNA but more protein than chromosome arms (Wanner et al. 1991; Iwano et al. 1997; Wanner and Formanek 2000; Schroeder-Reiter and Wanner 2009). Bailey et al. (2013) showed that epigenetic modifications of the N-terminal tail of the centromeric histone variant CENH3 influence the physical properties of chromatin fibers in HeLa cells such that the chromatin organization at centromeres may be altered. Transcription of centromeric DNA during mitosis (Liu et al. 2021) could also contribute to this alteration.

Features of active rDNA might be maintained during mitosis, preventing a helical chromonema structure at NORs. Not only microscopy data but also our Hi-C data revealed a peculiar non-helical

chromatin architecture around the NORs and centromeres, manifested as regions without periodical contact patterns in Hi-C contact maps. Perhaps the local loss of long-range contacts is prevented by proteins associated with NORs and centromeres. Data obtained by chromatin conformation capture and analysis of nucleolus-associated chromatin domains in *Arabidopsis thaliana* support this hypothesis for NORs (Feng et al. 2014; Pontvianne et al. 2016) and centromeres (Grob and Grossniklaus 2017). Alternatively, perhaps the missing contacts in the Hi-C matrices are due to the absence of centromeric and rDNA sequences in the reference genome of barley and/or the highly repetitive nature of surrounding regions, precluding unique contact mapping.

Overall, we speculate that the missing helical arrangement and the relaxed chromatin allow kinetochores to be established at centromeres and maintain the structures of transcriptionally active NORs. The identification of several parallel ~80-nm chromatin fibers within both constrictions suggests a specific arrangement of the chromonema, which remains to be elucidated.

Lower-level chromatin organization – a network of chromatin globules and looped fibers

Without specific labeling, the tight compaction of metaphase chromosomes makes individual helical turns invisible. The intermingling of lower-order chromatin fibers between adjacent turns of the chromonema in barley (visualized by oligo-FISH) explains this observation. Super-resolution microscopy revealed a network of globular (clustered) and fibrous chromatin structures within and at the surface of barley metaphase chromatids, similar to the fibers and 'knobby' structures possibly corresponding to chromomeres (coiled solenoids) (Serra 1947; Zatsepina et al. 1983) observed by scanning electron microscopy at the surfaces of barley (Wanner et al. 1991; Iwano et al. 1997; Wanner and Formanek 2000; Sartsanga et al. 2021), Chinese hamster (Zatsepina et al. 1983), and human chromosomes (Sumner 1991). Because our Hi-C contact matrices from barley inter- and metaphase chromosomes, analyzed at 1 Mb resolution, do not show TADs or compartments, they could not be related to the observed globular structures.

Different levels of chromatin organization have been observed, depending on the species analyzed and the methods used (reviewed in Kusnetzova and Sheval 2016). Several studies showed that in vivo chromatin is basically organized in 10-nm fibers and not 30-nm fibers, as found after fixation (reviewed in Maeshima et al. 2019). We measured a mean lower-order chromatin fiber diameter of ~80 nm in DAPI-labeled barley metaphase chromosomes while scanning electron microscopy revealed 15- to 150-nm diameter fibers (Wanner et al. 1991), helium ion microscopy (with improved chromosome preparations preventing artifacts) revealed 11.6-nm fibers (Sartsanga et al. 2021), and reticulate chromatin fibers with a diameter of up to 30 nm were observed in human metaphase chromosomes (Wako et al. 2020). Due to the visualization of fluorescent signals via a point spread function, signal thickness measurements (such as DAPI signals) might be overestimated, depending on the settings. Consequently, electron microscopy-based measurements are regarded as more reliable.

Within the chromatin fiber network, we found minor chromatin-free regions of ~120×220 nm, but never larger cavities, as previously observed by electron microscopy in plant and human chromosomes (Hao et al. 1988, 1990; Hamano et al. 2014; Kuznetsova et al. 2017). Hamano et al. (2014) noted that the cavities were not visible when an ionic liquid method that keeps the chromosomes wet was used. Chen et al. (2017) also did not identify large cavities in human chromosomes. Thus, minor chromatin-free spaces occur within the condensed chromatin of mitotic chromosomes, whereas the previously observed larger cavities might be preparation artifacts (Beseda et al. 2020).

In conclusion, sister chromatids of large metaphase chromosomes in eukaryotes are formed by a helically arranged chromonema consisting of looped minor chromatin fibers, which may form clusters with small chromatin-free regions between them.

Material and Methods

Plant material

Barley (*Hordeum vulgare* L.) cv. Morex seeds were obtained from the Gene Bank of the Leibniz Institute of Plant Genetics and Crop Plant Research Gatersleben, Germany.

Preparation and sequencing of chromosome Hi-C libraries

Suspensions of barley metaphase chromosomes were prepared from root tip meristems after cell cycle synchronization as described in Lysák et al. (1999) with the following modifications. Barley seeds were germinated for two days at 4°C, followed by incubation at 25°C for three days. The roots were fixed in 2% formaldehyde in 1×PBS buffer for 12 min at 5°C. Fixed metaphase chromosomes were released by mechanical homogenization into LB01 buffer ([79]Doležel et al., 1989) and stained by 4',6-diamidino-2-phenylindole (DAPI) at a final concentration of 2 µg/ml. The chromosomes were purified by sorting using a FACSAria SORP flow cytometer (Becton Dickinson, San Jose, CA USA). The initial gating was performed on FSC-A vs. DAPI-A parameters. To discriminate doublets, the chromosome gate was drawn on a DAPI-A vs. DAPI-W scatterplot (Figure S16).

Three replicates of chromosome Hi-C libraries were prepared. For each replicate, five million chromosomes were flow-sorted into a 15-ml Falcon tube with 2 ml LB01, centrifuged at 500 g for 30 min at 4°C, and the supernatant removed except for 20 µl. The pelleted chromosomes were gently resuspended in the remaining supernatant, diluted with 8 ml ddH_20, and spun down at 500 g for 30 min at 4°C. The supernatant was removed except for 20 µl. The pelleted chromosomes were gently resuspended and the entire sample was transferred to a 0.2 ml Eppendorf tube. Further steps were carried out with an Arima Genomics Hi-C kit (Arima Genomics, San Diego, CA USA) according to the manufacturer's protocol. The sequencing libraries were prepared with a NEBNext Ultra II DNA library preparation kit (NEB, Ipswitch, MA, USA) with 10 cycles of PCR amplification. Libraries were sequenced on an Illumina NovaSeq 6000 instrument (Illumina, San Diego, USA) in 150-bp paired-end mode. The parameters of the generated Hi-C data are summarized in Table S4.

The data for chromosome model simulation were generated by an alternative protocol. Eight million chromosomes were sorted into a 15-ml Falcon tube with 2 ml isolation buffer (Šimková et al. 2003), centrifuged at 500 g for 30 min at 4°C, and the supernatant removed except for 45 µl. Pelleted chromosomes were gently resuspended in the remaining supernatant and mixed with low-gelling agarose to create a 90 µl 1% agarose plug. The plug was washed twice for 30 min in 2 ml TE buffer (10 mM Tris-HCl, 1 mM EDTA, pH 8) on ice. Subsequent Hi-C library preparation steps, including DNA digestion, biotin fill-in, ligation, and chromatin release from the plug, were performed according to the "In situ Hi-C in agar plugs protocol" of Rao et al. (2014) with minor modifications: the DNA was digested by 800 U HindIII, and biotin-14-dATP was replaced by biotin-14-dCTP. The completed Hi-C library was sequenced on the HiSeq2500 system in 100-bp paired-end mode.

Hi-C reads were mapped against the barley cv. Morex genome version 2 (v2; Monat et al. 2019) using a previously described computational pipeline (Beier et al. 2017; Monat et al. 2019). Contact matrices were visualized in the R statistical environment (R Core Team 2020).

Contact probabilities from Hi-C data

All contacting pairs from Hi-C data were counted and mapped to the Morex genome version 2 (v2), as a function of the genomic distance between them (*d*). All values of distance *d* were split into bins on a logarithmic scale from 100 kb to 1 Gb. The contact probability of each bin was calculated as the sum of all observed pairs within the distance range of this bin, divided by the number of all genomic loci within the same distance range.

Quantification of Hi-C local contacts in metaphase chromosomes

The chromosomes were divided into 5-Mb-long non-overlapping regions. For each region, we considered only Hi-C pairs with at least one side of the contacting pair inside of this region or with both sides of this pair spanning this region (Figure S3). For each region, the pairs were counted based on the genomic distance between them (*d*). The counted pairs as a function of *d* are well described by the sum of an exponential and a Gaussian distribution. The Gaussian distribution coincides with the bump characteristic of a helical arrangement (Figure 1B-D), and its center indicates the turn length of the helical arrangement around the analyzed region. The center of the Gaussian distribution was assigned as the turn length for each region and was used to build the graphics in Figure 1E.

Building the helical path with a changing radius and estimating the turn number

The monomers selected as the loop basis were constrained to a helical path in the Cartesian space. A turn length (in base pairs) I_i was assigned to each monomer i according to the values calculated from the Hi-C data. With this value, we calculated how many monomers (n_i) from the helical path would fit in this turn, with monomer size (in base pairs) m and the average major loop size (in monomers) I_o (equation 1). Each monomer was then assigned a height z_i and an angle θ_i relative to the previous monomer. The height z_i is equal to the constant turn height (400 nm) divided by n_i, and the angle θ_i is the full turn (360°) divided by n_i (equation 2). The radius r_i was calculated from the turn length (n_i multiplied by the distance d between monomers) and the turn height as in equation 3, from the Pythagorean theorem. The cartesian coordinates were then retrieved by these cylindrical coordinates.

$$n_i = l_i/m/l_o \quad (1)$$

$$z_i = z_{i-1} + 400/n_i \qquad \theta_i = \theta_{i-1} + 360/n_i \quad (2)$$

$$(dn_i)^2 = (2\pi r_i)^2 + 400^2 \quad (3)$$

The number of turns is the number of cycles in the function *cos(θ)*, using 1 Mb as the monomer size and 1 monomer as the average major loop size.

Plant growth and treatment for FISH

Barley seeds were incubated for three days in the dark at room temperature. Roots were collected in cold tap water and incubated on ice for 24 hours (h). The roots were transferred into an ethanol:acetic acid (3:1) fixation solution and placed under a vacuum for 5 min. The roots were stored in this solution overnight at room temperature (RT).

Plant growth and treatment for EdU labeling of SCEs

Barley seeds were incubated for three days in the dark, followed by incubation in 20 µM EdU in Hoagland medium for 17 h at RT. The seedlings were transferred into fresh Hoagland medium and incubated for 19 h in the dark at RT (recovery phase). Roots were cut from the seedlings and incubated in ice-cold water for an additional 24 h. Finally, the roots were fixed in ethanol:acetic acid (3:1) for 5 min under a vacuum and overnight at RT.

Chromosome spread preparation

Selected roots were washed twice in ice water for 5 min and once in a citric buffer for 5 min. The roots were digested in an enzyme mixture [1% Pectolyase (Sigma); 1% Cytohelicase (Sigma); 0.7% Cellulase R-10 (Duchefa), and 0.7% Cellulase (Calbiochem) in 0.1 M citric buffer] at 37°C for 45 min. Following enzymatic digestion, the roots were washed twice in ice-cold water for 5 min and twice in ice-cold ethanol for 5 min. Root tips without root caps were collected into the tube containing ethanol:acetic acid (3:1) and mashed. 7 µl of this suspension was dropped onto a cold wet slide, transferred to a hot plate (55°C), and fixed with 25 µl of ethanol:acetic acid (3:1). The slides were allowed to dry at least for 1 h at RT.

To preserve the native volume of the chromosomes, metaphase chromosomes were flow-sorted into 1× meiocyte buffer A (1× buffer A salts, 0.32 M sorbitol, 1× DTT, 1× polyamines) and subsequently embedded into a 5% polyacrylamide gel as described (Bass et al. 1997; Howe et al. 2013) with minor modifications (Němečková et al. 2020).

FISH

To detect half and full helix turns within chromosome arm 5HL by fluorescence microscopy, oligo-FISH probes were designed against the chromosome-scale sequence assembly of the barley cv. Morex genome assembly version 1 (Morex v1; Beier et al. 2017; Mascher et al. 2017) using Abor Biosciences' proprietary software. Briefly, target sequences were cut into 43–47 nucleotide-long overlapping probe candidate sequences that were compared to the rest of the genome sequence to exclude any candidates with potential cross-hybridization based on a predicted *Tm* of hybridization. Non-overlapping target-specific oligonucleotides were selected for the final sets and synthesized as myTAGs® Labeled Libraries (Arbor Bioscience, Ann Arbor, MI USA).

To validate the lengths of intervals covered by the particular oligo-FISH probes, we verified the completeness of the Morex v2 genome assembly in the analyzed region of 5H using an optical map constructed from barley cv. Morex on the Saphyr platform of Bionano Genomics (Figure S8). The optical map contigs were aligned to the selected interval (442–599 Mb) in the chromosome 5H pseudomolecule using RefAligner version 9232 (Bionano Genomics). Query-to-anchor comparison was performed with default parameters and a p-value threshold of 1e−10. The alignment was visualized in Bionano Access version 1.5. The coordinates from the original design were replaced and are now based on the improved Morex assembly v2 (Monat et al., 2019). The labeled region starts at position 442.1 Mb. For simplicity, the designed probes were given the names of different bird species and labeled in different colors: Stork-Atto647N, Eagle-Alexa488, Ostrich-Atto594, Rhea-Alexa488, Moa-Atto594, and Flamingo-Alexa488 (Figure 2C; Figures S6, S7; Table S2).

Subtelomeres were labeled with the HvT01 oligo-probe (Belostotsky and Ananiev 1990; Schubert et al. 1998) using TexasRed, and telomeres were labeled with the *Arabidopsis* telomere-type oligo probe (Richards and Ausubel 1988) using Cy5. The centromeres were labeled with the probe for

centromeric repeats (GA)15 (Zhang et al. 2019) using FAM, and the NORs were labeled with the 45S rDNA probe using the clone pTa71 and Alexa488 (Gerlach and Bedbrook 1979).
For FISH, the slides were incubated in 45% acetic acid at RT for 10 min and washed in 2×SSC at RT for 10 min. When strong background signals due to cytoplasm were present, 50 µl of pepsin solution (0.1% in 0.01M HCl) was added to the slide, which was then covered with parafilm and incubated in a wet chamber at 37°C for 10 min. The slides were washed twice in 2×SSC for 5 min and post-fixed with 4% formaldehyde in 2×SSC at RT for 10 min. The slides were then washed 3 times in 2×SSC at RT for 4 min and immediately dehydrated in an ethanol gradient (70%, 85% and 100%, 2 min each). The slides were air-dried for at least one hour. In the meantime, all selected oligo probes were pooled into a microtube and the solutions evaporated using a SpeedVac concentrator (Eppendorf). The probes were reconstituted in 1 µl of ddH_2O and 19 µl of hybridization mixture (50% formamide; 10% dextran sulfate; 10% salmon sperm DNA; 2×SSC). The entire volume of the reconstituted probe was added to the slide, covered with a coverslip, and sealed with rubber cement. The slides were incubated for 20 min at 37°C and denatured on a hot plate (70°C) for 3 min. Finally, the slides were directly placed into a wet chamber and hybridized for 22 h at 37°C. Post-hybridization washing was carried out as follows: the slides were briefly washed in 2×SSC at RT to remove the coverslip, washed with shaking at 58°C for 20 min, followed by 5 min in 2×SSC at RT, dehydrated in an ethanol series (70%, 90% and 96%, 2 min each), air-dried in the dark, and counterstained with 8 µl DAPI (2 µg/ml in Vectashield).

Combination of EdU labeling and FISH

Seedling growth and treatment were performed as described for the EdU labeling experiment. Slides containing metaphase spreads with EdU-labeled SCEs were pre-selected and used for oligo-FISH. Depending on the cytoplasm background, the slides were incubated in 45% acetic acid at RT for 10 min and washed in 2×SSC at RT for 10 min or directly post-fixed with 4% formaldehyde in 2×SSC at RT for 10 min. The subsequent steps were identical to the FISH procedure described above.

Super-resolution microscopy and measurement of FISH signal volume

To detect the ultrastructural chromatin organization of chromosomes at a resolution of ~120 nm (super-resolution achieved with a 488 nm laser excitation), spatial structured illumination microscopy (3D-SIM) was performed with an Elyra PS.1 microscope system with a 63×/1.4 Oil Plan-Apochromat objective using ZENBlack software (Carl Zeiss GmbH). Images were captured separately for each fluorochrome using the 642, 561, 488, and 405 nm laser lines for excitation and appropriate emission filters (Weisshart et al. 2016). Maximum intensity projections of whole cells were calculated using ZENBlack software. Zoomed-in sections were presented as single slices to indicate the subnuclear chromatin structures at super-resolution. 3D rendering to produce spatial animations was performed based on SIM image stacks using Imaris 9.6 (Bitplane) software. The FISH signal and DAPI-labeled whole chromosome volumes were generated and measured with the Imaris tool 'Surface'.

Polymer simulation

A simulation for barley metaphase chromatin organization was performed based on a 10 nm chromatin fiber and the bottle-brush model of chicken containing a protein scaffold as described in Gibcus et al. (2018). We assumed that the individual 400 nm fiber turns consisted of larger and

smaller flexible loops. Therefore, a partial intermingling of the minor loops originating from adjacent turns occurred (Figure S10).

In all simulations, the chromatin was modeled as a beads-on-a-string homo-polymer. Molecular Dynamics simulations (MD) were performed using the OpenMM Python application programming interface (Eastman et al. 2017) and the OpenMM-lib library (https://github.com/mirnylab/). The motion of the polymer was simulated based on Langevin dynamics, with a temperature of 300 K, a collision frequency of 0.001 ps^{-1}, and a variable time step (Gibcus et al. 2018). In this simulation, three internal forces are applied to the polymer: (1) a harmonic force covalently binding two neighboring beads; (2) a harmonic angular force between three sequential beads with a spring constant of l k_BT/rad^2; and (3) a polynomial repulsive force allowing for the crossing of the fiber by setting an energy truncation value of 1.5 k_BT, when the distance between two non-bonded beads is zero. In the bottle-brush model, the entire polymer is organized into side-by-side major loops divided into side-by-side minor loops, as proposed by Gibcus et al. (2018). The lengths of both types of loops are randomly chosen following an exponential distribution. Two external forces are applied to constrain the polymer in a cylindrical bottle-brush model: (1) the monomers forming the base of the major loops are tethered to a helical path by a harmonic potential with a spring constant of 4 k_BT/nm^2; and (2) this helical path is at the center of a cylinder, whose boundaries are defined by a harmonically increasing potential with a spring constant of 10 k_BT/nm^2. Apart from these characteristics, the bottle-brush model is defined by four parameters: (1) the average length of major loops; (2) the average length of minor loops; (3) the turn height, and (4) the turn length of the helical path. These parameters are explicitly mentioned for each model we tested (Figure S12C). All simulations start with a conformation where the base of the major loops follow a calculated helical path, and the loops emerge radially. All monomers in the helical path are assigned cylindrical coordinates (angle, radius, and height). These coordinates are calculated so that the monomers are equally separated given the specified total number of major loops and the turn height and converted to Cartesian coordinates. The simulation runs until the contact probability is equilibrated.

To reproduce the contact probability of chicken chromosome 1 at prometaphase (30 min after the release of G2 arrest), as described by Gibcus et al. (2018), with major loops of 400 kb (average length), minor loops of 80 kb (average length), 150 nm turn height, and 8 Mb turn length, we used a coarse-grained model where each monomer represents one nucleosome. Covalent bonds were separated by 10 nm average distance and 1 nm wiggle distance, cylindrical confinement secured a volume of 11^3 nm^3 per monomer, and the monomers in the helical path were separated by 50 nm. Using the same parameters, we built four models to reproduce the contact probability of metaphase barley chromosome 5H, varying the average length of major and minor loops, the turn height, and the turn length. These models simulate a region with 5 turns of the helical path (Figure S12D, E).

To compare helical and half-helical arrangements, we used the same coarse-grained model described above but simulated a 10-Mb region with 2-Mb turn length, 100-nm turn height, 100kb major loops, and 10-kb minor loops. The radius of the helical path was set to 100 nm, and no cylindrical confinement was set. The half helical arrangement differed from the helical arrangement only in terms of the position of the major loops' basis: only the absolute values of the x-coordinate were considered in the conversion from cylindrical to Cartesian coordinates. Ten replicates per model were used to calculate the contact probability.

To observe the changing turn length, we simulated the ~600 Mb of chromosome 5H with a coarse-grained model where each monomer represents 2 kb. In agreement with the volume measured for the entire chromosome (~43^3 nm^3/2 kb), we set covalent bonds that were separated by an average

distance of 40 nm and a wiggle distance of 4 nm. The cylindrical confinement was set separately for each major loop, i.e., 800 nm in height around the position of the loop basis and radius proportional to the turn length, with a minimum of 500 nm and a maximum of 900 nm following our chromatid width measurements after EdU labeling (Movie 12). Major and minor loops were 1 Mb and 400 kb long, respectively. Monomers in the helical path were separated by 50 nm. The helical path was calculated with a constant turn height of 350 nm and a radius proportional to the local turn length, as previously calculated from our Hi-C data. At the constriction regions, where no helical arrangement occurs, the position of the major loops' basis follows a straight line on the z-axis and minor loops are only 40 kb long, a value that approximately mimics the observed size of the primary constriction.

Contact probabilities of polymer models

To measure the contact probabilities of the equilibrated models, the final conformation of each simulation was calculated by counting all monomers spatially close to each other by no more than 51 nm, as in ([34]Gibcus et al., 2018). These pairs of monomers were then grouped according to their distance in the linear genome. The sum of observed contacts in each group was divided by the sum of all possible contacts between two monomers separated by this group distance in the linear genome. The contact probability as a function of the linear genomic distance was directly compared to the experimental data obtained by Hi-C experiments upon normalization of all probability functions to be equal to 1 for 100 kb.

Acknowledgments

This work was supported by the Deutsche Forschungsgemeinschaft (Schu 762/11-1), DFG-GACR project (award No. 18-14450J) and by the ERDF project ''Plants as a tool for sustainable global development" (No. CZ.02.1.01/0.0/0.0/16_019/0000827). We thank Katrin Kumke and Ines Walde for excellent technical assistance, and Ingo Schubert for critical reading of the manuscript.

Figure legends

Figure 1. The presence of periodical Hi-C contacts reveals the helical organization of somatic barley metaphase chromosomes. A) Hi-C contact matrix of barley chromosome 5H in inter- and metaphase. The anti-parallel diagonal in interphase (green arrow) indicates the Rabl configuration, while metaphase chromosomes show a parallel diagonal (blue arrow), indicating that a periodical contact pattern is missing around the centromere and NOR (black arrows). **B)** Average Hi-C contact probabilities of all chromosomes as a function of the distance between two contacting sites in meta- and interphase. The characteristic bump (solid arrow) relates to the second diagonal observed in the Hi-C metaphase contact matrix (blue arrow in **(A)**. The bump follows a decrease at half of its position (dashed arrow). This pattern indicates an arrangement into turns, where sites distant by one turn (solid arrow) are more likely to come in contact than sites a half-turn apart (dashed arrow). The bump position indicates the turn length. Intra-turn contacts below 10-Mb distance (gray area) indicate the lower-order chromatin organization, where nested loops are packed within each turn (Gibcus et al. 2018). **C)** The three contact types observed with different contact probability patterns **(B)** are represented in a helical arrangement. Sites separated by one turn are closer to each other (solid arrow, inter-turn contacts) than sites separated by a half-turn (dashed arrow, half-turn contacts), and contacts between adjacent loops (inset) constitute a lower-order organization with higher contact probability (gray region). **D)** Schema of a metaphase chromosome arranged into turns, as inferred from the Hi-C matrix **(A)** and the contact probability **(B)**. The color gradient along the turns relates to the linear genomic sequence. **E)** Turn length along all chromosomes based on the local contacts observed in the Hi-C experiments (Table S1). Positions of primary (dashed arrows) and secondary (solid arrows) chromosome constrictions can be recognized by zero turn length. All interstitial regions show similar turn lengths, decreasing towards the telomeres. Abrupt peaks, such as in chromosome 7H at 160, 195, and 330 Mb, relate to gaps or assembly errors in the genome sequence. The total turn number per chromosome is indicated.

Figure 2. FISH using oligo probes reveal the helical organization of barley metaphase chromosomes. (A) Density of predicted single-copy oligo probes along chromosome 5H. The distal 157 Mb-long region of the long arm of chromosome 5H is enriched in single-copy sequences suitable for the detection by oligo-FISH. **(B)** Karyogram of barley indicating the distribution of applied centromere-, NOR-, subtelomere-, and telomere-specific FISH probes. **(C)** Design of the oligo-FISH probes (named after different birds for simplicity) covering the 157 Mb-long region of chromosome 5HL. Precise probe coordinates are given in Table S2. Stork and Eagle together cover a ~1.2 turn, and Ostrich, Rhea, and Moa cover a ~1.5 turn. Flamingo covers the subterminal part of the long arm. **(D)** Metaphase chromosome spread labeled with the FISH probes shown in **(B)**. The enlarged oligo-painted region of 5HL (asterisks) shows the chromatin arrangement in both sister chromatids as predicted by the Hi-C-based helical chromatin arrangement model (Figure 1D). Due to chromosome tilting, Moa (in a top-side view) shows the spiral organization of the ~430 nm thick chromatin fiber (marked with yellow lines). **(E)** Positions of telomeres and subtelomeres vary at both termini of different chromosomes. Subtelomeres form ring-like structures (right, arrows). Chromatin was counterstained with DAPI (blue).

Figure 2 continued. (F) Turn lengths (blue line) across the 300 Mb region of 5HL encompassing the designed oligo-FISH probes calculated from the Hi-C data. The regions covered by each probe are colored according to the probe color. **(G)** Helical arrangement of the target region illustrating

the changes in the turn lengths according to the region shown in (F). The model is compatible with a helical arrangement with similar turn heights and volumes (see H) and with varying turn lengths. **(H, I)** Box-plots showing the relative measured signal heights **(H)** and volumes **(I)** in percent per whole chromosome of the oligo-labeled half (Stork and Eagle)- and full-turn regions (absolute values are visualized in Figure S9). The numbers of measured chromosomes per oligo probe are shown in parentheses. The boxplots show the mean/median (cross/yellow line), lower, and upper quartiles with explicit values. Whiskers extend to 150% of the interquartile region below and above the box (Williamson et al. 1989). The high variability within each probe is due to difficulties in signal detection. The black dots in the right diagram **(I)** are the expected chromosome volume (%) for each probe if the chromatin density were uniform along the entire chromosome. For all probes, this volume is higher than the observed mean, reflecting an underestimation in the measurements. The exception is the Flamingo probe, the only one with a higher observed than expected mean volume. This indicates that the Flamingo region is less dense than the other measured chromosome regions. The signal heights were measured within SIM image stacks using ZENBlack software, and the volumes (see Figure 6C) were measured using the surface rendering tool of Imaris 9.6.

Figure 3. Sister chromatid exchanges (SCEs) confirm the helical organization of barley metaphase chromosomes. (a) Metaphase chromosome spread labeled with EdU to detect SCEs creating a harlequin pattern. Some exchanged chromatin regions appear as thin bands with a minimum height of ~400 nm (enlarged regions * and ** in dashed rectangles). The sizes of these regions correspond to the ~430 nm chromatin fiber (chromonema) detected by the oligo-FISH probes (Figure 2D, H, S9A), reflecting a helix within the chromatid arms. **(B)** Scatter plot of 257 measured SCEs of different heights (along the chromosome longitudinal axis) and widths (in the chromatid). The color code indicates how much of the chromatid width is covered by the SCE: dark green indicates complete coverage. The schematic chromosomes around the diagram show examples of measured SCEs. The lack of values in the dashed region indicates that SCEs > ~400 nm and not covering the complete chromatid width never occurred. The black line indicates the median height (~380 nm) of SCEs with incomplete width (less than chromatid width), and the gray area spans the lower and upper quartiles. The observed possible configurations of SCEs imply that the chromatids are formed by ~400 nm high chromatin units. These configurations are compatible with a helical arrangement, as illustrated in the scheme below. The small SCEs in the centromeric, NOR and telomeric regions were not considered. **(C)** At centromeres (top), the EdU labeling indicates the presence of a straight, thin connection between the ~400 nm high fibers. Immediately next to the centromere, due to chromatin tilting, a ~400 nm thick turn is visible in the pericentromeric region (arrow). At the NOR (bottom), thin chromatin fibers also occur. **(D)** SCE units of ~400 nm are also evident at the chromosomal termini (arrows). Chromatin was counterstained by DAPI (blue/white).

Figure 4. A combination of oligo-FISH and EdU labeled SCEs support the helical organization of chromatin. Metaphase chromosome spread (top) showing all barley chromosomes after EdU and oligo-FISH labeling. In both homologous oligo-FISH-painted 5HL regions, two thin exchanged regions occurred (bottom). The one on the left does not span the entire chromatid width, but the one on the right does (insets in the merged images). The SCEs are present at the transition from the Rhea region to the unlabeled Moa (left, red arrow) and Ostrich (right, white arrow) regions. The heights of the SCEs, oligo-FISH probe and EdU-free regions are similar (~380-450 nm).

Figure 5. Primary (centromere) and secondary (NORs) chromosome constrictions are not organized as a helix. Instead, these regions (marked by red and blue dashed rectangles) contain parallel chromatin fibers (red and white arrows; also see Figure 3C). At chromosome arms, the DAPI-labeled chromatin (white) occurs as a network of looped fibers within the ~400 nm fiber. The fibers contain chromatin clusters (yellow arrows), and in between them, small chromatin-free regions (green arrows). No large continuous cavities were observed, as demonstrated in Movies 9 and 10, representing the whole chromosome volume.

Figure 6. Simulated Hi-C data-based polymer chromosome model based on cytological findings. (A) Metaphase chromosome 5H labeled by different FISH probes (marked by an asterisk in Figure 2D). The chromatids are separated by a dashed line. The ortho-view (Movie 3) **(B)** and surface rendering (Movie 5) **(C)** of the same chromosome prove that the FISH signals are present throughout the whole chromosome volume. **(D)** A polymer model of a single chromatid based on the turn lengths calculated from the experimental Hi-C data (Figure S14). The simulated model, built as a bottle brush, is formed by large loops, whose bases follow a helical arrangement (right). The large loops are further divided into minor loops, which internally and externally fill the space surrounding the helical arrangement. Thus arranged, the loops form thicker helical turns of chromatin. Each monomer in the model represents ten nucleosomes (~2 kb). The entire polymer contains 300,000 monomers corresponding to ~600 Mb. The multi-colored region follows the design of the oligo-FISH probes (Figure 2C). The model can be used to illustrate the number and changing sizes of the turns along the chromatid arms, but it has to be adapted according to the observed FISH-labeling pattern, e.g., the NOR appears larger via FISH labeling than that simulated based on the Hi-C data.

Figure 7. Helical model of the higher-order chromatid organization of a somatic plant metaphase chromosome based on data from barley.
Both chromatids (the highest level of chromatin organization) are formed by a ~400 nm thick chromatin fiber (chromonema) arranged in a helix of identical handedness (Figure S11). The chromatids are filled with chromatin without large cavities. Adjacent chromonema turns intermingle due to the flexibility of the smaller 80 nm fibers present within the chromonema. The helical order is interrupted at centromeres and secondary constrictions, which mainly display straight 80-nm chromatin fibers. The chromosomal termini contain less condensed, more flexible chromatin. Due to this flexibility, the telomeres may be embedded into the subtelomeric chromatin and not appear at the very end of the chromatid. The left long arm chromatid is shown as a stretched helix representing their higher-order chromatin folding based on oligo-FISH labeling. The different colors represent half (white + green) and complete (red + green) chromonema turns, respectively. The chromonema is formed by looped, thinner 80 nm chromatin fibers. This lower-order chromatin arrangement (colorless inset) is still under debate. According to previous findings ([9]Thoma et al. 1979), at the lowest hierarchical level, 147 bp of left-handed DNA is wrapped around a nucleosome core. Nucleosomes with DNA linkers in between them form the 10-nm chromatin fiber. Several nucleosomes associate into thicker 80 nm chromatin fibers, which form loops within the chromonema.

Figure S1. Hi-C contact matrices of all barley chromosomes (except 5H shown in Figure 1A) at interphase and metaphase from the first replicate of the Hi-C experiment. The anti-parallel diagonal in interphase (green arrows) indicates the Rabl configuration, while metaphase chromosomes show a parallel diagonal (blue arrows), indicating that a periodical contact pattern is missing at the NOR of 6H and the centromeres (black arrows).

Figure S2. Contact probabilities calculated from the three Hi-C experimental replicates of interphase chromatin (A, B) and metaphase (C, D) chromosomes. In all graphics, each line represents one chromosome and each color one replicate. In **(A)** and **(C),** the probabilities are normalized to have the same value at 100 kb. In **(B)** and **(D),** the probabilities are exponentially normalized to have the same values at 100 kb and 30 Mb. In **(D),** the exponential normalization withdraws experimental variability and highlights the position of the bump characteristic of the metaphase contact probability. (**E**) Derivative of the contact probability log comparing metaphase **(D)** and interphase **(B).** (**F**) Contact probability ratio between metaphase **(D)** and interphase **(B)**. The dashed lines in **(E, F)** correspond to the observed peaks. In interphase, both peaks relate to the Rabl conformation reminiscent of anaphase. In metaphase, the first peak corresponds to the size of chromatin loops and the second to the size of helical turns. In the ratio of metaphase/interphase contact probabilities, the peaks highlight the differences between metaphase and interphase conformations.

Figure S3. Quantification of Hi-C local contacts in metaphase chromosomes. The chromosomes were divided into 5-Mb-long non-overlapping regions. All Hi-C pairs within or spanning each region **(A)** were analyzed as a function of the distance between the contacting sites. For each region, this function was plotted as the number of contacts separated by 1 Mb, 2 Mb, ... until 100 Mb **(B)**. Normalized, the results can be interpreted as a local contact probability (similar to Figure 1B). This function is well described by the sum of an exponential and a Gaussian distribution. The Gaussian distribution coincides with the bump characteristic of a helical arrangement (see Figure 1). Its center indicates the turn length of the helical arrangement around the analyzed region, which was used to build the graphics in Figure 1C.

Figure S4. Number of local contacts at nine different positions (100–550 Mb) of chromosome 5H retrieved from experimental Hi-C data. At all positions, a prominent bump is present, with the center at slightly different positions. The bump represents a contact increase followed by a decrease at half of its position. This pattern indicates that the chromatin is arranged into turns, with turn length corresponding to the center of the bump. The bump position at any region along chromosome 5H was calculated as described in Figure S3. The placement of the bump for all 5 Mb regions (119), separated by 5 Mb along the 5H sequence, is visualized in Movie 1.

Figure S5. Predicted oligo density along all barley chromosomes (except 5H shown in Figure 2A) used to design the oligo-FISH experiment. The x-axis shows the positions of the oligos on the chromosome in the Morex v2 genome. The y-axis represents the number of oligos within 40-Mb bins.

Figure S6. Graphical representation of the oligo density based on the barley cv. Morex v2 assembly covering the Stork and Moa regions subjected to oligo-FISH. (A) The 33,987 oligos of 45 nucleotides (on average) of the Stork probe homogeneously cover a 0.6-turn of the helix,

with minor gaps arising from the lack of unique sequences. **(B)** The 108,831 oligos of 45 nucleotides (on average) of the Moa probe homogeneously cover a 1.6-turn of the helix without significant gaps. Orange marks the threshold of a minimum of three oligos per kilobase. Green denotes a sufficient number of oligos for FISH in the selected region.

Figure S7. Graphical representation of the oligo densities of all designed probes at the long arm of chromosome 5H. The lower diagram shows an enlarged view of the region covered by the oligo probes.

Figure S8. Validation of chromosome 5H interval 442–599 Mb in the Morex V2 genome assembly by optical mapping. The selected sequence segment (green bars) shows good alignment to the optical map contigs 1, 55, and 17 (blue bars), indicating the overall correctness and completeness of the sequence (top), except for a region around 491 Mb, where non-aligned overhangs of contigs 1 and 55 indicate a missing sequence of at least 403 kb (bottom).

Figure S9. Box-plots showing the measured signal heights (A) and volumes (B) of the oligo-labeled regions on chromosome 5HL.
The variable heights of the probes are consistent with the different turn lengths along the mitotic chromosome (Figure 2) and the different degrees of metaphase chromosome condensation. Volumes were measured after surface rendering using Imaris 9.6, and the values correspond to a single chromatid. The numbers of measured chromosomes per oligo probe are shown in parentheses.

Figure S10. Adjacent helix-turns are partially intermingled. The differentially oligo-FISH labeled turns at chromosome arm 5HL intermingle. Smaller looped chromatin fibers forming the turned chromonema (indicated by dashed lines and marked by different colors) invade each other's space (arrows in the right enlarged image). Chromatin was counterstained with DAPI (blue).

Figure S11. In both chromatids, the 400-nm fibers turn in the same direction. (A) The oligo-FISH probes (two examples of Stork, Eagle, and Ostrich are shown) reveal that the sister chromatids coil in the same direction, and not in a mirrored manner. In the merged image, the sister chromatids are divided by a dashed line. **(B)** The schemata show arrangements that were observed (top and middle) and not observed (bottom).

Figure S12. Comparison of applied bottle brush models for condensed barley vs. chicken chromosomes. (A) Contact probability of a barley polymer model generated with the settings described by Gibcus et al. ([34]2018) compared with the Hi-C contact probability for chromosome 1 of chicken at prometaphase ([34]Gibcus et al., 2018). **(B)** Contact probabilities of four barley polymer models, with the same settings as in **(A)**, but with varying helical arrangement parameters as shown in table **(C)**. The models are compared with the Hi-C contact probability of barley chromosome 5H at metaphase. All probabilities are normalized to be equal to 1 at 100 kb. **(D, E)** Conformations of barley models 3 **(D)** and 5 **(E)**. The 30-Mb turns are colored in alternating red and green. From left to right: the bases of major loops form the helical path; the bases of the minor loops are shown in white; a single major loop is divided into minor loops; all loops together complete the model. In **(D)** the bases of major loops (model 3) follow a helical path where the monomers are ~10 nm apart. In **(E),** the bases of the major loops (model 5) follow the same path, but the monomers are

~100 nm apart. Thus, the helical structure is not as constrained as in **(D)**. Consequently, in **(D)**, a backbone scaffold is formed. In **(E)**, the scaffold appears dispersed.

Figure S13. Contact probabilities of polymer models support a helical chromatid organization. The diagram shows the contact probabilities of different polymer models predicted for equilibrium and fractal globules, for simulated helical organization, as suggested by Gibcus et al. (2018), and for a simulated half-helical arrangement with changing handedness, as suggested by Chu et al. (2020). In all spatial models, the polymer is colored as shown for the unfolded polymer. For the helical and half-helical organizations, the polymer is transparent, and the basis of the loops appears as white spheres arranged in turns. Only the helical model creates the contact probability bump.

Figure S14. Nine replicates of the simulated Hi-C data-based polymer chromosome model. The simulations were based on the turn lengths calculated from the experimental Hi-C data. The different patterns arose from the varying loop distributions. Their positions and sizes were chosen at random according to an exponential distribution to reach the same average loop size.

Figure S15. Comparison of Hi-C-based contact probabilities of mitotic chromosomes in chicken vs. barley. (A) Contact probabilities of barley chromosome 5H at metaphase and chicken chromosome 1 at prometaphase (Gibcus et al. 2018). The right diagram shows the derivative of the log of the same contact probabilities, clearly indicating the bump position. The dashed line marks the average size of the nested loops **(B)** Contact probabilities of all barley chromosomes at metaphase and **(C)** all chicken chromosomes at prometaphase (Gibcus et al. 2018). All probabilities were normalized to be equal to 1 at 100 kb.

Figure S16: Flow sorting of barley metaphase chromosomes. Flow karyotype of barley cv. Morex. Initial gating was set on relative DAPI fluorescence vs. forward scatter parameters (P0); the dependent sorting gate was drawn based on the DAPI-area vs. DAPI-width scatter plot (P1).

Tables

Table 1: Parameters of helically organized somatic metaphase chromosomes of barley compared to other species. Chromatid helix turn sizes and nested loop sizes are based on Hi-C data and a bottle brush-like model except for mouse and human.

Table S1: Values of local turn length of each chromosome calculated for 5-Mb bins, as described in the supplementary materials and Figure S4. These values are graphically shown in Figure 1E. The first three lines display the sequence length of each chromosome and the positions of the primary (centromere) and secondary constriction (NOR) at the short arms of 5H and 6H, as predicted from Hi-C data.

Table S2: Coordinates of the oligo-FISH probes (named after different birds) adjacent to the 5HL subtelomere based on the barley cv. Morex v2 genome assembly.

Table S3: Volumes of barley satellite chromosomes 5H and 6H (identified based on their secondary constriction and centromere positions) and NOR-free (1H-4H, 7H) chromosomes. The measurements were done on polyacrylamide embedded spatially preserved chromosomes.

Table S4: Statistics of the metaphase Hi-C datasets. Seven libraries were analyzed: three replicates from interphase libraries, three replicates from metaphase libraries, and one metaphase library generated with an alternative protocol, which yielded fewer unspecific contacts, for comparison with polymer modeling. For each library, the total number of contact reads (all reads), percentage of PCR duplicated reads (duplicated), number of non-duplicated reads with a mapping quality (MAPQ) of at least 10 (high-quality reads), number of intra-chromosome contacts separated by more than 1 kb (1 kb separation), number of intra-chromosome contacts separated by more than 1 Mb (1 Mb separation), and number of inter-chromosome contacts (inter-chromosome) were computed. * percentage of all reads: ** percentage of reads relative to the number of high-quality reads; *** percentage of reads separated by more than 1 kb.

Movies

Movie 1. Bump position along chromosome 5H, indicating the turn sizes. Placement of the bump calculated for 119 different positions in the sequence of chromosome 5H separated by 5 Mb.

Movie 2. The 14 somatic barley metaphase chromosomes labeled by FISH, as described in Figure 2B-D. The movie clearly shows that the oligo-FISH labeled 5HL region is also labeled inside of the chromosome arms.

Movie 3. Slices of a chromosome 5H SIM image stack shown in ortho view (Figure 6B), indicating the complete FISH labeling of the inner chromatin.

Movie 4: Spatial minor chromatin fiber intermingling of adjacent chromonema turns at chromosome arm 5HL labeled in different colors by oligo-FISH (Figure S10).

Movie 5. Spatial surface rendering of chromosome 5H (Figure 6C) showing that FISH signals are present within the whole chromosome volume.

Movie 6. Spatial arrangements of telomeres and subtelomeres (Figure 6E).

Movie 7. Spatial arrangement of the oligo-FISH and EdU labeled region of the left 5H chromosome (*) shown in Figure 4.

Movie 8. Spatial arrangement of the oligo-FISH and EdU labeled region of the right 5H chromosome (**) shown in Figure 4.

Movie 9. Single SIM image stack slices of a DAPI-labeled 6H chromosome showing a network of minor ~80 nm looped chromatin fibers free of large cavities throughout the chromosome arms. Within the centromere and NOR, straight ~80 nm chromatin fibers occur.

Movie 10. Spatial organization of the same 6H chromosome shown in Movie 9.

Movie 11. Animation of the polymer simulation model shown in Figure 6D for a single FISH-labeled 5H chromatid.

Movie 12. Polymer simulation of two helical chromonema half-turns (red and green) of a metaphase chromatid within a cylinder.

References

Albert, P.S., Zhang, T., Semrau, K., Rouillard, J.M., Kao, Y.H., Wang, C.R., Danilova, T.V., Jiang, J., and Birchler, J.A. (2019). Whole-chromosome paints in maize reveal rearrangements, nuclear domains, and chromosomal relationships. Proc. Natl. Acad. Sci. U S A *116*, 1679-1685.

Aurich-Costa, J., Zamechek, L., Keenan, P., and Bradley, S. (2007). Oligo fluorescence in situ hybridization (oligo-FISH), a new strategy for enumerating chromosomes in interphase nuclei. Fertil. Steril. *88*, S86-S86.

Bailey, A.O., Panchenko, T., Sathyan, K.M., Petkowski, J.J., Pai, P.J., Bai, D.L., Russell, D.H., Macara, I.G., Shabanowitz, J., Hunt, D.F.*, et al.* (2013). Posttranslational modification of CENP-A influences the conformation of centromeric chromatin. Proc. Natl. Acad. Sci. U S A *110*, 11827-11832.

Bak, A.L., Zeuthen, J., and Crick, F.H. (1977). Higher-order structure of human mitotic chromosomes. Proc. Natl. Acad. Sci. U S A *74*, 1595-1599.

Baranetzky, J. (1880). Die Kerntheilung in den Pollenmutterzellen einiger Tradescantien. Bot. Zeitschr. *38*, 281-296.

Baroux, C., and Schubert, V. (2018). Technical review: microscopy and image processing tools to analyze plant chromatin: practical considerations. In: Plant chromatin dynamics: methods and protocols, Bemer, M., and M.B.C. Baroux, (eds.), Springer NY, pp. 537-589.

Bass, H.W., Marshall, W.F., Sedat, J.W., Agard, D.A., and Cande, W.Z. (1997). Telomeres cluster de novo before the initiation of synapsis: A three-dimensional spatial analysis of telomere positions before and during meiotic prophase. J. Cell Biol. *137*, 5-18.

Beier, S., Himmelbach, A., Colmsee, C., Zhang, X.Q., Barrero, R.A., Zhang, Q., Li, L., Bayer, M., Bolser, D., Taudien, S.*, et al.* (2017). Construction of a map-based reference genome sequence for barley, *Hordeum vulgare* L. Sci. Data *4*, 170044.

Belmont, A.S., Braunfeld, M.B., Sedat, J.W., and Agard, D.A. (1989). Large-scale chromatin structural domains within mitotic and interphase chromosomes in vivo and in vitro. Chromosoma *98*, 129-143.

Belmont, A.S., Sedat, J.W., and Agard, D.A. (1987). A three-dimensional approach to mitotic chromosome structure: evidence for a complex hierarchical organization. J. Cell. Biol. *105*, 77-92.

Belostotsky, D.A., and Ananiev, E.V. (1990). Characterization of relic DNA from barley genome. Theor. Appl. Genet. *80*, 374-380.

Beseda, T., Capal, P., Kubalová, I., Schubert, V., Doležel, J., and Šimková, H. (2020). Mitotic chromosome organization: General rules meet species-specific variability. Comput. Struct. Biotechnol. J. *18*, 1311-1319.

Bi, Y., Zhao, Q., Yan, W., Li, M., Liu, Y., Cheng, C., Zhang, L., Yu, X., Li, J., Qian, C.*, et al.* (2019). Flexible chromosome painting based on multiplex PCR of oligonucleotides and its application for comparative chromosome analyses in Cucumis. Plant J. *102*,178–186.

Boy de la Tour, E., and Laemmli, U.K. (1988). The metaphase scaffold is helically folded: sister chromatids have predominantly opposite helical handedness. Cell *55*, 937-944.

Braz, G.T., He, L., Zhao, H., Zhang, T., Semrau, K., Rouillard, J.M., Torres, G.A., and Jiang, J. (2018). Comparative oligo-FISH mapping: an efficient and powerful methodology to reveal karyotypic and chromosomal evolution. Genetics *208*, 513-523.

Callan, H.G. (1966). Chromosomes and nucleoli of the axolotl, *Ambystoma mexicanum*. J. Cell Sci. *1*, 85-108.

Chen, B., Yusuf, M., Hashimoto, T., Estandarte, A.K., Thompson, G., and Robinson, I. (2017). Three-dimensional positioning and structure of chromosomes in a human prophase nucleus. Sci. Advances *3*, e1602231.

Chu, L., Liang, Z., Mukhina, M., Fisher, J., Vincenten, N., Zhang, Z., Hutchinson, J., Zickler, D., and Kleckner, N. (2020). The 3D topography of mitotic chromosomes. Mol. Cell *79*, 902-916, e906.

Daban, J.R. (2020) Supramolecular multilayer organization of chromosomes: possible functional roles of planar chromatin in gene expression and DNA replication and repair. FEBS Lett. *594*, 395-411.

Döbel, P., and Schubert, I. (1981). Banding-Techniken und differentielle Markierung durch Basenanaloga - Beiträge zu Chromsomenstruktur, zum Zellzyklus und zur Entstehung chromosomaler Strukturumbauten pflanzlicher Chromosomen. Akademie der Wissenschaften der DDR (Gatersleben), 175 pp.

Doležel, J., Cížková , J. Šimková, H. and Bartoš, J. (2018). One major challenge of sequencing large plant genomes is to know how big they really are. Int. J. Mol. Sci. 19.

Earnshaw, W.C., and Laemmli, U.K. (1983). Architecture of metaphase chromosomes and chromosome scaffolds. J. Cell Biol. *96*, 84-93.

Eastman, P., Swails, J., Chodera, J.D., McGibbon, R.T., Zhao, Y., Beauchamp, K.A., Wang, L.P., Simmonett, A.C., Harrigan, M.P., Stern, C.D.*, et al.* (2017). OpenMM 7: rapid development of high performance algorithms for molecular dynamics. PLoS Comput. Biol. *13*, e1005659.

Feng, S., Cokus, S.J., Schubert, V., Zhai, J., Pellegrini, M., and Jacobsen, S.E. (2014). Genome-wide Hi-C analyses in wild-type and mutants reveal high-resolution chromatin interactions in Arabidopsis. Mol. Cell *55*, 694-707.

Finch, J.T., and Klug, A. (1976). Solenoidal model for superstructure in chromatin. Proc. Natl. Acad. Sci. U S A *73*, 1897-1901.

Fornasiero, E.F., and Opazo, F. (2015). Super-resolution imaging for cell biologists: concepts, applications, current challenges and developments. Bioessays *37*, 436-451.

Fukui, K., and Uchiyama, S. (2007). Chromosome protein framework from proteome analysis of isolated human metaphase chromosomes. Chem. Rec. *7*, 230-237.

Gerlach, W.L., and Bedbrook, J.R. (1979). Cloning and characterization of ribosomal RNA genes from wheat and barley. Nucleic Acids Res. *7*, 1869-1885.

Gibcus, J.H., Samejima, K., Goloborodko, A., Samejima, I., Naumova, N., Nuebler, J., Kanemaki, M.T., Xie, L., Paulson, J.R., Earnshaw, W.C.*, et al.* (2018). A pathway for mitotic chromosome formation. Science *359*.

Grigoryev, S.A., Bascom, G., Buckwalter, J.M., Schubert, M.B., Woodcock, C.L., and Schlick, T. (2016). Hierarchical looping of zigzag nucleosome chains in metaphase chromosomes. Proc. Natl. Acad. Sci. U S A *113*, 1238-1243.

Grob, S., and Grossniklaus, U. (2017). Chromosome conformation capture-based studies reveal novel features of plant nuclear architecture. Curr. Opin. Plant Biol. *36*, 149-157.

Hamano, T., Dwiranti, A., Kaneyoshi, K., Fukuda, S., Kometani, R., Nakao, M., Takata, H., Uchiyama, S., Ohmido, N., and Fukui, K. (2014). Chromosome interior observation by focused ion beam/scanning electron microscopy (FIB/SEM) using ionic liquid technique. Microsc. Microanal. *20*, 1340-1347.

Han, Y., Zhang, T., Thammapichai, P., Weng, Y., and Jiang, J. (2015). Chromosome-specific painting in *Cucumis* species using bulked oligonucleotides. Genetics *200*, 771-779.

Hao, S., Jiao, M.D., and Huang, B.C. (1990). Chromosome organization revealed upon the decondensation of telophase chromosomes in *Allium*. Chromosoma *99*, 371-378.

Hao, S., Xing, M., and Jiao, M. (1988). Chromatin-free compartments and their contents in anaphase chromosomes of higher plants. Cell Biol. Intern. Rep. *12*, 627-635.

Hayashida, M., Phengchat, R., Malac, M., Harada, K., Akashi, T., Ohmido, N., and Fukui, K. (2021). Higher-order structure of human chromosomes observed by electron diffraction and electron tomography. Microsc. Microanal. *27*, 149-155.

Hoang, P.T.N., Rouillard, J.M., Macas, J., Kubalova, I., Schubert, V., and Schubert, I. (2021). Limitation of current probe design for oligo-cross-FISH, exemplified by chromosome evolution studies in duckweeds. Chromosoma *130*, 15-25.

Hoencamp, C., Dudchenko, O., Elbatsh, A.M.O., Brahmachari, S., Raaijmakers, J.A., van Schaik, T., Sedeno Cacciatore, A., Contessoto, V.G., van Heesbeen, R., van den Broek, B.*, et al.* (2021). 3D genomics across the tree of life reveals condensin II as a determinant of architecture type. Science *372*, 984-989.

Howe, E.S., Murphy, S.P., and Bass, H.W. (2013). Three-dimensional acrylamide fluorescence in situ hybridization for plant cells. Methods Mol. Biol. *990*, 53-66.

Iino, A. (1971). Observations on human somatic chromosomes treated with hyaluronidase. Cytogenetics *10*, 286-294.

Inaga, S., Tanaka, K., and Iino, A. (2002). Three-dimensional helical coiling structures and band patterns of hydrous metaphase chromosomes observed by low vacuum scanning electron microscopy. Arch. Histol. Cytol. *65*, 415-423.

Iwano, M., Fukui, K., Takaichi, S., and Isogai, A. (1997). Globular and fibrous structure in barley chromosomes revealed by high-resolution scanning electron microscopy. Chromosome Res. *5*, 341-349.

Jasencakova, Z., Meister, A., and Schubert, I. (2001). Chromatin organization and its relation to replication and histone acetylation during the cell cycle in barley. Chromosoma *110*, 83-92.

Jordan, R., Edington, J., Evans, H.H., and Schwartz, J.L. (1999). Detection of chromosome aberrations by FISH as a function of cell division cycle (harlequin-FISH). Biotechniques *26*, 532-534.

Kempfer, R., and Pombo, A. (2020). Methods for mapping 3D chromosome architecture. Nat Rev Genet. *21*, 207-226.

Kireeva, N., Lakonishok, M., Kireev, I., Hirano, T., and Belmont, A.S. (2004). Visualization of early chromosome condensation: a hierarchical folding, axial glue model of chromosome structure. J. Cell Biol. *166*, 775-785.

Kubalová, I., Němečková, A., Weisshart, K., Hřibová, E., and Schubert, V. (2021). Comparing super-resolution microscopy techniques to analyze chromosomes. Int. J. Mol. Sci. *22*.

Kuznetsova, M.A., Chaban, I.A., and Sheval, E.V. (2017). Visualization of chromosome condensation in plants with large chromosomes. BMC Plant Biol. *17*, 153.

Kuznetsova, M.A., and Sheval, E.V. (2016). Chromatin fibers: from classical descriptions to modern interpretation. Cell Biol. Int. *40*, 1140-1151.

Latt, S.A. (1973). Microfluorometric detection of deoxyribonucleic acid replication in human metaphase chromosomes. Proc. Natl. Acad. Sci. U S A *70*, 3395-3399.

Li, G., Zhang, T., Yu, Z., Wang, H., Yang, E., and Yang, Z. (2021). An efficient Oligo-FISH painting system for revealing chromosome rearrangements and polyploidization in *Triticeae*. Plant J. *105*, 978-993.

Lieberman-Aiden, E., van Berkum, N.L., Williams, L., Imakaev, M., Ragoczy, T., Telling, A., Amit, I., Lajoie, B.R., Sabo, P.J., Dorschner, M.O.*, et al.* (2009). Comprehensive mapping of long-range interactions reveals folding principles of the human genome. Science *326*, 289-293.

Liu, Q., Liu, Y., Shi, Q., Su, H., Wang, C., Birchler, J.A., and Han, F. (2021). Emerging roles of centromeric RNAs in centromere formation and function. Genes Genomics *43*, 217-226.

Liu, X., Sun, S., Wu, Y., Zhou, Y., Gu, S., Yu, H., Yi, C., Gu, M., Jiang, J., Liu, B., *et al.* (2020a). Dual-color oligo-FISH can reveal chromosomal variations and evolution in Oryza species. Plant J. *101*, 112-121.

Liu, Y., Wang, X., Wei, Y., Liu, Z., Lu, Q., Liu, F., Zhang, T., and Peng, R. (2020b). Chromosome Painting Based on Bulked Oligonucleotides in Cotton. Front. Plant Sci. *11*, 802.

Lysak, M.A., Cihalikova, J., Kubalakova, M., Šimková, H., Künzel, G., and Doležel, J. (1999). Flow karyotyping and sorting of mitotic chromosomes of barley (*Hordeum vulgare* L.). Chromosome Res. *7*, 431-444.

Maeshima, K., Eltsov, M., and Laemmli, U.K. (2005). Chromosome structure: improved immunolabeling for electron microscopy. Chromosoma *114*, 365-375.

Maeshima, K., Hibino, K., and Hudson, D.F. (2018). Condensins under the microscope. J. Cell Biol. *217*, 2229-2231.

Maeshima, K., Hihara, S., and Eltsov, M. (2010a). Chromatin structure: does the 30-nm fibre exist in vivo? Curr. Opin. Cell Biol. *22*, 291-297.

Maeshima, K., Hihara, S., and Takata, H. (2010b). New insight into the mitotic chromosome structure: irregular folding of nucleosome fibers without 30-nm chromatin structure. Cold Spring Harb. Symp. Quant. Biol. *75*, 439-444.

Maeshima, K., Ide, S., and Babokhov, M. (2019). Dynamic chromatin organization without the 30-nm fiber. Curr. Opin. Cell Biol. *58*, 95-104.

Maeshima, K., Ide, S., Hibino, K., and Sasai, M. (2016). Liquid-like behavior of chromatin. Curr. Opin. Genet. Dev. *37*, 36-45.

Maeshima, K., and Laemmli, U.K. (2003). A two-step scaffolding model for mitotic chromosome assembly. Dev. Cell *4*, 467-480.

Manton, I. (1950). The spiral structure of chromosomes. Biol. Rev. *25*, 486-508.

Manton, I., and Smiles, J. (1943). Observations on the spiral structure of somatic chromosomes in *Osmunda* with the aid of ultra-violet light. Ann. Bot. *7*, 195-212.

Manuelidis, L., and Chen, T.L. (1990). A unified model of eukaryotic chromosomes. Cytometry *11*, 8-25.

Marko, J.F. (2011). The mitotic chromosome: structure and mechanics. In: Genome Organization and Function in the Cell Nucleus, 1th Ed., Rippe, ed., Wiley-VCH Verlag GmgH & Co KGaA, pp. 449–485.

Marsden, M.P., and Laemmli, U.K. (1979). Metaphase chromosome structure: evidence for a radial loop model. Cell *17*, 849-858.

Maruyama, K. (1983). Stereoscopic scanning electron microscopy of the chromosomes in *Vicia faba* (broad beans). J. Ultrastruct. Res. *82*, 322-326.

Mascher, M., Gundlach, H., Himmelbach, A., Beier, S., Twardziok, S.O., Wicker, T., Radchuk, V., Dockter, C., Hedley, P.E., Russell, J., *et al.* (2017). A chromosome conformation capture ordered sequence of the barley genome. Nature *544*, 427-433.

Matsuura, H. (1935). Chromosome studies on *Trillium kamtschaticum* PALL. I. The number of coils in the chromonema of the normal and abnormal meiotic chromosomes and its relation to the volume of chromosomes. Cytologia, Tokyo *6*, 270-280.

Matsuura, H. (1938). Chromosome studies in *Trillium kamtschaticum* Pall. XI. A simple new method for the demonstration of spiral structure in chromosomes. Cytologia, Tokyo *9*, 243-248.

McClintock, B. (1934). The relationship of a particular chromosomal element to the development of the nucleoli in *Zea mays*. Zeitschr. Zellforsch. Mikr. Anat. *21*, 294–328.

Mirny, L.A. (2011). The fractal globule as a model of chromatin architecture in the cell. Chromosome Res. *19*, 37-51.

Monat, C., Padmarasu, S., Lux, T., Wicker, T., Gundlach, H., Himmelbach, A., Ens, J., Li, C., Muehlbauer, G.J., Schulman, A.H., *et al.* (2019). TRITEX: chromosome-scale sequence assembly of *Triticeae* genomes with open-source tools. Genome Biol. *20*, 284.

Municio, C., Antosz, W., Grasser, K.D., Kornobis, E., Van Bel, M., Eguinoa, I., Coppens, F., Brautigam, A., Lermontova, I., Bruckmann, A., *et al.* (2021). The Arabidopsis condensin CAP-D subunits arrange interphase chromatin. New Phytol. *230*, 972-987.

Murayama, K. (1983). Stereoscopic scanning electron microscopy of the chromosomes in *Vicia faba* (broad beans). J. Ultrastruct. Res. *82*, 322–326.

Musacchio, A., and Desai, A. (2017). A Molecular View of Kinetochore Assembly and Function. Biology (Basel) *6*.

Nagasaka, K., Hossain, M.J., Roberti, M.J., Ellenberg, J., and Hirota, T. (2016). Sister chromatid resolution is an intrinsic part of chromosome organization in prophase. Nat. Cell Bio.l *18*, 692-699.

Naumova, N., Imakaev, M., Fudenberg, G., Zhan, Y., Lajoie, B.R., Mirny, L.A., and Dekker, J. (2013). Organization of the mitotic chromosome. Science *342*, 948-953.

Nebel, B.R. (1932a). Chromosome structure in *Tradescantiae* I. Methods and morphology. Z. Zellforsch. *16*, 251-284.

Nebel, B.R. (1932b). Chromosome structure in *Tradescantiae* II. The direction of coiling of the chromonema in *Tradescantia reflexa* Raf., *T. virginiana* L., *Zebrina pendula* Schnizl. and *Rhoeo discolor* Hance. Z. Zellforsch. *16*, 285–304.

Nebel, B.R. (1939). Chromosome structure. Bot. Rev. *5*, 1-14.

Nebel, B.R., and Ruttle, M.L. (1936a). Chromosome Structure in *Tradescantiae*. VII. Further Observations on the Direction of Coiling in *Tradescantia reflexa* Raf. The American Naturalist *70*, 226-236.

Nebel, B.R., and Ruttle, M.L. (1936b). Chromosome Structure in *Tradescantiae* VIII. The direction of coiling in *Tradescantia reflexa* Raf. as related to the mode of crossing-over. Cytologia *6*, 457-464.

Němečková, A., Koláčková, V., Vrána, J., Doležel , J., and Hřibová, E. (2020). DNA replication and chromosome positioning throughout the interphase in three-dimensional space of plant nuclei. J. Exp. Bot. *71*, 6262-6272.

Neumann, P., Navratilova, A., Schroeder-Reiter, E., Koblizkova, A., Steinbauerova, V., Chocholova, E., Novak, P., Wanner, G., and Macas, J. (2012). Stretching the rules: monocentric chromosomes with multiple centromere domains. PLoS Genet. *8*, e1002777.

Nishino, Y., Eltsov, M., Joti, Y., Ito, K., Takata, H., Takahashi, Y., Hihara, S., Frangakis, A.S., Imamoto, N., Ishikawa, T., *et al.* (2012). Human mitotic chromosomes consist predominantly of irregularly folded nucleosome fibres without a 30-nm chromatin structure. EMBO J. *31*, 1644-1653.

Nokkala, S., and Nokkala, C. (1985). Spiral structures of meiotic chromosomes in plants. Hereditas *103*, 187-194.

Nokkala, S., and Nokkala, C. (1986). Coiled internal structure of chromonema within chromosomes suggesting hierarchical coil model for chromosome structure. Hereditas *104*, 29-40.

Ohnuki, Y. (1965). Demonstration of the spiral structure of human chromosomes. Nature *208*, 916-917.

Ohnuki, Y. (1968). Structure of chromosomes. I. Morphological studies of the spiral structure of human somatic chromosomes. Chromosoma *25*, 402-428.

Ohta, S., Taniguchi, T., Sato, N., Hamada, M., Taniguchi, H., and Rappsilber, J. (2019). Quantitative proteomics of the mitotic chromosome scaffold reveals the association of BAZ1B with chromosomal axes. Mol. Cell Proteomics *18*, 169-181.

Oluwadare, O., Highsmith, M., and Cheng, J. (2019). An overview of methods for reconstructing 3-D chromosome and genome structures from Hi-C data. Biol. Proced. Online *21*, 7.

Paulson, J.R., and Laemmli, U.K. (1977). The structure of histone-depleted metaphase chromosomes. Cell *12*, 817-828.

Perry, P., and Wolff, S. (1974). New Giemsa method for the differential staining of sister chromatids. Nature *251*, 156-158.

Phengchat, R., Hayashida, M., Ohmido, N., Homeniuk, D., and Fukui, K. (2019). 3D observation of chromosome scaffold structure using a 360 degrees electron tomography sample holder. Micron *126*, 102736.

Pienta, K.J., and Coffey, D.S. (1984). A structural analysis of the role of the nuclear matrix and DNA loops in the organization of the nucleus and chromosome. J. Cell Sci. Suppl 1, 123-135.

Poirier, M.G., and Marko, J.F. (2002). Mitotic chromosomes are chromatin networks without a mechanically contiguous protein scaffold. Proc. Natl. Acad. Sci. U S A *99*, 15393-15397.

Pontvianne, F., Carpentier, M.C., Durut, N., Pavlistova, V., Jaske, K., Schorova, S., Parrinello, H., Rohmer, M., Pikaard, C.S., Fojtova, M., *et al.* (2016). Identification of nucleolus-associated chromatin domains reveals a role for the nucleolus in 3D organization of the *A. thaliana* genome. Cell Rep. *16*, 1574-1587.

Rabl, C. (1885). Über Zelltheilung. Morph. Jb. *10*, 214-330.

Rachel, A.J., Sharma, T., and Menon, V.V. (1991). Harlequin Banding and Localization of Sister-Chromatid Exchanges. Mutat. Res. *264*, 71-80.

Rao, S. S., Huntley, M. H., Durand, N. C., Stamenova, E. K., Bochkov, I. D., Robinson, J. T., Sanborn, A. L., Machol, I., Omer, A. D., Lander, E. S., and Aiden, E. L. (2014). A 3D map of the human genome at kilobase resolution reveals principles of chromatin looping. Cell *159*, 1665-1680.

Rattner, J.B. (1987). The organization of the mammalian kinetochore: a scanning electron microscope study. Chromosoma *95*, 175-181.

Rattner, J.B., and Lin, C.C. (1985). Radial loops and helical coils coexist in metaphase chromosomes. Cell *42*, 291-296.

Rattner, J.B., and Lin, C.C. (1987). The higher order structure of the centromere. Genome *29*, 588-593.

R Core Team (2020). R: A language and environment for statistical computing. R Foundation for Statistical Computing, Vienna, Austria. www.r-project.org/index.html

Rego, E.H., Shao, L., Macklin, J.J., Winoto, L., Johansson, G.A., Kamps-Hughes, N., Davidson, M.W., and Gustafsson, M.G. (2012). Nonlinear structured-illumination microscopy with a photoswitchable protein reveals cellular structures at 50-nm resolution. Proc. Natl. Acad. Sci. U S A *109*, E135-143.

Richards, E.J., and Ausubel, F.M. (1988). Isolation of a higher eukaryotic telomere from *Arabidopsis thaliana*. Cell *53*, 127-136.

Ris, H. (1981). Stereoscopic electron microscopy of chromosomes. Methods Cell. Biol. *22*, 77-96.

Rosin, L.F., Gil Jr., J., Drinnenberg, I.A., and Lei, E.P. (2021). Oligopaint DNA FISH as a tool for investigating meiotic chromosome dynamics in the silkworm,*Bombyx mori*. bioRxiv preprint.

Ruch, F. (1950). Über den Schraubenbau der meiotischen Chromosomen. Chromosoma *3*, 357-392.

Saitoh, Y., and Laemmli, U.K. (1994). Metaphase chromosome structure: bands arise from a differential folding path of the highly AT-rich scaffold. Cell *76*, 609-622.

Sartsanga, C., Phengchat, R., Fukui, K., Wako, T., and Ohmido, N. (2021). Surface structures consisting of chromatin fibers in isolated barley (Hordeum vulgare) chromosomes revealed by helium ion microscopy. Chromosome Res., doi.org/10.1007/s10577-021-09649-2

Sax, K. (1935). Chromosome structure in the meiotic chromosomes of *Rhoeo discolor* Hance. J. Arnold Arboretum *61*, 216-224.

Sax, K., and Humphrey, L.M. (1934). Structure of Meiotic Chromosomes in Microsporogenesis of *Tradescantia*. Bot. Gazette *96*, 354-362.

Schloissnig, S., Kawaguchi, A., Nowoshilow, S., Falcon, F., Otsuki, L., Tardivo, P., Timoshevskaya, N., Keinath, M.C., Smith, J.J., Voss, S.R., *et al.* (2021). The giant axolotl genome uncovers the evolution, scaling, and transcriptional control of complex gene loci. Proc. Natl. Acad. Sci. U S A *118*. doi: 10.1073/pnas.2017176118

Schöfer, C., and Weipoltshammer, K. (2018). Nucleolus and chromatin. Histochem Cell Biol *150*, 209-225.

Schroeder-Reiter, E., Perez-Willard, F., Zeile, U., and Wanner, G. (2009). Focused ion beam (FIB) combined with high resolution scanning electron microscopy: A promising tool for 3D analysis of chromosome architecture. J.Struct. Biol. *165*, 97-106.

Schroeder-Reiter, E., Sanei, M., Houben, A., and Wanner, G. (2012). Current SEM techniques for de- and re-construction of centromeres to determine 3D CENH3 distribution in barley mitotic chromosomes. J. Microscopy *246*, 96-106.

Schroeder-Reiter, E., and Wanner, G. (2009). Chromosome centromeres: structural and analytical investigations with high resolution scanning electron microscopy in combination with focused ion beam milling. Cytogenet. Genome Res. *124*, 239-250.

Schubert, I., Schubert, V., and Fuchs, J. (2011). No evidence for "break-induced replication" in a higher plant – but break-induced conversion may occur. Front.Plant Genet. Genomics *2*, 8.

Schubert, I., Shi, F., Fuchs, J., and Endo, T.R. (1998). An efficient screening for terminal deletions and translocations of barley chromosomes added to common wheat. Plant J. *14*, 489-495.

Schubert, V. (2017). Super-resolution microscopy - applications in plant cell research. Front. Plant Sci. *8*, 531.

Schubert, V., Neumann, P., Marques, A., Heckmann, S., Macas, J., Pedrosa-Harand, A., Schubert, I., Jang, T.S., and Houben, A. (2020). Super-resolution microscopy reveals diversity of plant centromere architecture. Int. J. Mol. Sci. *21*.

Schubert, V., Ruban, A., and Houben, A. (2016a). Chromatin ring formation at plant centromeres. Front. Plant Sci. *7*, 28.

Schubert, V., Zelkowski, M., Klemme, S., and Houben, A. (2016b). Similar sister chromatid arrangement in mono- and holocentric plant chromosomes. Cytogenet. Genome Res. *149*, 218-225.

Schvartzman, J.B. (1987). Sister-chromatid exchanges in higher plant cells - past and perspectives. Mutat. Res. *181*, 127-145.

Schvartzman, J.B., and Cortes, F. (1977). Sister Chromatid Exchanges in *Allium cepa*. Chromosoma *62*, 119-131.

Schvartzman, J.B., Cortes, F., and Lopez-Saez, J.F. (1978). Sister subchromatid exchanged segments and chromosome structure. Exp. Cell Res. *114*, 443-446.

Sedat, J., and Manuelidis, L. (1978). A direct approach to the structure of eukaryotic chromosomes. Cold Spring Harb. Symp. Quant. Biol. *42 Pt 1*, 331-350.

Serra, J.A. (1947). Contribution to a physiological interpretation of mitosis and meiosis. II. The prophasic appearing of the spiralization. . Portugaliae Acta Biol. *2*, 45-90.

Seto, T. (1972). The spiral structure of amphibian somatic chromosomes as observed with a light microscope. Mem. Fac. Educ., Shimane Univ. (Nat. Sci.), 99-104.

Shi, G., and Thirumalai, D. (2021). From Hi-C contact map to three-dimensional organization of interphase human chromosomes. Physical Rev. X 11. 011051.

Šimková, H., Číhalíková, J., Vrána, J., Lysák, M.A., and Doležel, J. (2003). Preparation of HMW DNA from plant nuclei and chromosomes isolated from root tips. Biol. Plant. *46*: 369-373.

Šimoníková, D., Němečková, A., Karafiátová, M., Uwimana, B., Swennen, R., Doležel, J., and Hřibová, E. (2019). Chromosome Painting Facilitates Anchoring Reference Genome Sequence to Chromosomes In Situ and Integrated Karyotyping in Banana (Musa Spp.). Front. Plant Sci. *10*, 1503.

Smith, J.J., Timoshevskaya, N., Timoshevskiy, V.A., Keinath, M.C., Hardy, D., and Voss, S.R. (2019). A chromosome-scale assembly of the axolotl genome. Genome Res. 29, 317-324.

Sorsa, V. (1986). Distribution of chromomeres as a basis of chromosomal coiling. J Cell Sci *80*, 193-205.

Strukov, Y.G., and Belmont, A.S. (2009). Mitotic chromosome structure: reproducibility of folding and symmetry between sister chromatids. Biophys. J. *96*, 1617-1628.

Strukov, Y.G., Sural, T.H., Kuroda, M.I., and Sedat, J.W. (2011). Evidence of activity-specific, radial organization of mitotic chromosomes in Drosophila. PLoS Biol. *9*, e1000574.

Strukov, Y.G., Wang, Y., and Belmont, A.S. (2003). Engineered chromosome regions with altered sequence composition demonstrate hierarchical large-scale folding within metaphase chromosomes. J. Cell Biol. *162*, 23-35.

Sumner, A.T. (1991). Scanning electron microscopy of mammalian chromosomes from prophase to telophase. Chromosoma *100*, 410-418.

Sumner, A.T. (1998). The mitotic chromosome. Adv. Genome Biol. *5A*, pp. 211-261.

Sun, M., Biggs, R., Hornick, J., and Marko, J.F. (2018). Condensin controls mitotic chromosome stiffness and stability without forming a structurally contiguous scaffold. Chromosome Res. *26*, 277-295.

Sureka, R., Wadhwa, R., Thakur, S.S., Pathak, R.U., and Mishra, R.K. (2018). Comparison of nuclear matrix and mitotic chromosome scaffold proteins in Drosophila S2 cells-transmission of hallmarks of nuclear organization through mitosis. Mol. Cell. Proteomics *17*, 1965-1978.

Szabo, Q., Bantignies, F., and Cavalli, G. (2019). Principles of genome folding into topologically associating domains. Sci. Adv. *5*, eaaw1668.

Szabo, Q., Jost, D., Chang, J.M., Cattoni, D.I., Papadopoulos, G.L., Bonev, B., Sexton, T., Gurgo, J., Jacquier, C., Nollmann, M.*, et al.* (2018). TADs are 3D structural units of higher-order chromosome organization in *Drosophila*. Sci. Adv. *4*, eaar8082.

Takayama, S., and Taniguchi, T. (1986). Light and scanning electron microscopic observations on the two contrasting types of sister chromatid differential staining after ultraviolet light irradiation. Chromosoma 93, 404-408.

Tang, S., Tang, Z., Qiu, L., Yang, Z., Li, G., Lang, T., Zhu, W., Zhang, J., and Fu, S. (2018). Developing new oligo probes to distinguish specific chromosomal segments and the A, B, D genomes of Wheat (*Triticum aestivum* L.) using ND-FISH. Front. Plant Sci. *9*, 1104.

Thoma, F., Koller, T., and Klug, A. (1979). Involvement of histone H1 in the organization of the nucleosome and of the salt-dependent superstructures of chromatin. J. Cell Biol. *83*, 403-427.

Utsumi, K.R. (1982). Scanning electron microscopy of Giemsa-stained chromosomes and surface-spread chromosomes. Chromosoma *86*, 683-702.

Valarik, M., Bartos, J., Kovarova, P., Kubalakova, M., de Jong, J.H., and Doležel, J. (2004). High-resolution FISH on super-stretched flow-sorted plant chromosomes. Plant J. *37*, 940-950.

van Berkum, N.L., Lieberman-Aiden, E., Williams, L., Imakaev, M., Gnirke, A., Mirny, L.A., Dekker, J., Lander, E.S. (2010). Hi-C: a method to study the three-dimensional architecture of genomes. J. Vis. Exp. *39*, e1869.

Wako, T., Yoshida, A., Kato, J., Otsuka, Y., Ogawa, S., Kaneyoshi, K., Takata, H., and Fukui, K. (2020). Human metaphase chromosome consists of randomly arranged chromatin fibres with up to 30-nm diameter. Sci. Rep. *10*, 8948.

Walther, N., Hossain, M.J., Politi, A.Z., Koch, B., Kueblbeck, M., Odegard-Fougner, O., Lampe, M., and Ellenberg, J. (2018). A quantitative map of human condensins provides new insights into mitotic chromosome architecture. J. Cell Biol. *217*, 2309-2328.

Wanner, G., and Formanek, H. (2000). A new chromosome model. J. Struct. Biol. *132*, 147-161.

Wanner, G., Formanek, H., Martin, R., and Herrmann, R.G. (1991). High-Resolution Scanning Electron-Microscopy of Plant Chromosomes. Chromosoma *100*, 103-109.

Weisshart, K., Fuchs, J., and Schubert, V. (2016). Structured illumination microscopy (SIM) and photoactivated localization microscopy (PALM) to analyze the abundance and distribution of RNA polymerase II molecules in flow-sorted Arabidopsis nuclei. Bio-protocol 6(3): e1725.

Williams, S.P., Athey, B.D., Muglia, L.J., Schappe, R.S., Gough, A.H., and Langmore, J.P. (1986). Chromatin fibers are left-handed double helices with diameter and mass per unit length that depend on linker length. Biophys. J. *49*, 233-248.

Wilson, D.M., 3rd, and Thompson, L.H. (2007). Molecular mechanisms of sister-chromatid exchange. Mutat. Res. *616*, 11-23.

Xin, H., Zhang, T., Wu, Y., Zhang, W., Zhang, P., Xi, M., and Jiang, J. (2020). An extraordinarily stable karyotype of the woody Populus species revealed by chromosome painting. Plant J. *101*, 253-264.

Zatsepina, O.V., Polyakov, V.Y., and Chentsov, Y.S. (1983). Chromonema and chromomere - structural units of mitotic and interphase chromosomes. Chromosoma *88*, 91-97.

Zhang, S., Zhu, M., Shang, Y., Wang, J., Dawadundup, Zhuang, L., Zhang, J., Chu, C., and Qi, Z. (2019). Physical organization of repetitive sequences and chromosome diversity of barley revealed by fluorescence in situ hybridization (FISH). Genome *62*, 329-339.

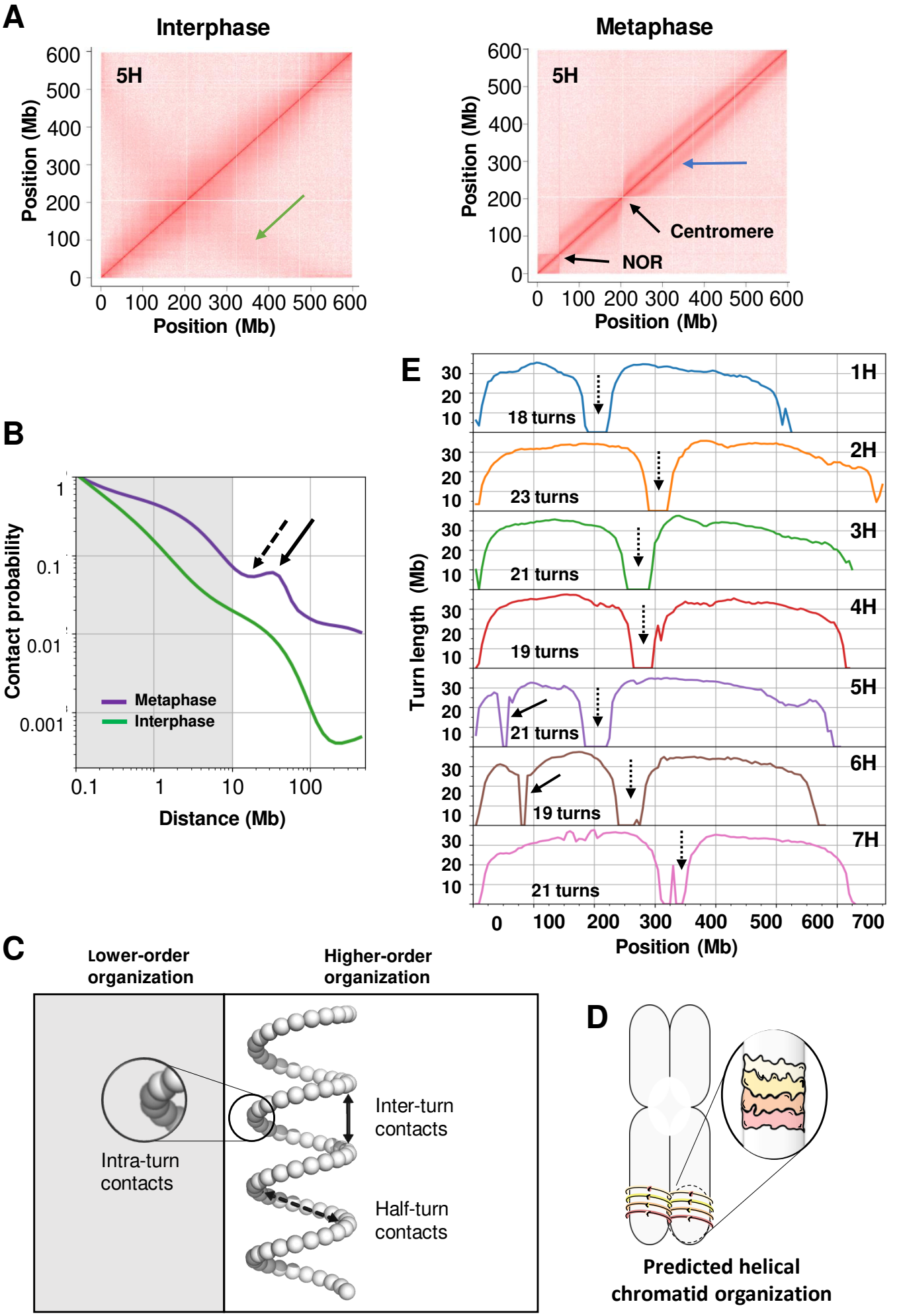
A
Interphase
Metaphase
5H
5H
Position (Mb)
Position (Mb)
Centromere
NOR
B
Contact probability
Distance (Mb)
Metaphase
Interphase
E
Turn length (Mb)
Position (Mb)
1H
18 turns
2H
23 turns
3H
21 turns
4H
19 turns
5H
21 turns
6H
19 turns
7H
21 turns
C
Lower-order organization
Higher-order organization
Intra-turn contacts
Inter-turn contacts
Half-turn contacts
D
Predicted helical chromatid organization

Figure 1

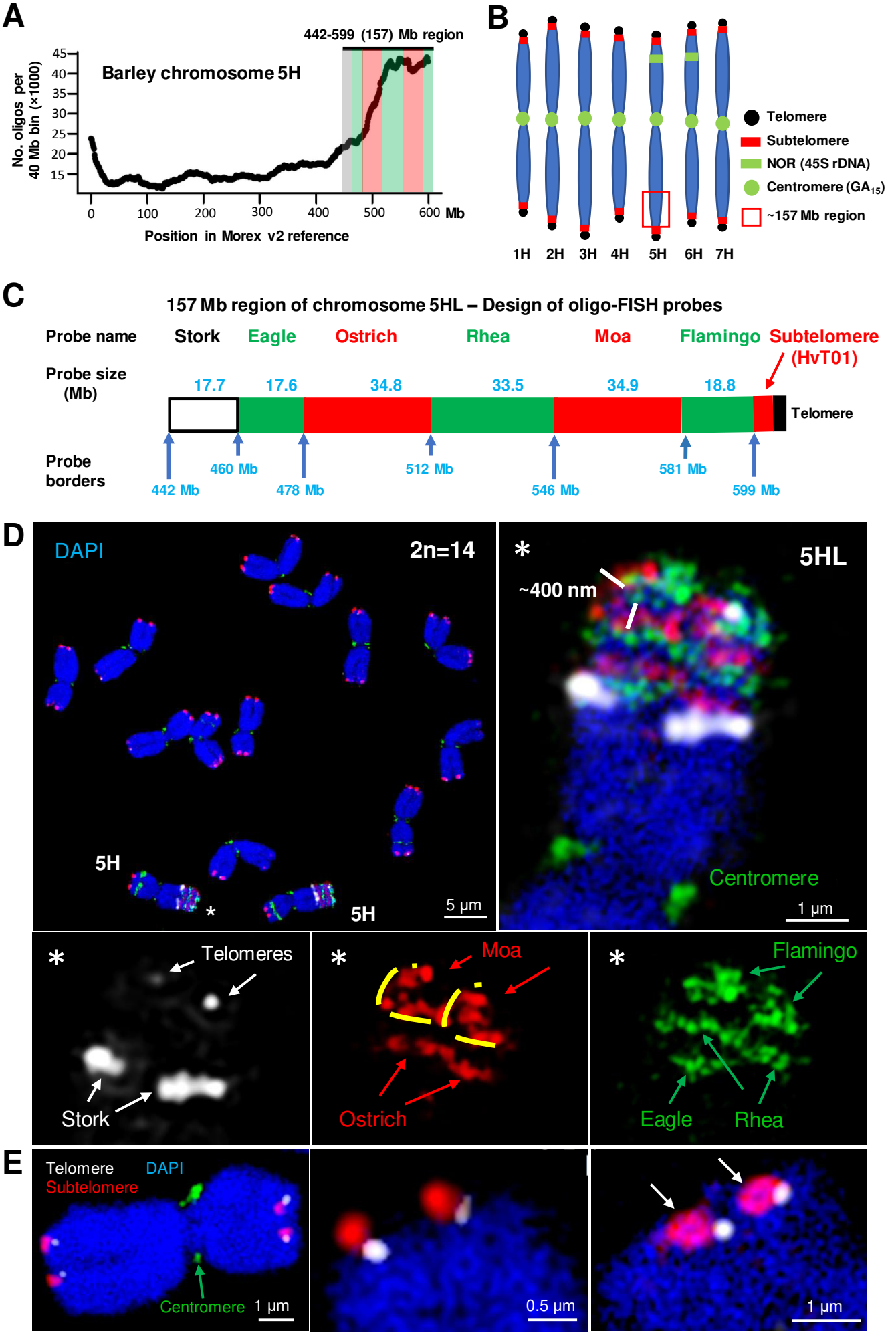
A
442-599 (157) Mb region
Barley chromosome 5H
No. oligos per 40 Mb bin (×1000)
45
40
35
30
25
20
15
0
100
200
300
400
500
600 Mb
Position in Morex v2 reference
B
Telomere
Subtelomere
NOR (45S rDNA)
Centromere (GA15)
~157 Mb region
1H
2H
3H
4H
5H
6H
7H
C
157 Mb region of chromosome 5HL – Design of oligo-FISH probes
Probe name
Stork
Eagle
Ostrich
Rhea
Moa
Flamingo
Subtelomere (HvT01)
Probe size (Mb)
17.7
17.6
34.8
33.5
34.9
18.8
Telomere
Probe borders
442 Mb
460 Mb
478 Mb
512 Mb
546 Mb
581 Mb
599 Mb
D
DAPI
2n=14
5H
5H
5 µm
*
5HL
~400 nm
Centromere
1 µm
*
Telomeres
Stork
*
Moa
Ostrich
*
Flamingo
Eagle
Rhea
E
Telomere
DAPI
Subtelomere
Centromere
1 µm
0.5 µm
1 µm

Figure 2

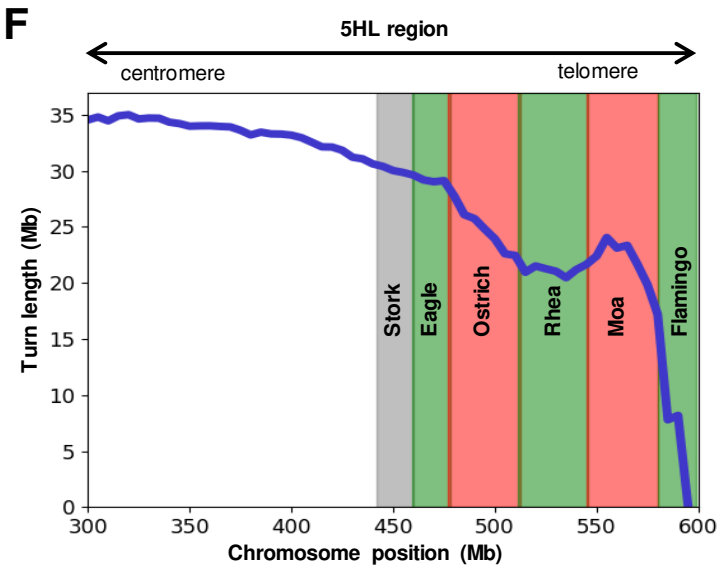

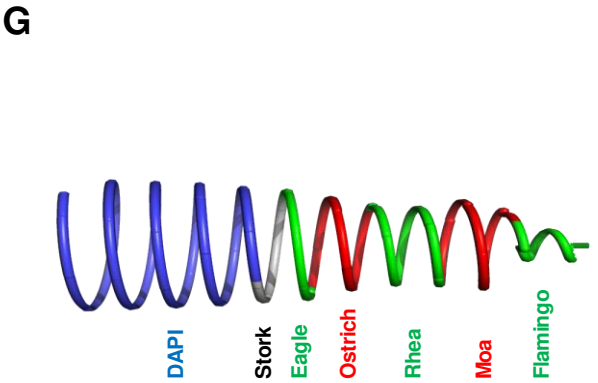

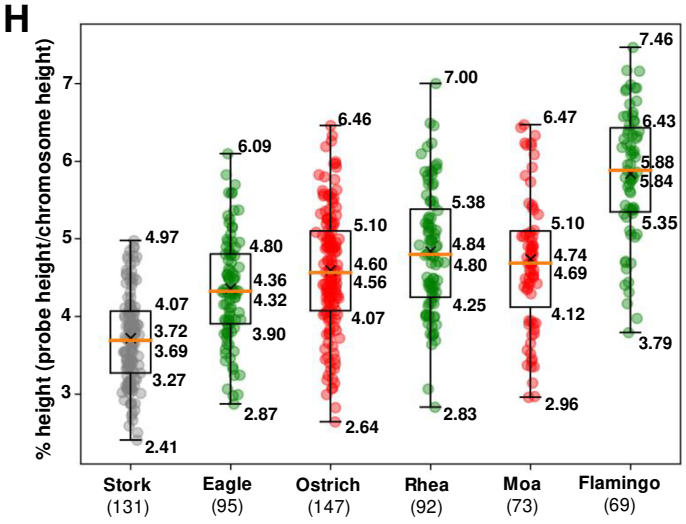

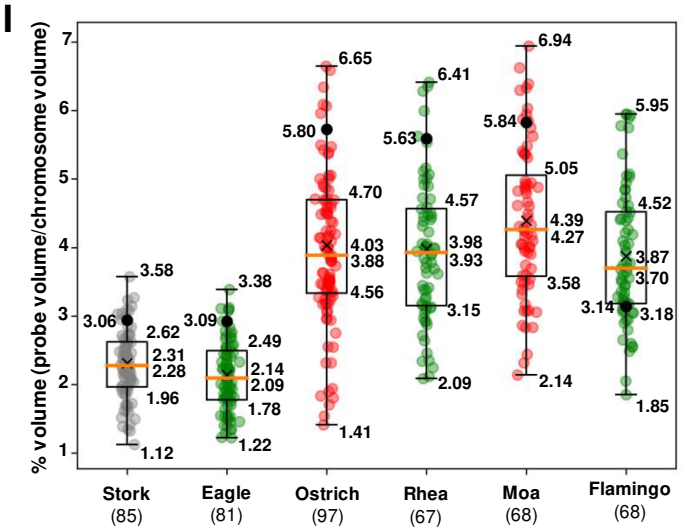

Figure 2 continued

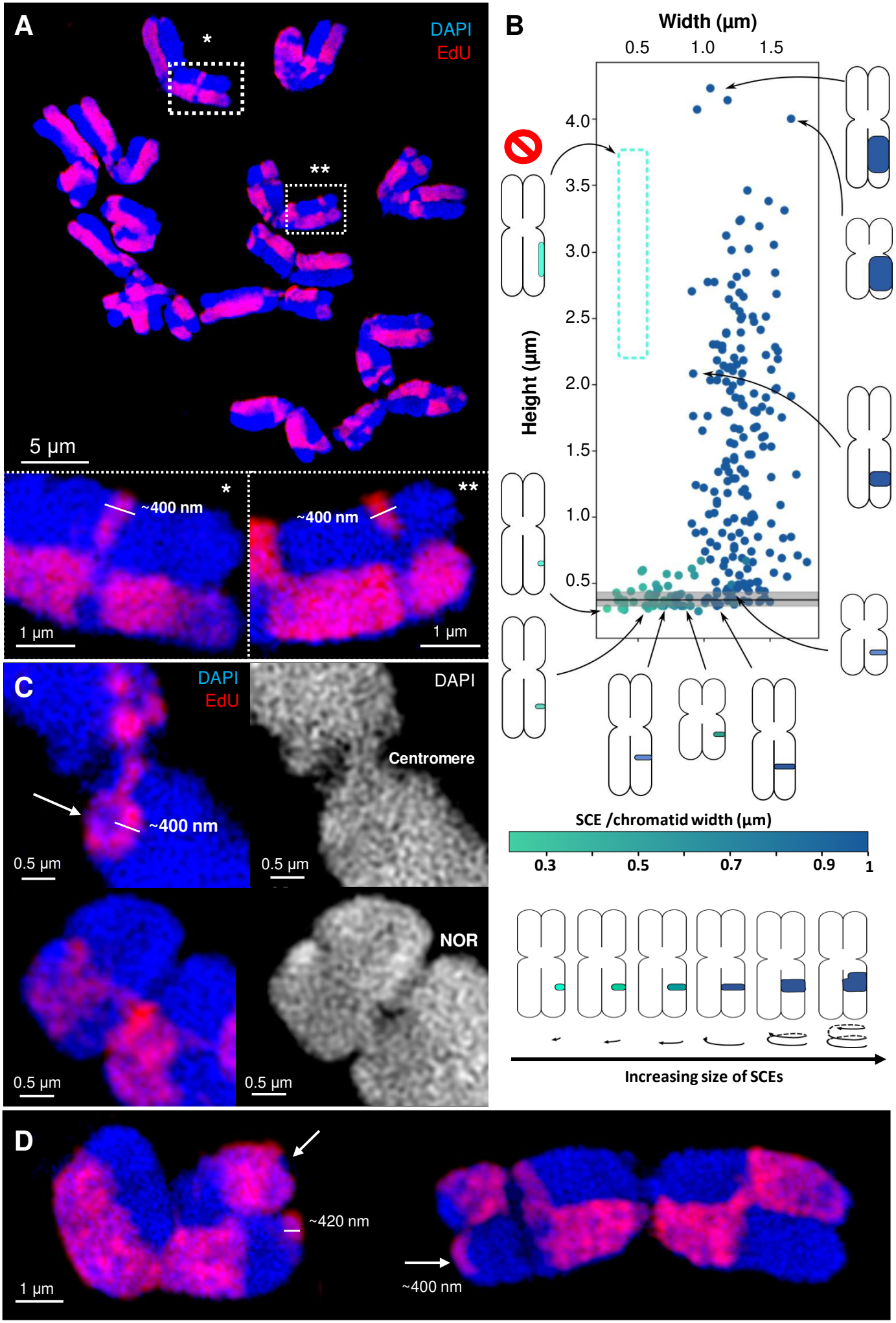
A
DAPI
EdU
*
**
5 µm
~400 nm
1 µm
B
Width (µm)
0.5
1.0
1.5
Height (µm)
4.0
3.5
3.0
2.5
2.0
1.5
1.0
0.5
SCE /chromatid width (µm)
0.3
0.5
0.7
0.9
1
Increasing size of SCEs
C
Centromere
NOR
0.5 µm
D
~420 nm
~400 nm

Figure 3

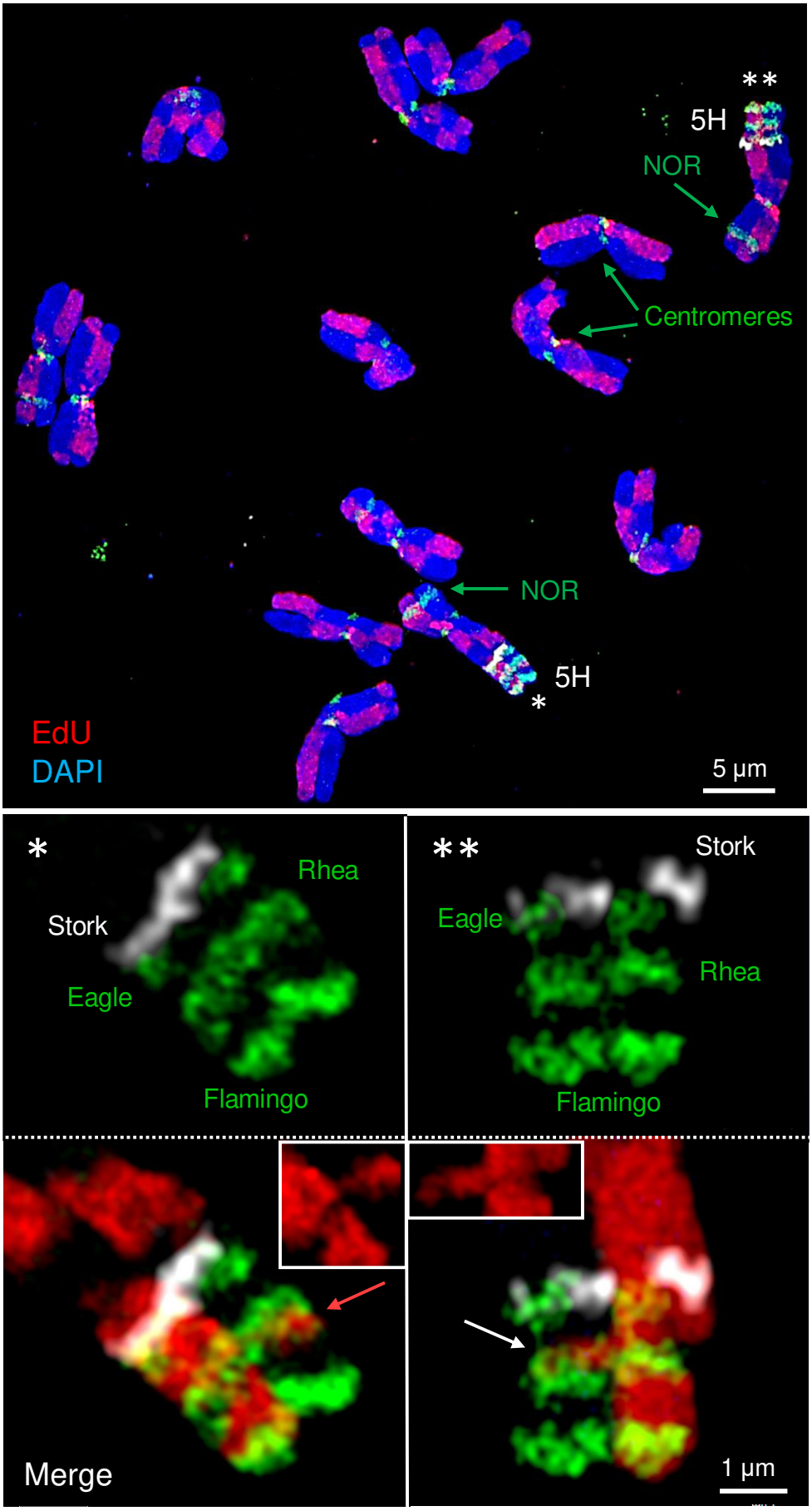
**
5H
NOR
Centromeres
NOR
5H
*
EdU
DAPI
5 µm
*
Rhea
Stork
Eagle
Flamingo
**
Stork
Eagle
Rhea
Flamingo
Merge
1 µm

Figure 4

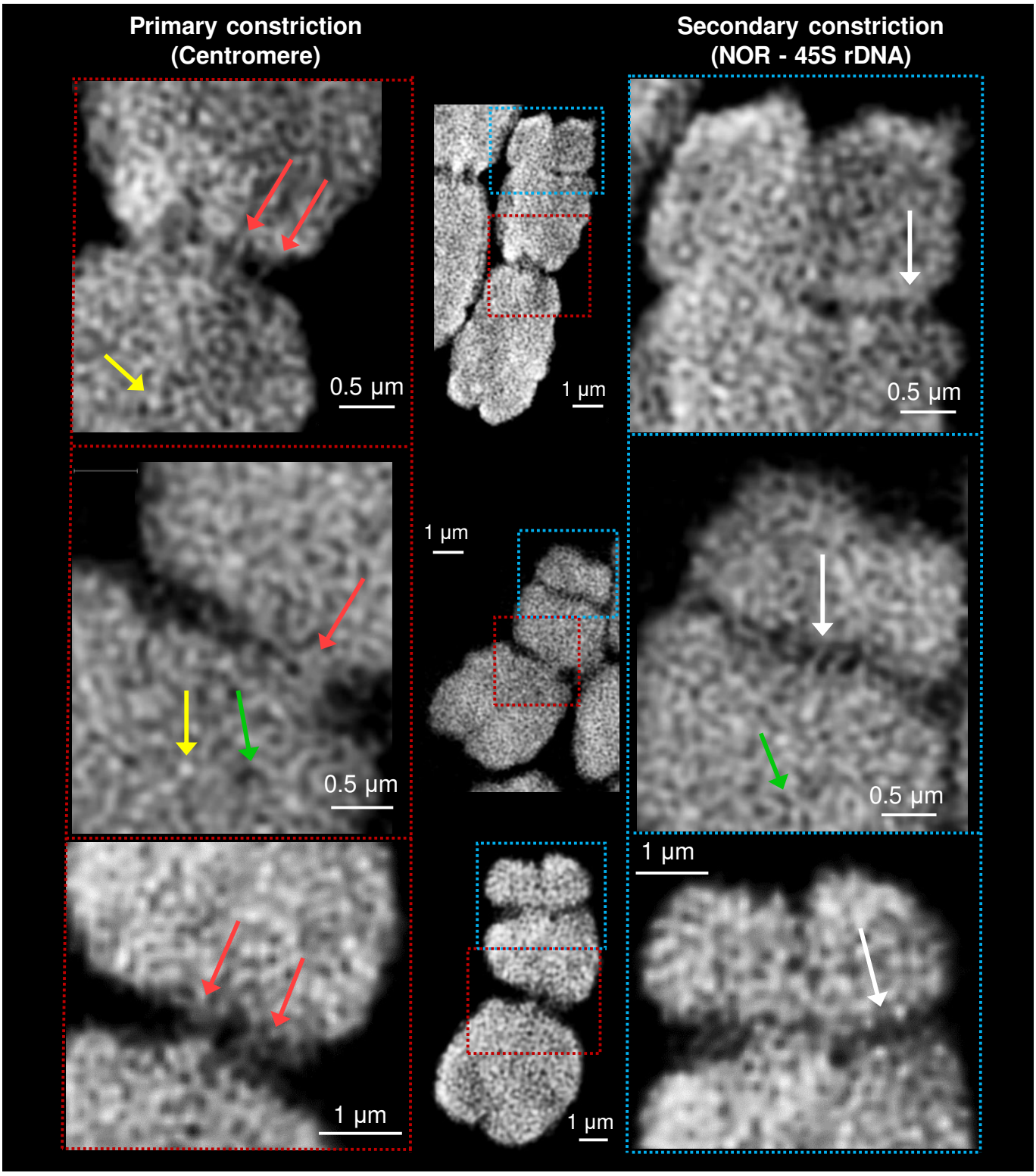
Primary constriction
(Centromere)
Secondary constriction
(NOR - 45S rDNA)
0.5 µm
1 µm
0.5 µm
1 µm
0.5 µm
0.5 µm
1 µm
1 µm
1 µm

Figure 5

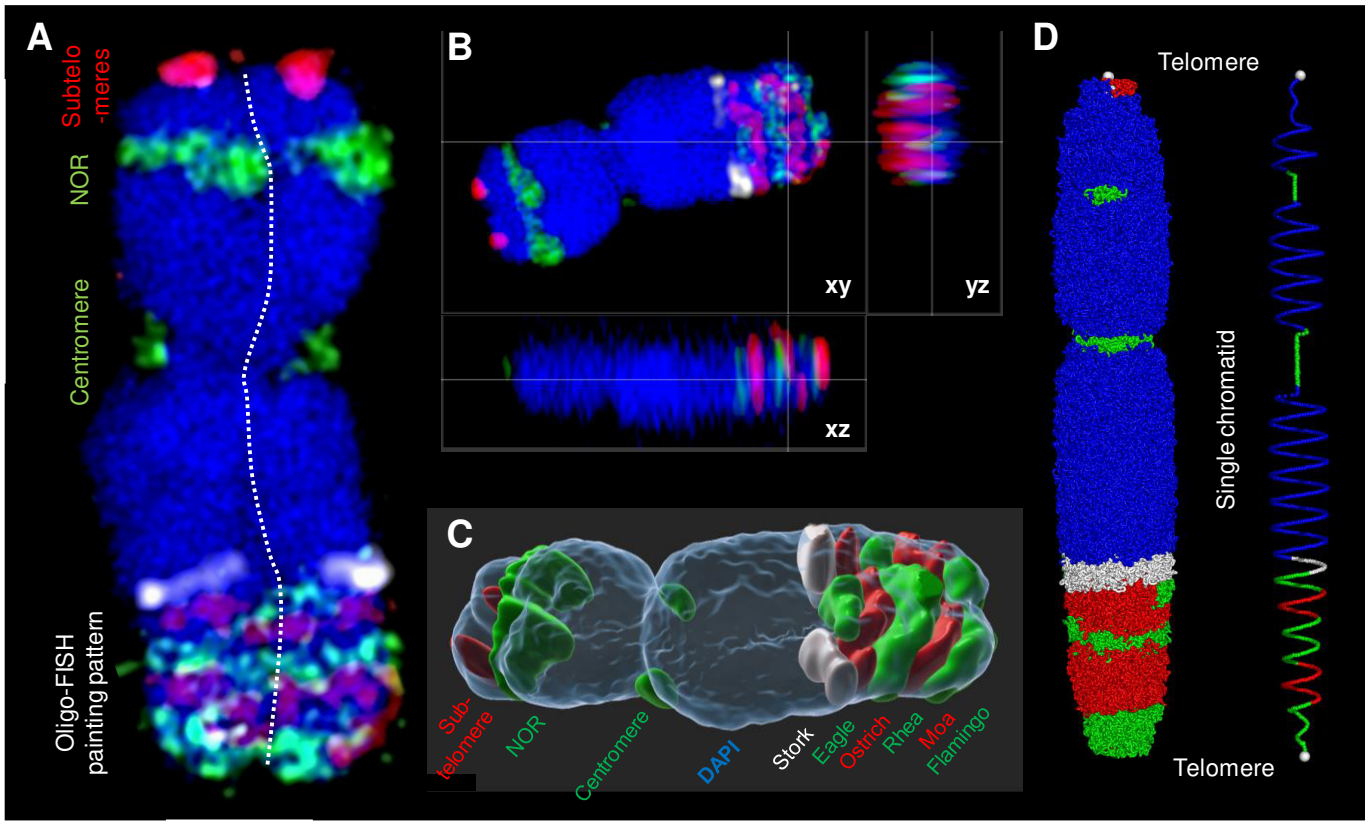
A
Subtelo
-meres
NOR
Centromere
Oligo-FISH
painting pattern
B
xy
yz
xz
C
Sub-
telomere
NOR
Centromere
DAPI
Stork
Eagle
Ostrich
Rhea
Moa
Flamingo
D
Telomere
Single chromatid
Telomere

Figure 6

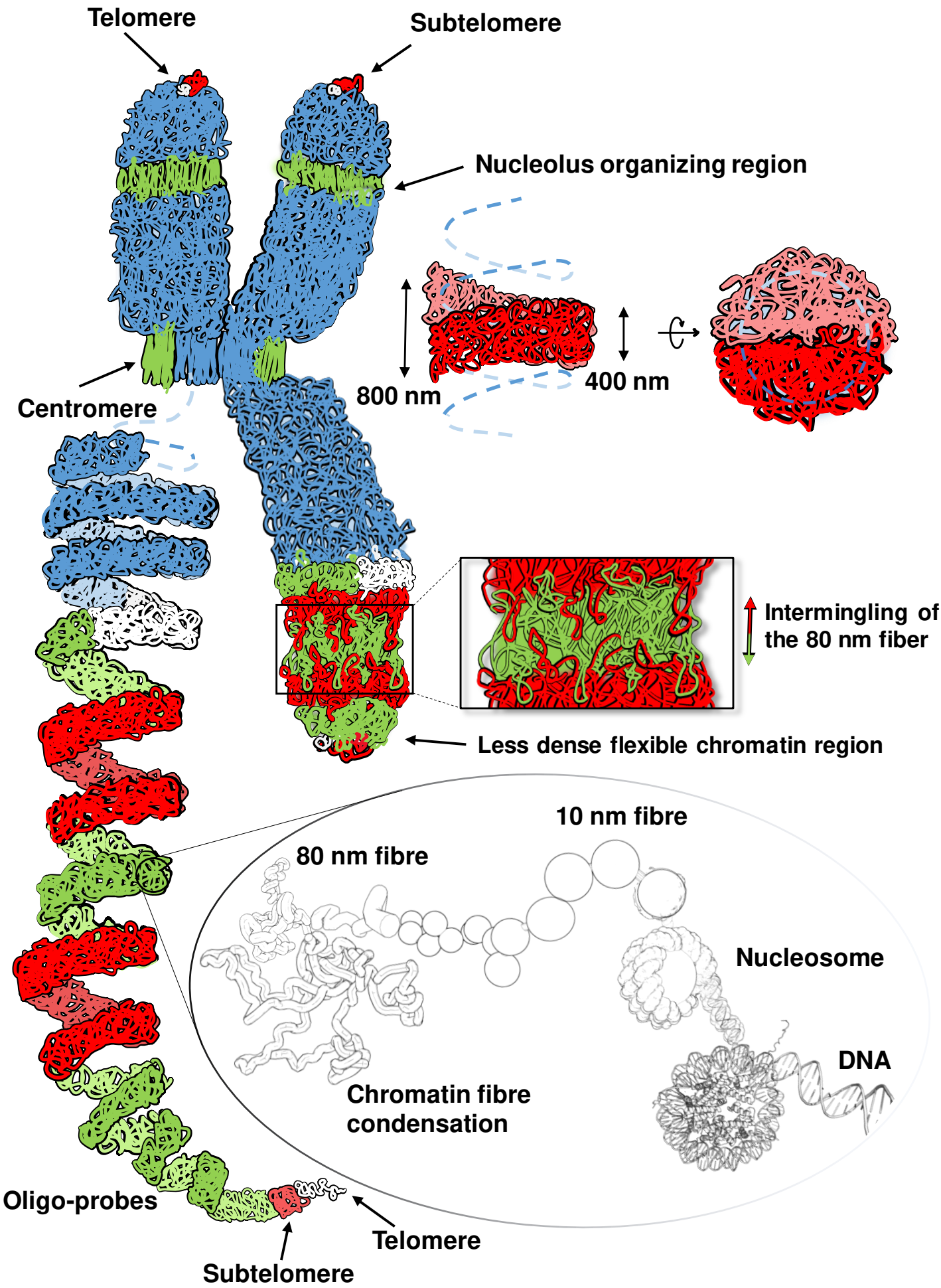
Telomere
Subtelomere
Nucleolus organizing region
800 nm
400 nm
Centromere
Intermingling of the 80 nm fiber
Less dense flexible chromatin region
10 nm fibre
80 nm fibre
Nucleosome
DNA
Chromatin fibre condensation
Oligo-probes
Telomere
Subtelomere

Figure 7

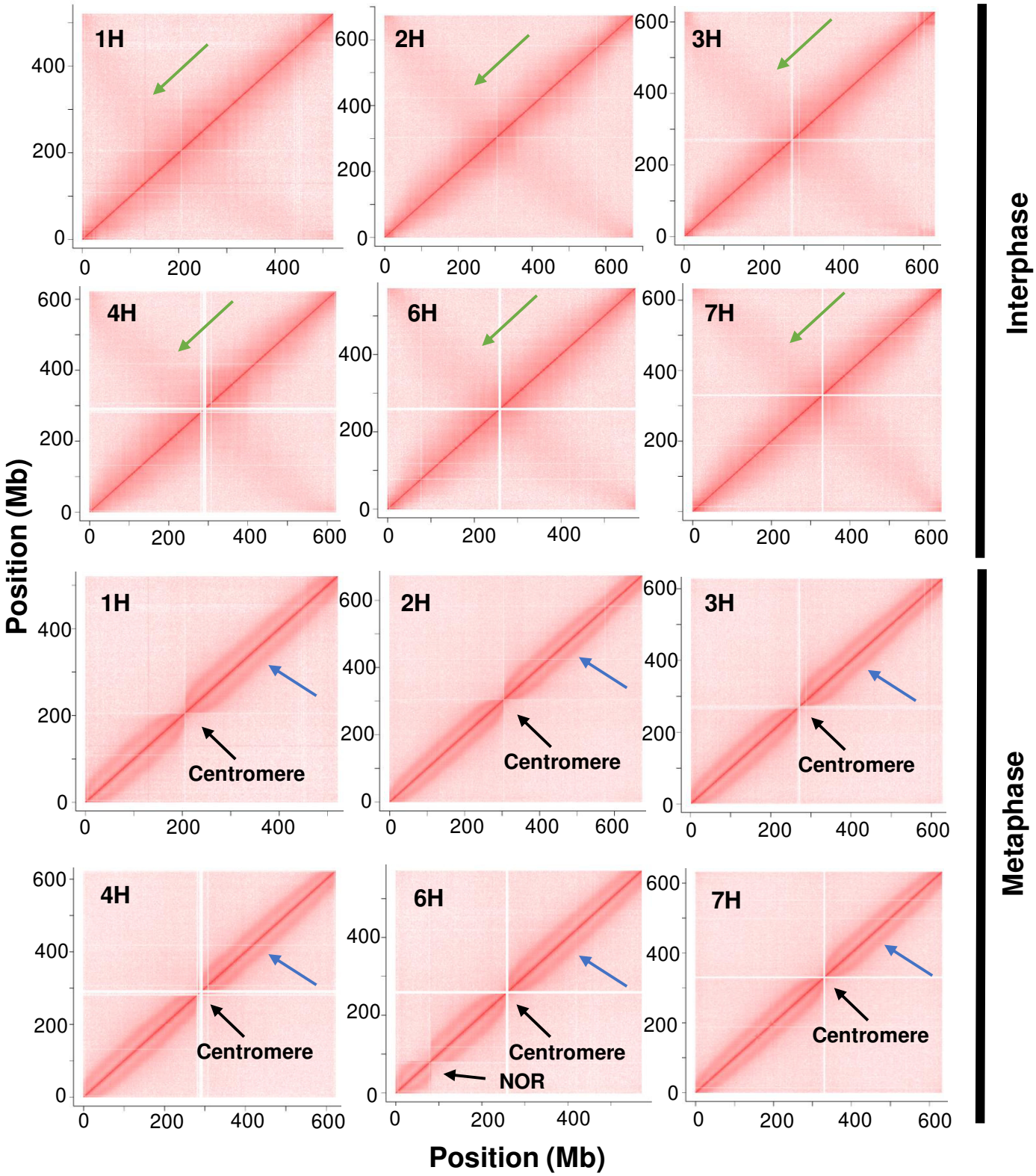
1H
2H
3H
4H
6H
7H
Interphase
Metaphase
Centromere
NOR
Position (Mb)
Position (Mb)

Figure S1

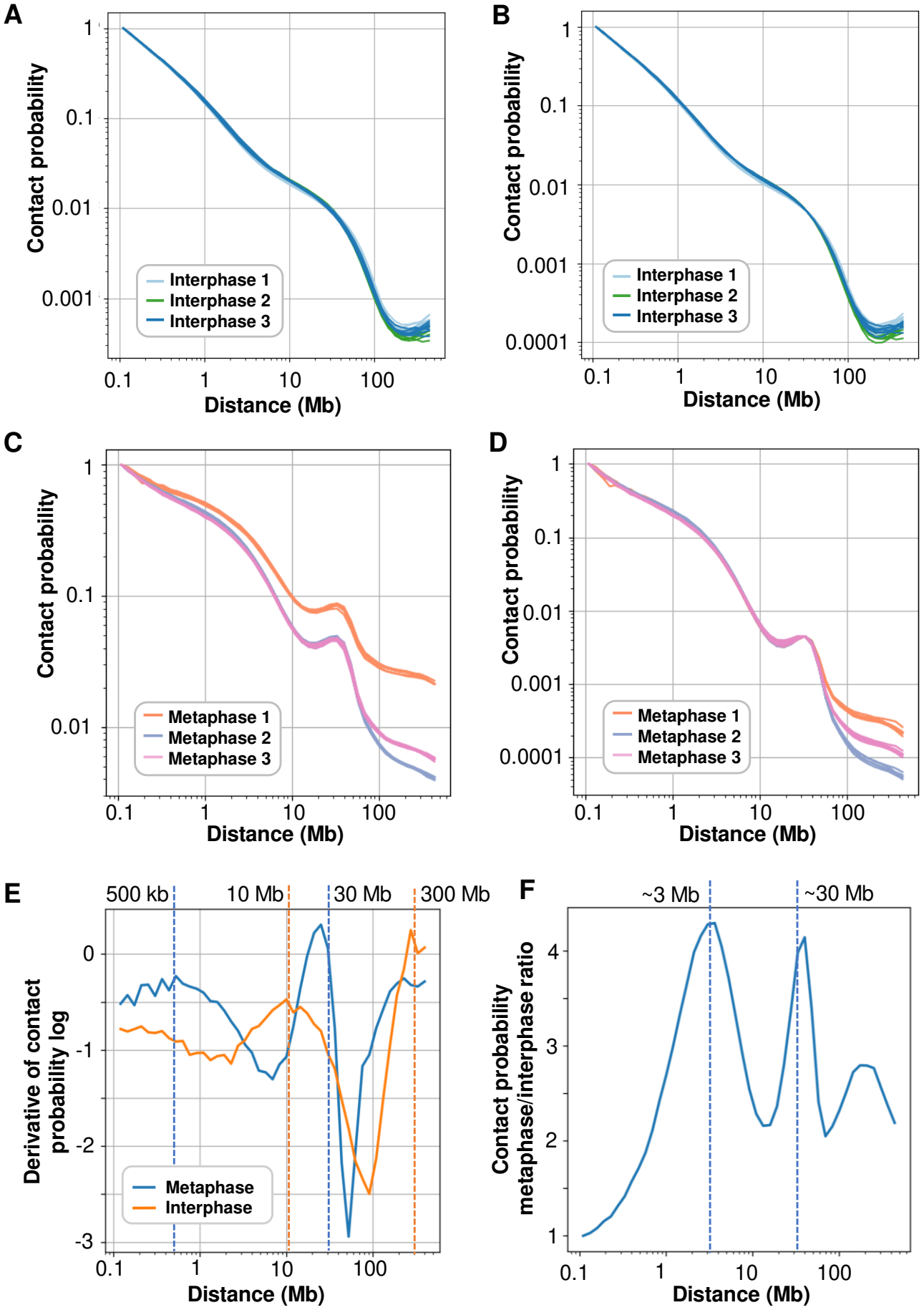
A
Contact probability
1
0.1
0.01
0.001
Interphase 1
Interphase 2
Interphase 3
0.1
1
10
100
Distance (Mb)
B
Contact probability
1
0.1
0.01
0.001
0.0001
Interphase 1
Interphase 2
Interphase 3
0.1
1
10
100
Distance (Mb)
C
Contact probability
1
0.1
0.01
Metaphase 1
Metaphase 2
Metaphase 3
0.1
1
10
100
Distance (Mb)
D
Contact probability
1
0.1
0.01
0.001
0.0001
Metaphase 1
Metaphase 2
Metaphase 3
0.1
1
10
100
Distance (Mb)
E
500 kb
10 Mb
30 Mb
300 Mb
Derivative of contact probability log
0
-1
-2
-3
Metaphase
Interphase
0.1
1
10
100
Distance (Mb)
F
~3 Mb
~30 Mb
Contact probability metaphase/interphase ratio
4
3
2
1
0.1
1
10
100
Distance (Mb)

Figure S2

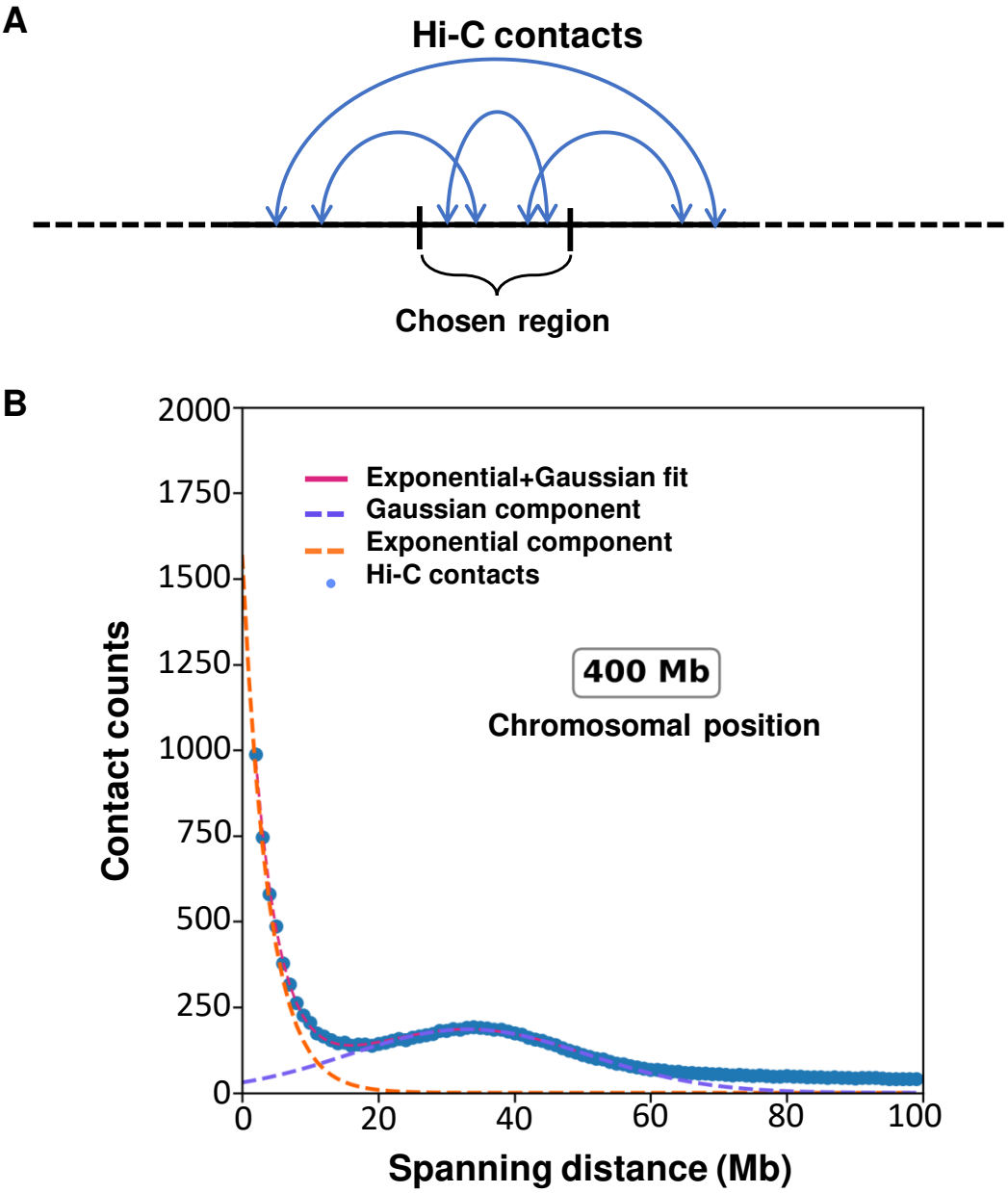
A
Hi-C contacts
Chosen region
B
Exponential+Gaussian fit
Gaussian component
Exponential component
Hi-C contacts
400 Mb
Chromosomal position
Contact counts
Spanning distance (Mb)
0
250
500
750
1000
1250
1500
1750
2000
0
20
40
60
80
100

Figure S3

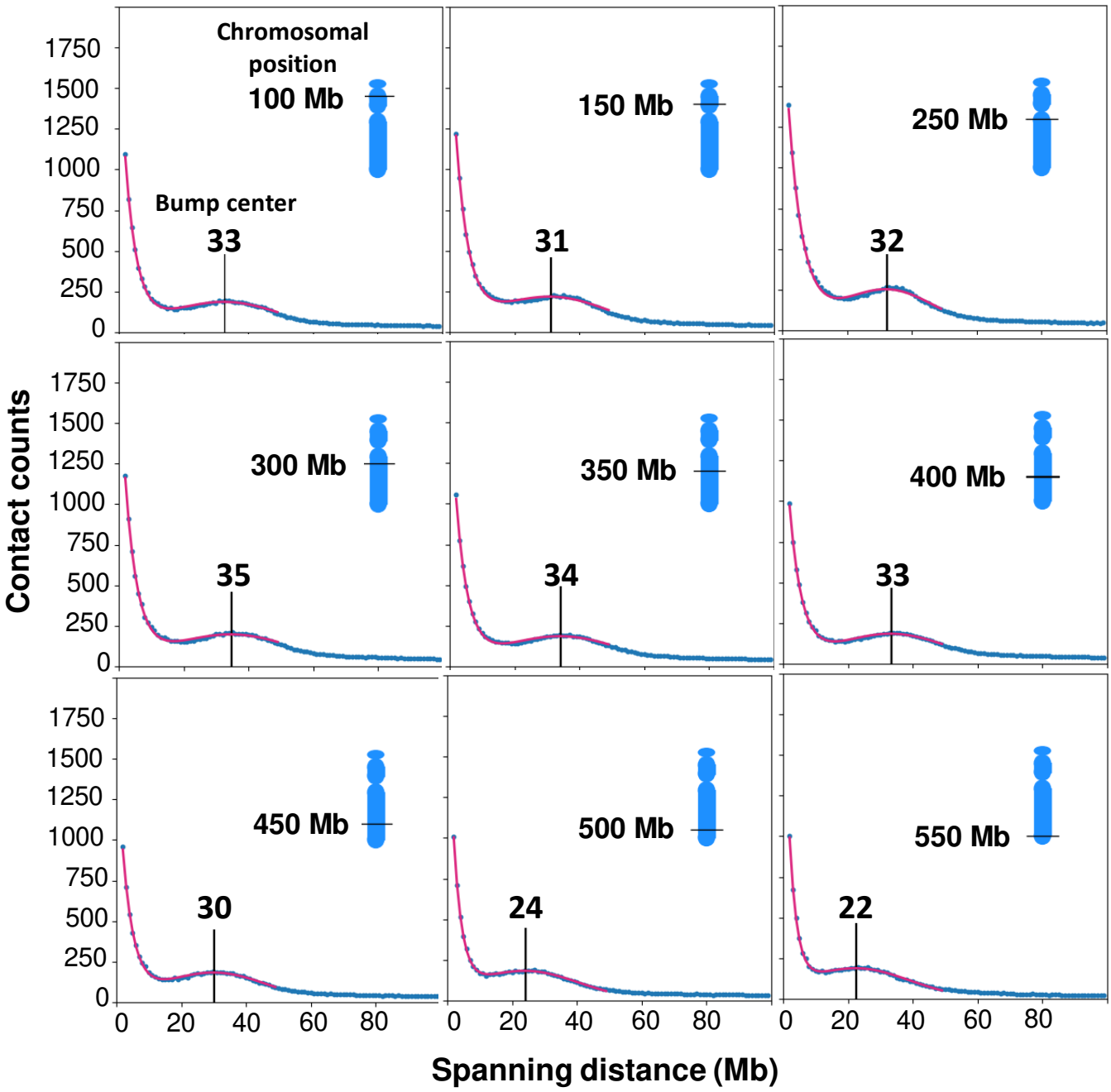
Chromosomal position
100 Mb
Bump center
33
150 Mb
31
250 Mb
32
300 Mb
35
350 Mb
34
400 Mb
33
450 Mb
30
500 Mb
24
550 Mb
22
Contact counts
Spanning distance (Mb)
0
250
500
750
1000
1250
1500
1750
0
20
40
60
80

Figure S4

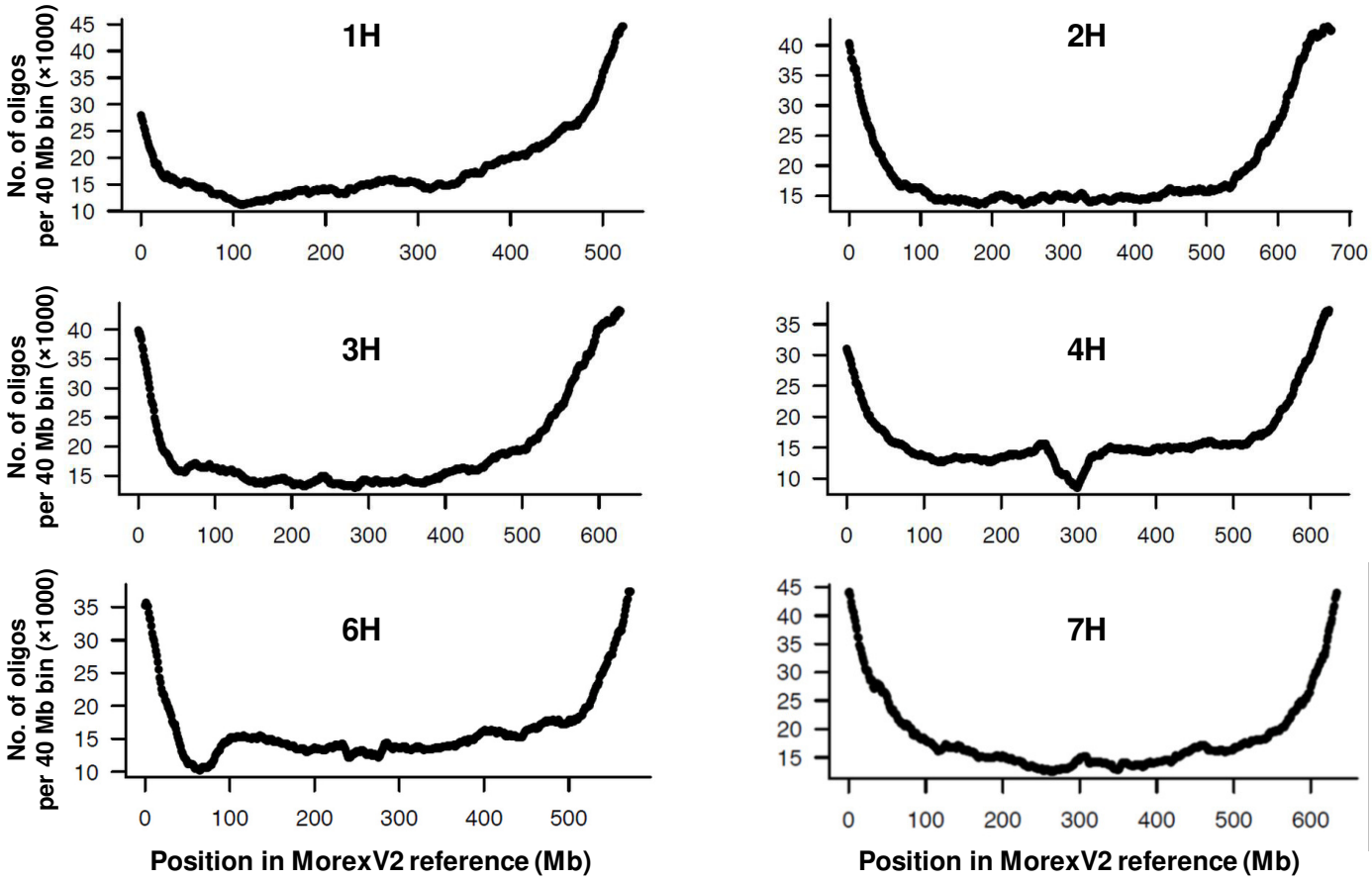
1H
2H
3H
4H
6H
7H
No. of oligos per 40 Mb bin (×1000)
Position in MorexV2 reference (Mb)

Figure S5

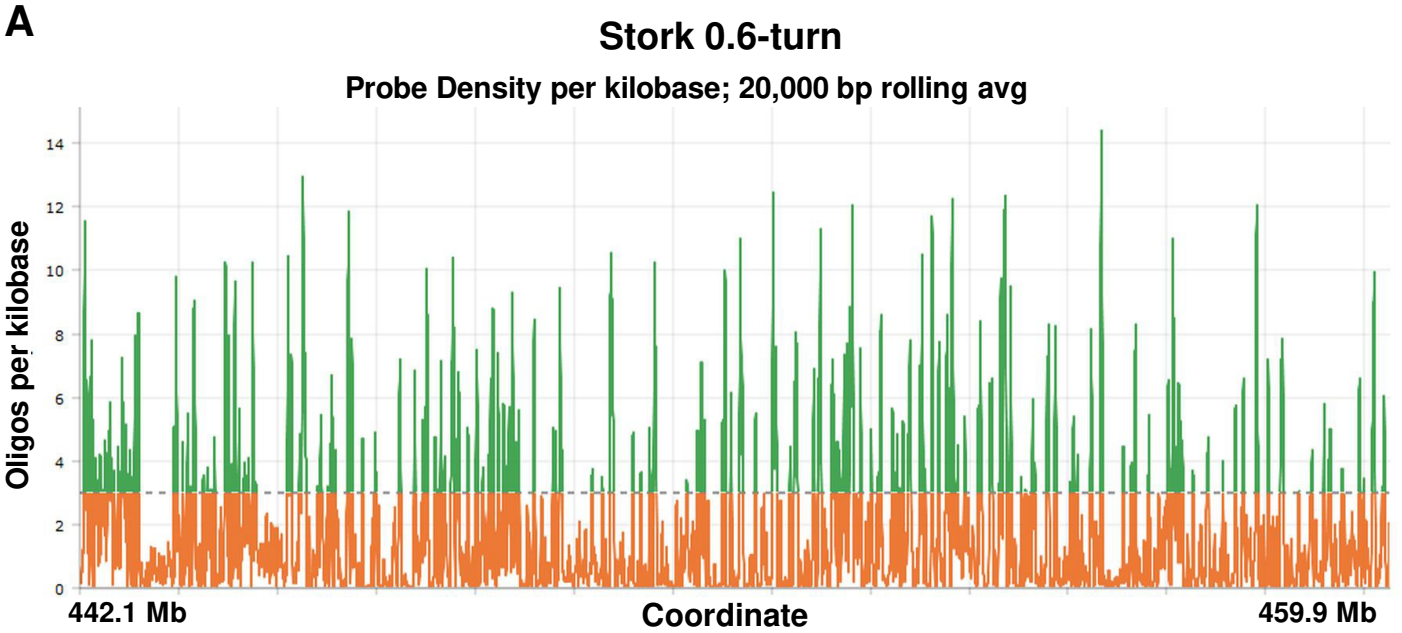
A
Stork 0.6-turn
Probe Density per kilobase; 20,000 bp rolling avg
Oligos per kilobase
0
2
4
6
8
10
12
14
442.1 Mb
Coordinate
459.9 Mb

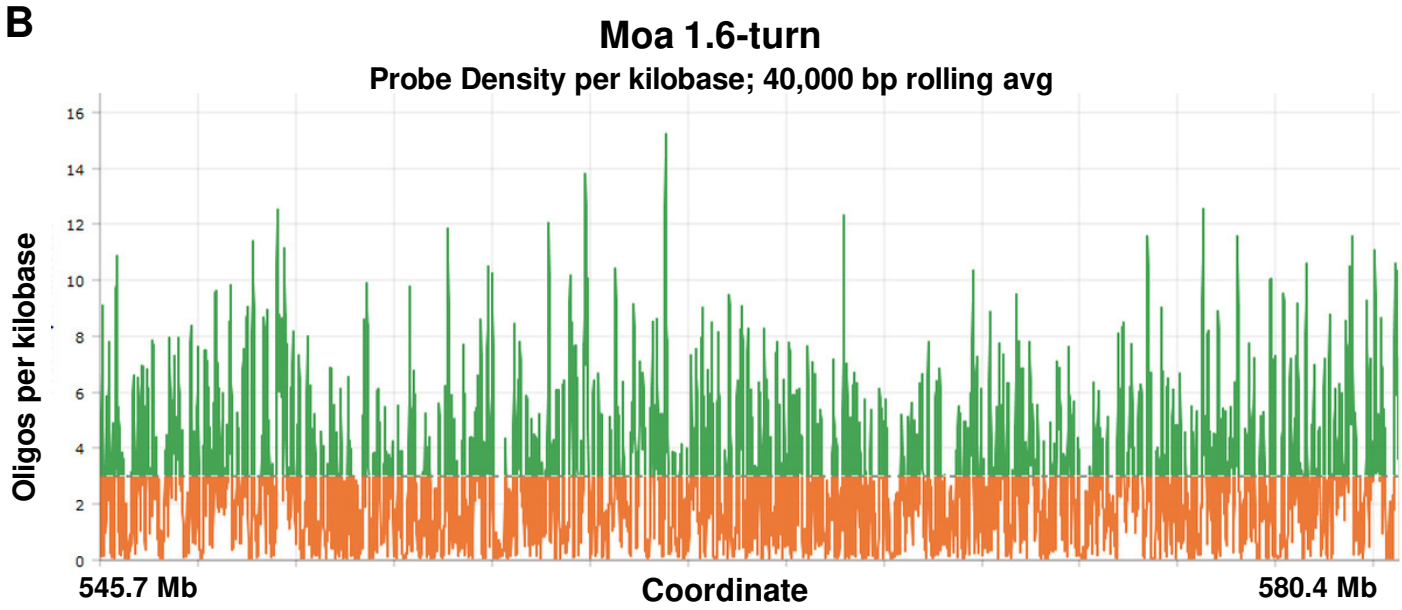
B
Moa 1.6-turn
Probe Density per kilobase; 40,000 bp rolling avg
Oligos per kilobase
0
2
4
6
8
10
12
14
16
545.7 Mb
Coordinate
580.4 Mb

Figure S6

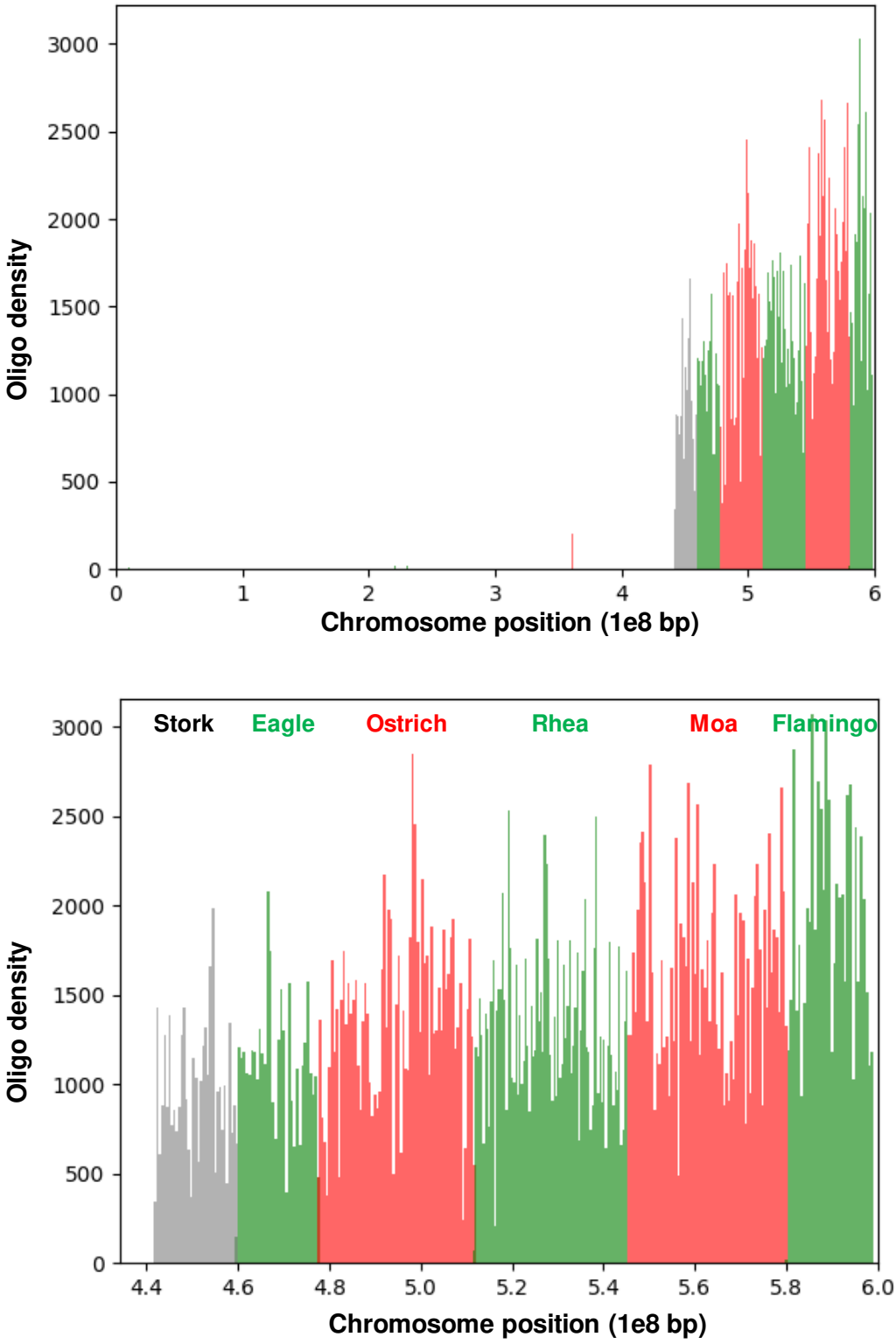
Oligo density
Chromosome position (1e8 bp)
Stork
Eagle
Ostrich
Rhea
Moa
Flamingo

Figure S7

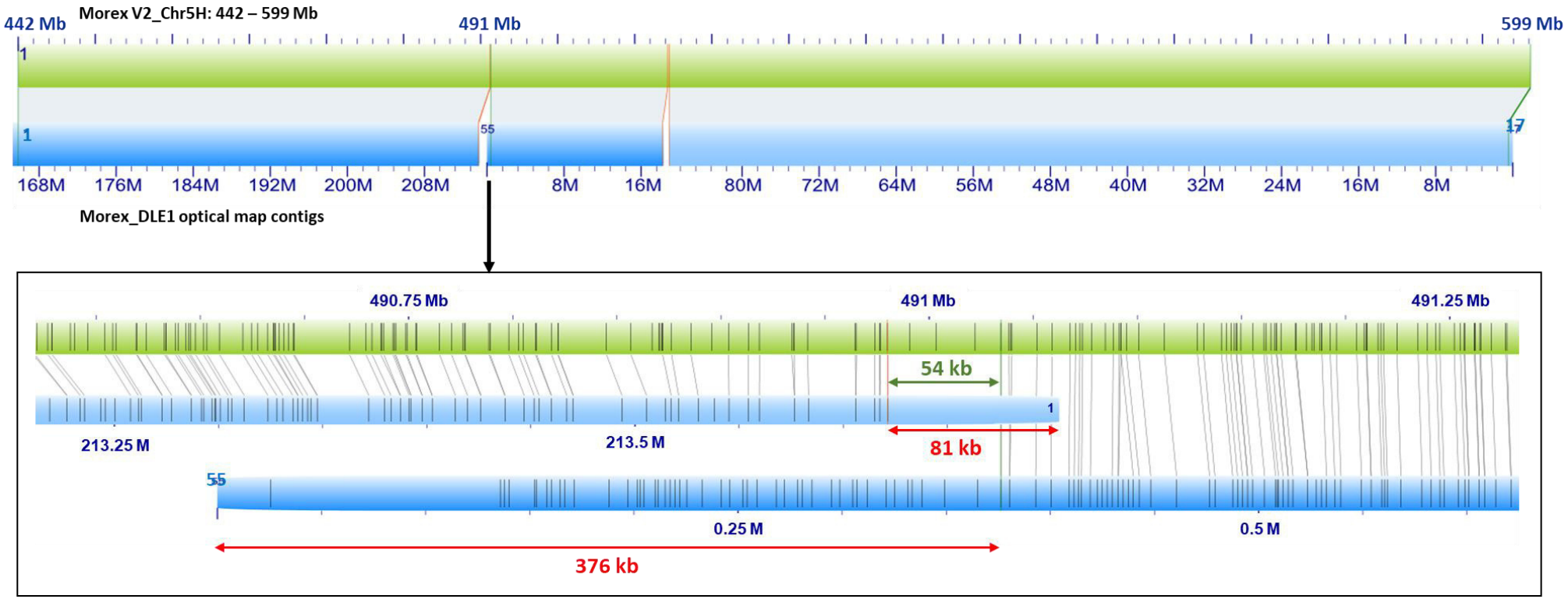
Morex V2_Chr5H: 442 – 599 Mb
442 Mb
491 Mb
599 Mb
1
55
17
168M
176M
184M
192M
200M
208M
8M
16M
80M
72M
64M
56M
48M
40M
32M
24M
16M
8M
Morex_DLE1 optical map contigs
490.75 Mb
491 Mb
491.25 Mb
54 kb
213.25 M
213.5 M
81 kb
0.25 M
0.5 M
376 kb

Figure S8

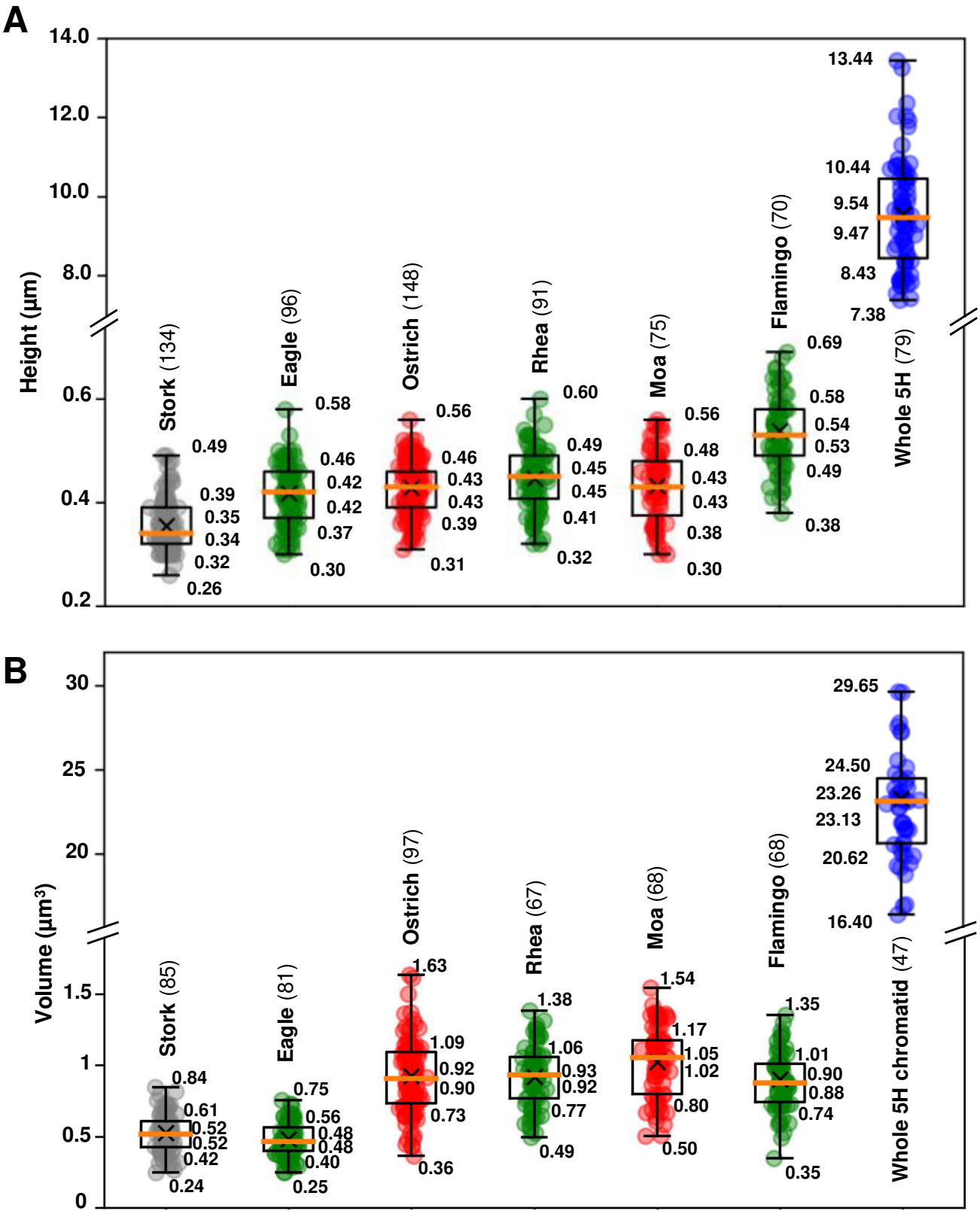
A
Height (µm)
14.0
12.0
10.0
8.0
0.6
0.4
0.2
Stork (134)
0.49
0.39
0.35
0.34
0.32
0.26
Eagle (96)
0.58
0.46
0.42
0.42
0.37
0.30
Ostrich (148)
0.56
0.46
0.43
0.43
0.39
0.31
Rhea (91)
0.60
0.49
0.45
0.45
0.41
0.32
Moa (75)
0.56
0.48
0.43
0.43
0.38
0.30
Flamingo (70)
0.69
0.58
0.54
0.53
0.49
0.38
Whole 5H (79)
13.44
10.44
9.54
9.47
8.43
7.38
B
Volume (µm³)
30
25
20
1.5
1
0.5
0
Stork (85)
0.84
0.61
0.52
0.52
0.42
0.24
Eagle (81)
0.75
0.56
0.48
0.48
0.40
0.25
Ostrich (97)
1.63
1.09
0.92
0.90
0.73
0.36
Rhea (67)
1.38
1.06
0.93
0.92
0.77
0.49
Moa (68)
1.54
1.17
1.05
1.02
0.80
0.50
Flamingo (68)
1.35
1.01
0.90
0.88
0.74
0.35
Whole 5H chromatid (47)
29.65
24.50
23.26
23.13
20.62
16.40

Figure S9

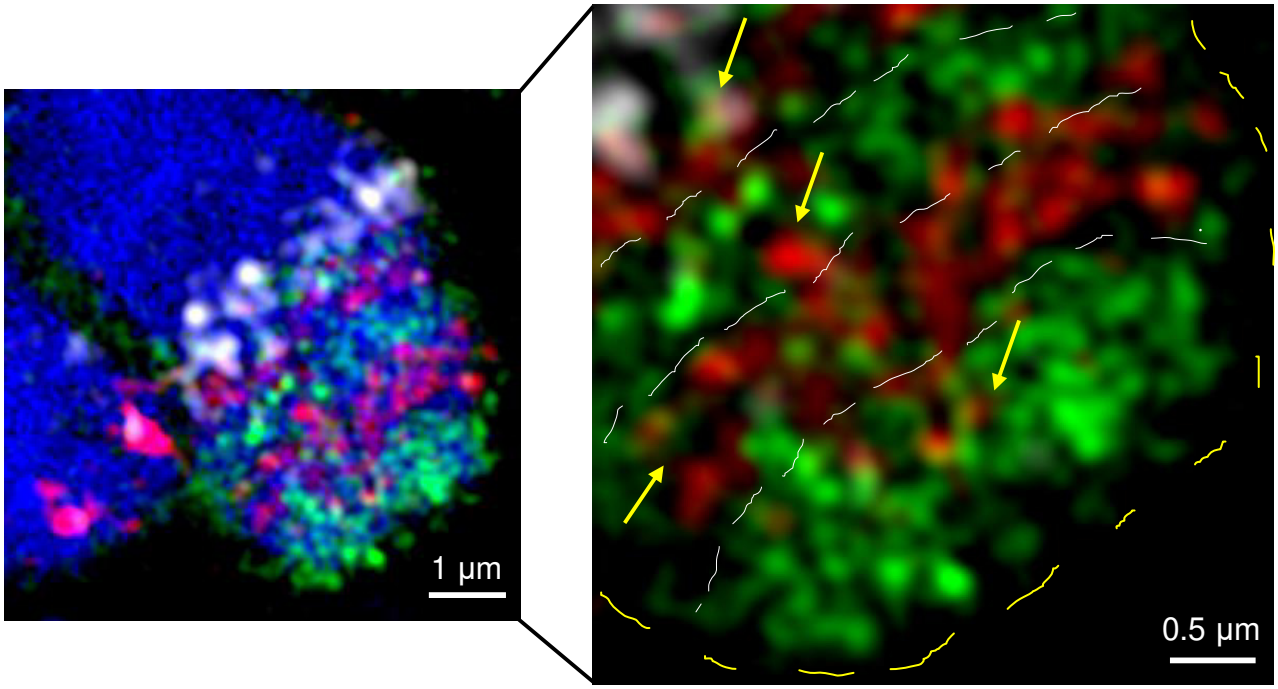

Figure S10

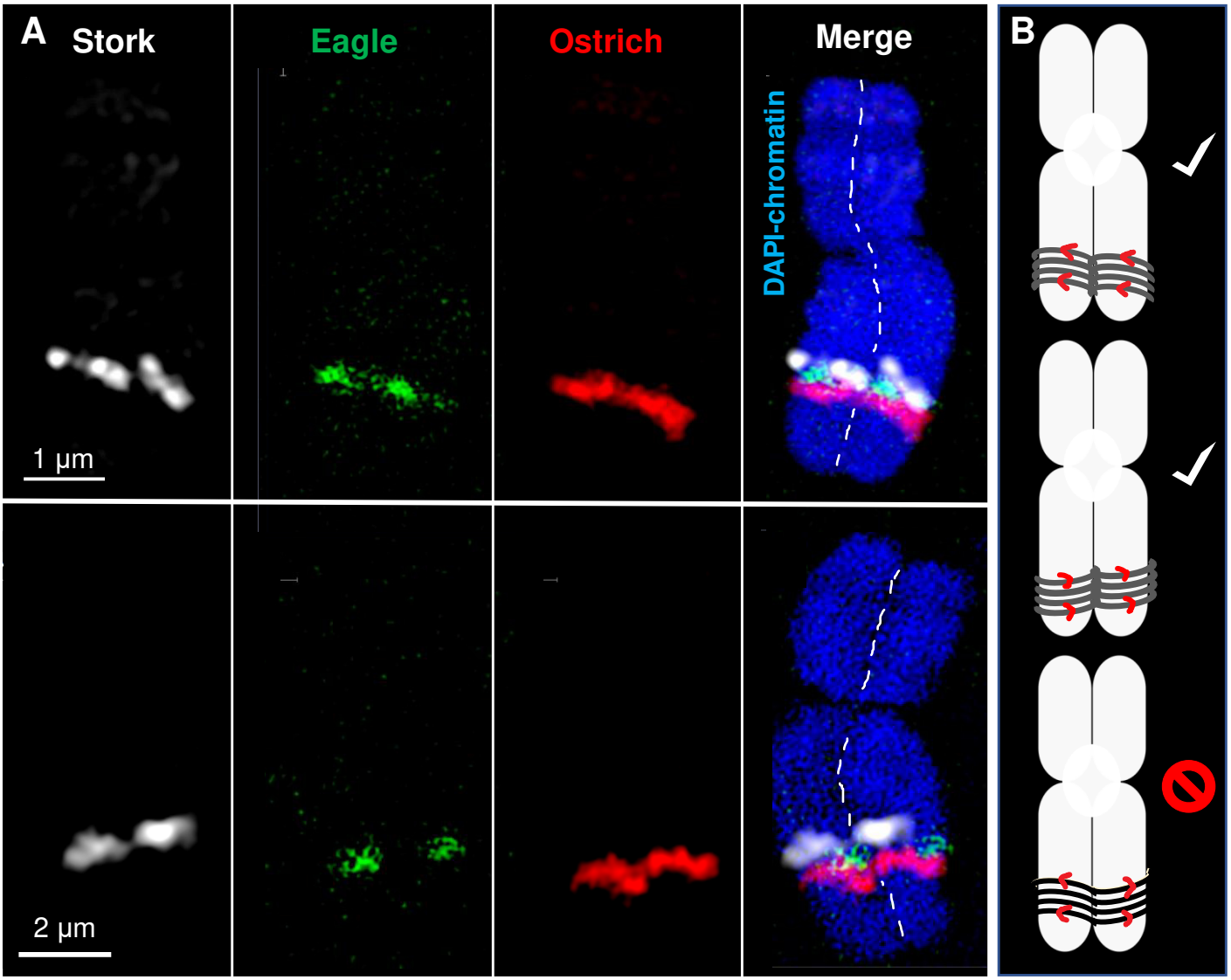

Figure S11

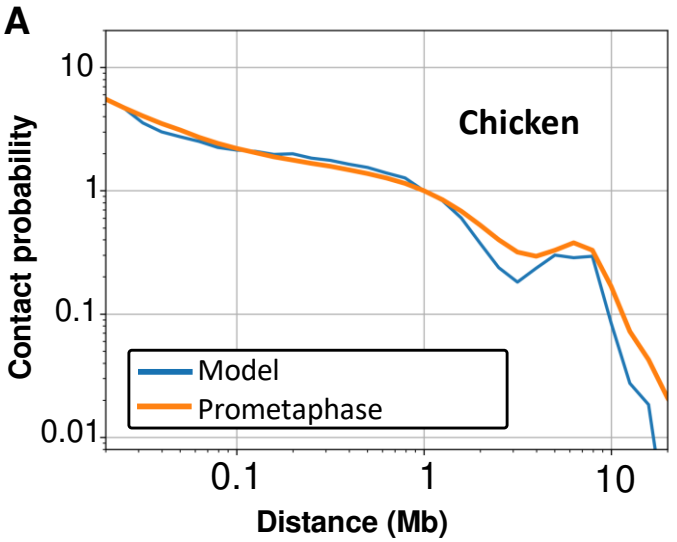

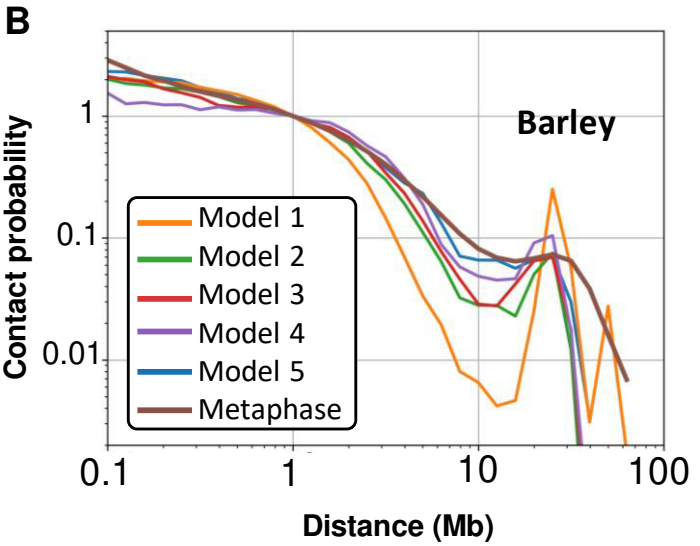

C

Simulated model parameters for barley

	Turn length (Mb)	Turn height (nm)	Major loop size (kb)	Minor loop size (kb)
Model 1	30	150	400	80
Model 2	30	400	400	80
Model 3	30	400	800	80
Model 4	30	400	800	160
Model 5	30	400	3,000	500

D

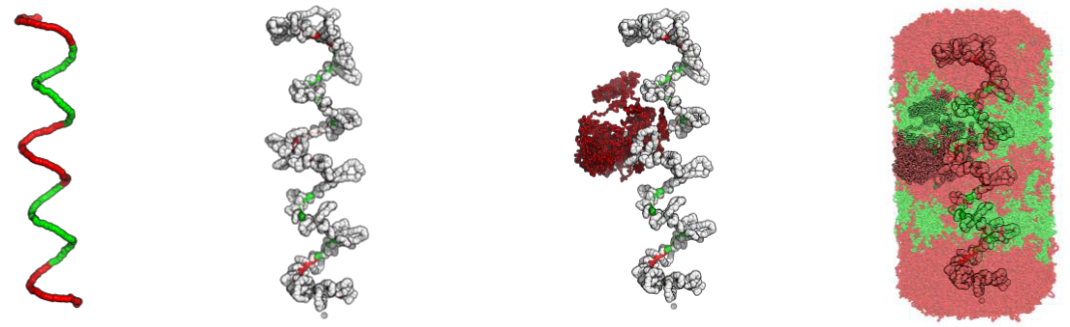

E

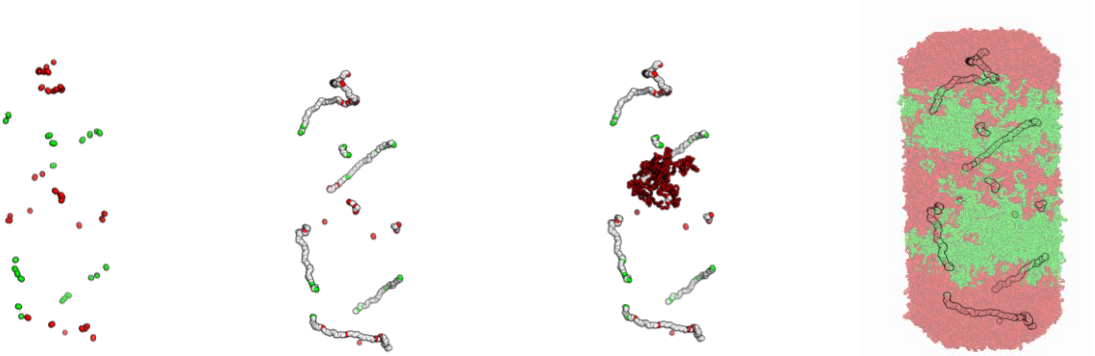

Figure S12

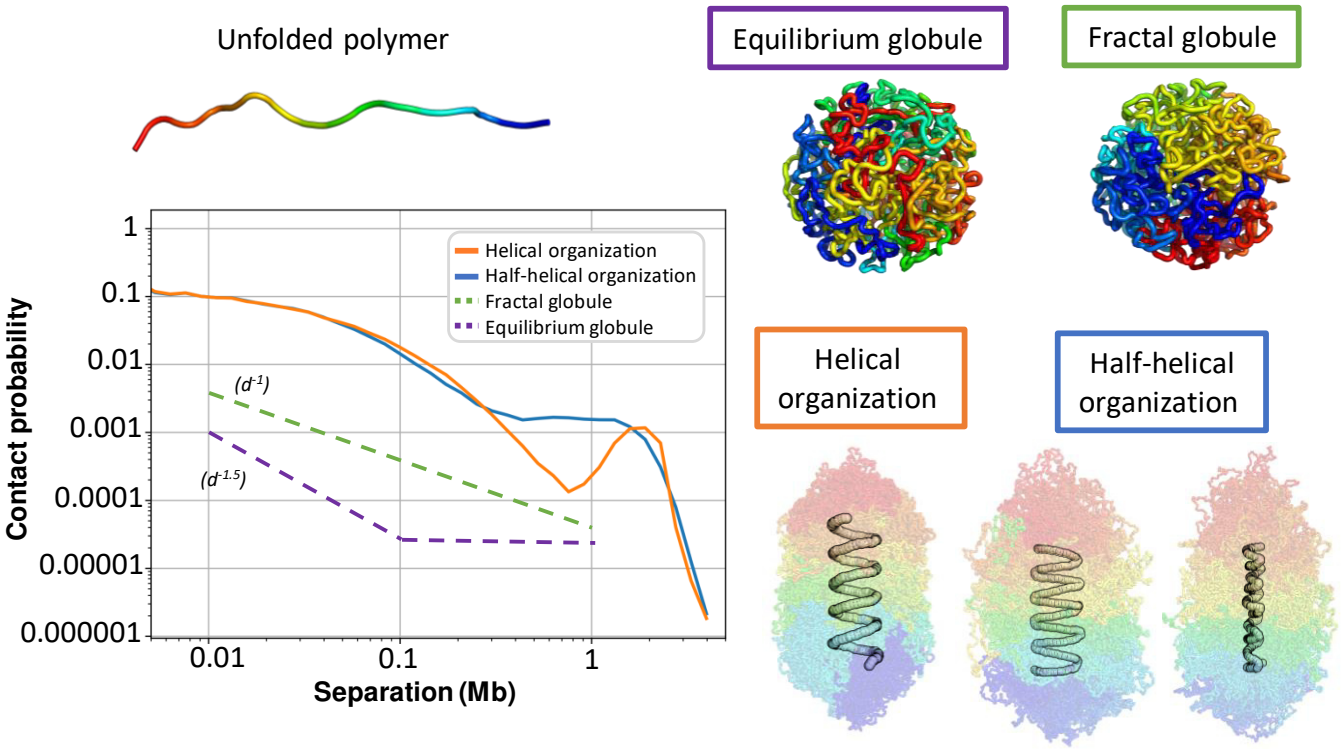
Unfolded polymer
Equilibrium globule
Fractal globule
Helical organization
Half-helical organization
Contact probability
Separation (Mb)
Helical organization
Half-helical organization
Fractal globule
Equilibrium globule
(d-1)
(d-1.5)
1
0.1
0.01
0.001
0.0001
0.00001
0.000001
0.01
0.1
1

Figure S13

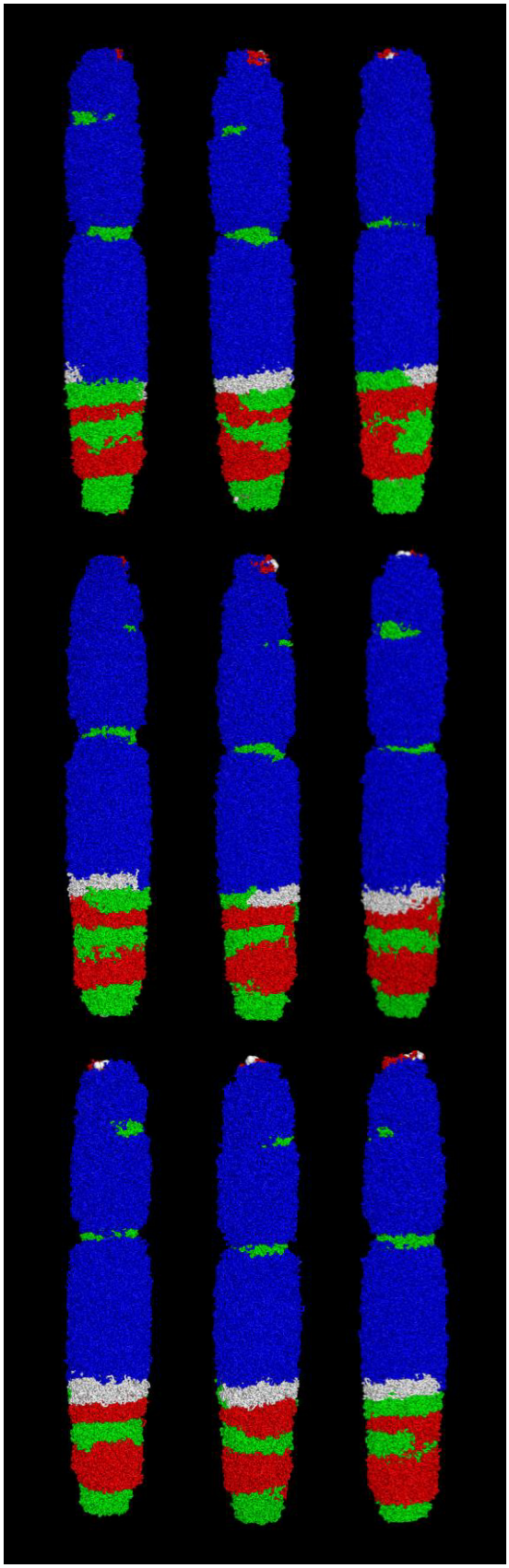

Figure S14

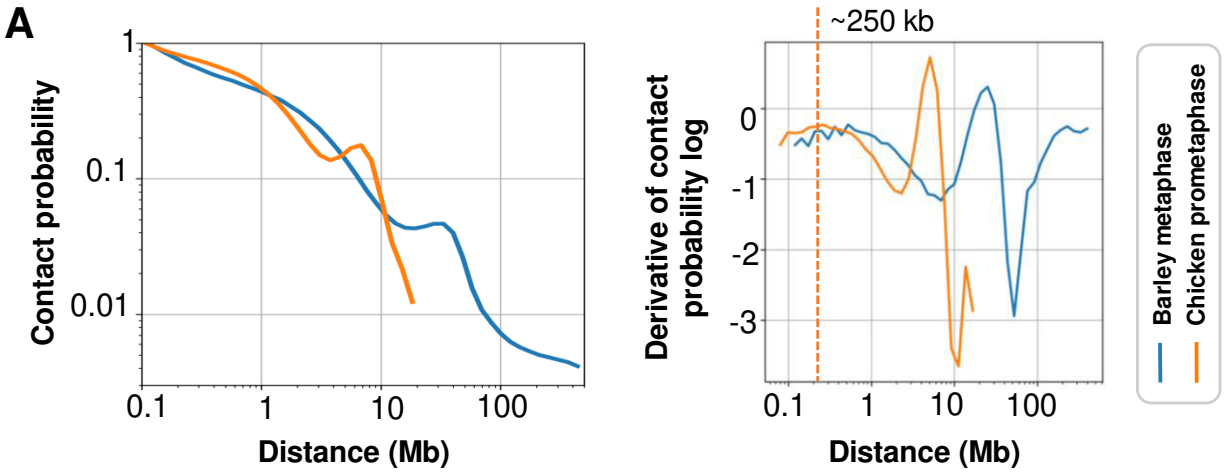
A
Contact probability
1
0.1
0.01
0.1
1
10
100
Distance (Mb)
~250 kb
Derivative of contact probability log
0
-1
-2
-3
0.1
1
10
100
Distance (Mb)
Barley metaphase
Chicken prometaphase

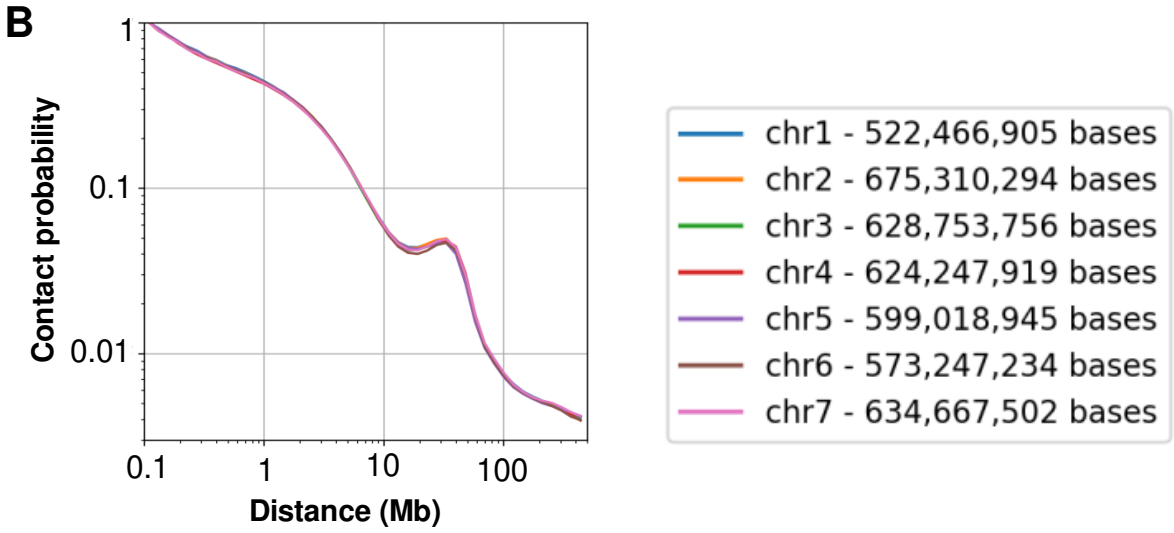
B
Contact probability
1
0.1
0.01
0.1
1
10
100
Distance (Mb)
chr1 - 522,466,905 bases
chr2 - 675,310,294 bases
chr3 - 628,753,756 bases
chr4 - 624,247,919 bases
chr5 - 599,018,945 bases
chr6 - 573,247,234 bases
chr7 - 634,667,502 bases

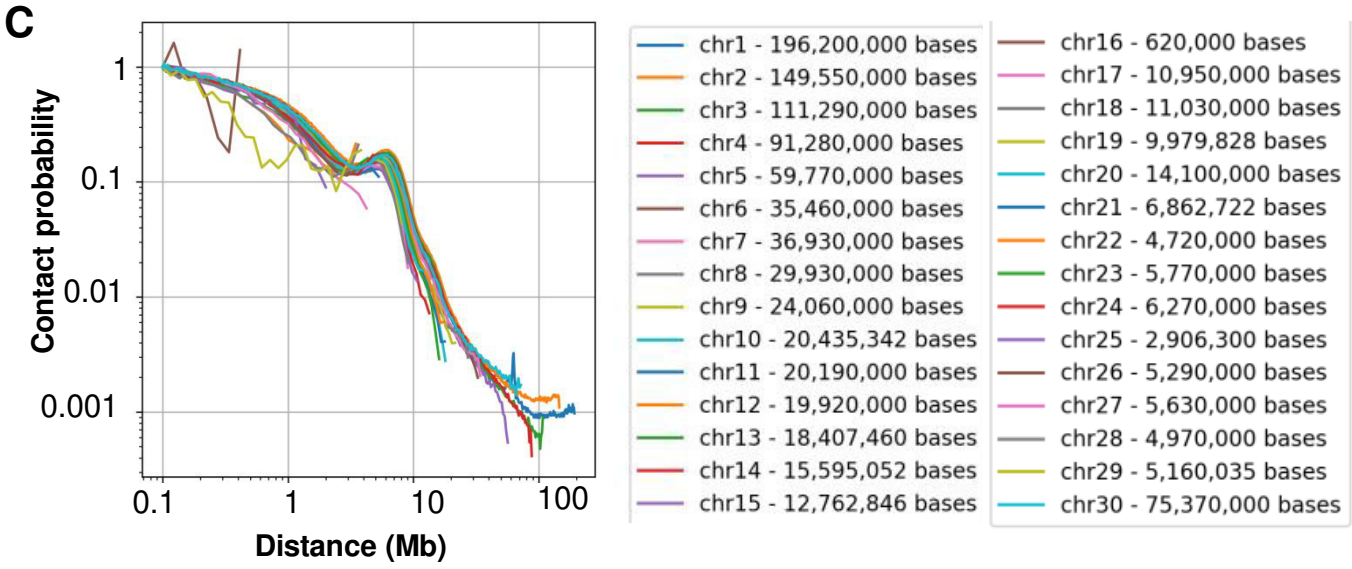
C
Contact probability
1
0.1
0.01
0.001
0.1
1
10
100
Distance (Mb)
chr1 - 196,200,000 bases
chr2 - 149,550,000 bases
chr3 - 111,290,000 bases
chr4 - 91,280,000 bases
chr5 - 59,770,000 bases
chr6 - 35,460,000 bases
chr7 - 36,930,000 bases
chr8 - 29,930,000 bases
chr9 - 24,060,000 bases
chr10 - 20,435,342 bases
chr11 - 20,190,000 bases
chr12 - 19,920,000 bases
chr13 - 18,407,460 bases
chr14 - 15,595,052 bases
chr15 - 12,762,846 bases
chr16 - 620,000 bases
chr17 - 10,950,000 bases
chr18 - 11,030,000 bases
chr19 - 9,979,828 bases
chr20 - 14,100,000 bases
chr21 - 6,862,722 bases
chr22 - 4,720,000 bases
chr23 - 5,770,000 bases
chr24 - 6,270,000 bases
chr25 - 2,906,300 bases
chr26 - 5,290,000 bases
chr27 - 5,630,000 bases
chr28 - 4,970,000 bases
chr29 - 5,160,035 bases
chr30 - 75,370,000 bases

Figure S15

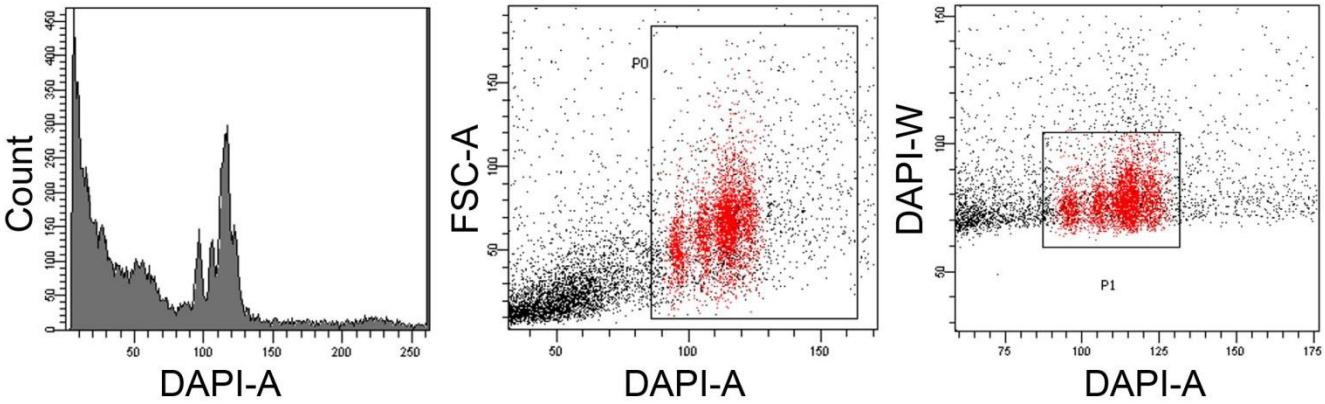

Figure S16

Table 1: Parameters of helically organized somatic metaphase chromosomes of barley compared to other species. Chromatid helix turn sizes and nested loop sizes are based on Hi-C data and a bottle brush-like model except for mouse and human.

Species	n	Haploid genome size (Gb)	Chromosome size (Mb)	Chromonema thickness (nm)	Turn length (Mb)	Nested loop length (Mb)	References
Barley	7	5	522 - 675	400	20-38	500[4]	This work
Onion/garlic	8	14.9/16.2	1800-2300	400-600[1], 400-550[2]	n. d.	n. d.	Niu et al., 1989; Hao et al., 1990, 1994
Axolotl	14	35	660 - 2,960	~250[5]	35	600[4]	Callan, 1966; Smith et al., 2019; Schloissnig et al., 2021
Chicken	34	1	0.6 - 196	150 - 200	12[5]	80[2, 6] (150[2, 4])	Gibcus et al., 2018
Mouse	21	2.6	61 - 195	200-300, 400[3]	n. d.	n. d.	Rattner and Lin, 1985; Summer, 1998
Human	23	3.1	47 - 247	150-200[3]	16.6[5]	60[6]	Bak et al., 1977; Ohnuki ,1968; Pienta and Coffey, 1984; Rattner and Lin, 1985; Takayama and Taniguchi, 1986; Gibcus et al., 2018; Hayashida et al., 2021

[1]In prometaphase
[2]In telophase
[3]Not Hi-C study
[4]First peak in the contact probability log derivative
[5]Calculated from the longest mitotic chromosome
[6]Corresponds to minor loop size
n. d. - not determined

Table S1: Values of local turn length of each chromosome calculated for 5 Mb bins, as described in supplementary materials and Figure S4. These values are graphically shown in Figure 1E. The three first lines display the sequence length of each chromosome, and the positions of the primary (centromere) and secondary constriction (NOR) at the short arms of 5H and 6H, as predicted from Hi-C data.

	1H	2H	3H	4H	5H	6H	7H
Chromosome size (Mb)	522.5	675.3	628.7	624.4	599.0	573.2	634.7
Centromere position (Mb)	205.5	305.8	271.9	282.4	206.0	260.0	328.8
NOR position (Mb)	-	-	-	-	50.3	79.5	-
Position (Mb)				**Turn length (Mb)**			
2.5-7.5	6.01674	3.41191	10.0504	5.60E-08	5.96904	4.30E-08	5.47E-09
7.5-12.5	3.3989	3.39141	1.24E-07	2.38075	19.6863	6.14956	5.96E-07
12.5-17.5	13.6668	13.0618	11.0963	12.0694	22.1876	13.5131	6.32619
17.5-22.5	19.7629	17.18	18.8189	18.0119	24.3624	21.5796	15.2778
22.5-27.5	25.619	19.5063	23.289	22.9052	25.8212	25.1436	20.3829
27.5-32.5	26.3202	22.5116	26.0755	25.7573	26.2016	27.3088	22.4413
32.5-37.5	28.6499	24.3615	27.7775	27.5784	27.6527	29.2685	23.6694
37.5-42.5	29.4102	25.5515	29.5156	29.6878	26.864	30.6588	25.1945
42.5-47.5	30.4477	26.9644	30.6173	30.8019	13.6946	31.102	25.793
47.5-52.5	30.447	28.0789	31.1308	31.3201	3.90E-08	30.6038	25.6596
52.5-57.5	30.3814	28.9819	32.008	31.8613	1.22E-07	29.8517	25.8668
57.5-62.5	30.7721	29.178	32.1477	32.8573	25.2976	27.7301	25.6354
62.5-67.5	30.6446	29.6516	32.7131	33.4771	22.4426	27.0497	26.2038
67.5-72.5	30.8399	30.7569	33.2433	33.8482	26.4577	26.0902	26.9197
72.5-77.5	31.2262	31.1721	32.958	34.242	29.1869	25.5726	28.3646
77.5-82.5	32.7546	31.5567	33.5336	34.3294	30.456	1.99E-12	28.5584
82.5-87.5	33.2509	31.2866	33.3311	34.6787	30.8924	1.54E-07	29.7553
87.5-92.5	34.091	31.3926	33.6411	34.8001	32.0145	25.3131	30.1972
92.5-97.5	34.819	31.5472	34.1038	35.2321	32.6105	25.6364	30.681
97.5-102.5	34.9206	31.4086	33.9768	35.0999	32.5178	27.1352	30.9678
102.5-107.5	35.4487	31.6383	34.6804	34.9774	32.1115	28.9428	31.1725
107.5-112.5	35.2697	31.4884	34.6192	35.2558	31.4494	30.3431	31.8339
112.5-117.5	34.7301	31.8003	34.8457	35.4576	30.6382	31.6458	32.1062
117.5-122.5	34.4552	31.733	35.1639	35.6888	31.0143	32.8772	32.3051
122.5-127.5	33.6035	31.9941	35.1249	36.0441	30.4393	33.6562	32.4979
127.5-132.5	32.8825	32.1363	35.4935	36.2429	29.8152	34.4415	33.0943
132.5-137.5	32.0877	32.9942	35.6706	36.4408	29.8695	34.5958	33.4276
137.5-142.5	30.6648	33.1226	35.3801	36.8475	29.2471	34.7721	33.8254
142.5-147.5	30.5385	33.591	35.0965	37.2356	29.4943	34.8878	33.4321
147.5-152.5	29.2401	33.6246	34.9161	37.4198	31.0086	35.2648	32.5287
152.5-157.5	28.9405	33.6886	34.9754	37.4845	30.27	36.1125	36.2879
157.5-162.5	28.4541	33.7891	34.8313	37.2513	29.1436	36.69	37.0673
162.5-167.5	27.8497	33.3587	34.8597	37.298	28.0698	37.1208	36.0702
167.5-172.5	26.2151	33.4029	34.3964	37.2553	25.5765	37.2073	31.7659
172.5-177.5	23.036	34.0477	34.0597	36.7538	22.9311	37.364	33.1757
177.5-182.5	18.3452	34.2014	33.3938	35.8105	13.1703	37.2536	33.0345
182.5-187.5	3.23232	34.2238	32.9613	35.0615	8.88E-09	36.7446	32.3794
187.5-192.5	5.77E-11	34.066	32.8202	34.7704	3.68E-08	36.3706	35.1794
192.5-197.5	4.26E-08	34.0345	32.7427	33.9533	1.34E-07	35.8814	37.3129
197.5-202.5	9.58E-10	33.9191	32.4727	32.2715	6.15E-09	34.4791	37.6781
202.5-207.5	1.14E-08	34.0749	32.1912	31.6223	9.65E-08	33.876	33.5086
207.5-212.5	4.94E-09	33.8319	31.8995	33.0899	1.26E-07	32.5153	34.6433
212.5-217.5	4.44E-15	33.7478	31.137	32.4271	1.36E-08	30.1152	35.8472
217.5-222.5	2.10E-07	33.3611	29.9599	31.3009	4.68E-07	28.3225	36.1778
222.5-227.5	7.7988	32.7032	29.071	31.0981	4.35708	26.2381	36.2295
227.5-232.5	20.0756	32.9118	27.7213	32.0108	22.6128	23.3928	36.4219
232.5-237.5	24.9688	32.6444	26.2091	30.793	26.6324	14.8782	36.5365

	1H	2H	3H	4H	5H	6H	7H
Position (Mb)				**Turn length (Mb)**			
237.5-242.5	27.9133	32.9266	21.9091	30.7244	28.6671	2.99E-07	36.2472
242.5-247.5	30.6028	32.0568	18.0876	28.7014	30.7917	7.12E-10	36.0978
247.5-252.2	32.3382	32.0024	7.76712	25.1582	32.184	1.36E-08	36.3516
252.5-257.5	33.1497	31.8705	7.42E-08	22.4684	33.04	7.06E-09	36.0632
257.5-262.5	33.7869	30.3695	2.14E-09	12.6957	33.606	1.45E-09	35.4676
262.5-267.5	34.3179	29.3664	5.56E-07	4.58E-11	33.6956	4.81E-08	35.0643
267.5-272.5	34.2778	27.3048	2.19E-06	3.78E-10	31.9944	2.80618	34.5308
272.5-277.5	34.3777	24.7343	1.70E-08	5.06E-09	32.4848	1.60E-07	33.081
277.5-282.5	34.6652	19.9785	2.99E-08	3.56E-08	33.2126	8.64977	31.6357
282.5-287.5	34.6182	12.539	1.21E-09	8.74E-07	34.098	20.4693	30.8667
287.5-292.5	34.519	2.44E-13	6.19E-12	2.85E-06	34.7032	25.0188	28.3714
292.5-297.5	34.1255	1.19E-06	10.0299	6.00E-13	34.7975	27.3963	27.165
297.5-302.5	33.8657	9.33E-13	23.7339	14.3295	34.5394	28.6435	22.2139
302.5-307.5	33.0197	8.39E-10	26.1005	21.6783	34.7994	29.3851	17.3955
307.5-312.5	33.1925	6.59E-10	30.108	14.0763	34.4565	33.7904	2.33809
312.5-317.5	33.4299	1.79E-08	32.716	22.1995	34.907	34.8424	3.94E-07
317.5-322.5	33.4936	7.70E-10	34.2683	26.508	35.0075	33.2338	4.64E-07
322.5-327.5	33.2605	9.41484	35.4378	27.5564	34.6288	34.2273	1.83E-06
327.5-332.5	32.7137	19.3441	36.6982	28.5718	34.7095	34.1128	19.4349
332.5-337.5	32.6454	22.8902	37.4345	30.9083	34.6917	34.5335	5.71E-08
337.5-342.5	32.088	26.9874	37.5309	31.8386	34.3407	34.5175	1.43E-09
342.5-347.5	31.8489	27.8013	36.8835	32.6608	34.2121	34.2827	1.48E-10
347.5-352.5	31.4395	31.0436	36.1659	33.8463	33.9803	34.5684	6.32615
352.5-357.5	31.0148	31.8322	35.7429	32.9708	34.01	34.6865	18.7447
357.5-362.5	31.3222	33.8545	35.2958	33.1092	34.0151	34.7757	24.8626
362.5-367.5	31.0258	34.6337	34.8958	32.6703	33.9587	34.9235	26.6516
367.5-372.5	30.9657	34.973	34.3256	33.118	33.9184	34.394	28.9271
372.5-377.5	30.9108	35.6196	33.4739	32.3202	33.6151	34.6627	31.3187
377.5-382.5	30.6854	35.6359	32.4056	33.0433	33.2048	34.3154	32.6222
382.5-387.5	30.726	35.6518	32.246	32.7307	33.4495	33.848	34.0566
387.5-392.5	30.9995	35.5138	33.215	31.5889	33.2956	33.5464	34.4456
392.5-397.5	31.3994	35.1389	33.804	32.0617	33.2773	33.8538	34.8513
397.5-402.5	31.0889	34.4437	34.0328	33.5815	33.1836	33.8478	35.2768
402.5-407.5	30.4093	33.7706	33.9275	34.0165	32.954	33.9513	35.0858
407.5-412.5	29.8711	33.7733	34.2662	34.1398	32.5537	33.8335	34.8808
412.5-417.5	29.1366	32.7707	34.1763	34.3838	32.1396	33.6421	34.9159
417.5-422.5	29.1749	32.1647	34.0588	34.8112	32.1213	34.6381	34.4724
422.5-427.5	28.6555	32.9012	33.7376	34.6444	31.8305	33.6526	34.0792
427.5-432.5	28.9366	32.9395	33.8082	35.519	31.2156	34.2223	34.1023
432.5-437.5	28.2459	33.4327	33.6258	34.8364	31.0672	34.1226	33.8582
437.5-442.5	28.9684	33.7228	33.1357	34.2773	30.6198	33.7286	33.8694
442.5-447.5	28.2041	33.89	32.7506	33.8143	30.3953	32.994	34.0414
447.5-452.5	28.2515	34.0404	32.2745	33.3632	30.0231	33.0358	33.8713
452.5-457.5	27.5916	34.4113	32.2374	33.5331	29.8501	32.2564	33.3055
457.5-462.5	26.291	34.2249	32.136	32.7541	29.6158	31.5048	33.2865
462.5-467.5	25.9303	34.5612	31.6487	32.743	29.184	32.3898	33.4259
467.5-472.5	25.4411	34.3868	31.4897	33.4705	29.0229	31.822	33.2463
472.5-477.5	23.9437	34.1271	31.4121	32.9942	29.1223	31.0097	33.3311
477.5-482.5	23.3546	34.209	30.8674	33.3189	27.7607	31.2104	33.4033
482.5-487.5	22.6197	34.0958	30.4565	33.4761	26.0865	31.0838	33.3216
487.5-492.5	21.7581	34.1659	29.9014	33.1369	25.7346	31.4538	33.0992
492.5-497.5	20.3533	34.0828	29.4672	33.0742	24.8074	30.3505	33.0381
497.5-502.5	17.3684	34.4562	28.3903	32.7133	23.9356	29.4287	32.731
502.5-507.5	12.2531	33.7769	28.2051	32.3605	22.5968	29.4079	32.3883
507.5-512.5	3.78151	33.7908	26.9858	32.0161	22.4535	29.1924	31.7152
512.5-517.5	12.0529	33.1738	26.6734	31.5706	20.9526	28.1931	32.112
517.5-522.5	6.13769	32.9463	26.9733	30.9844	21.5121	27.3251	32.3378
522.5-527.5		32.4902	26.0259	30.59	21.265	27.2698	31.6343
527.5-532.5		31.8125	26.2868	30.093	21.0415	26.2253	31.6827

	1H	2H	3H	4H	5H	6H	7H
Position (Mb)				**Turn length (Mb)**			
532.5-537.5		31.5727	26.074	29.7905	20.4688	25.9744	31.4727
537.5-542.5		30.5718	25.5686	30.3023	21.187	25.6962	31.7087
542.5-547.5		29.8406	25.6092	29.9643	21.6532	23.5544	31.4402
547.5-552.5		29.2722	25.4209	29.2289	22.4012	21.8487	30.7147
552.5-557.5		29.0004	24.5428	28.6189	24.049	17.465	30.7752
557.5-562.5		27.9736	23.806	28.1934	23.1059	11.6061	30.1034
562.5-567.5		27.0287	24.2538	27.9885	23.353	6.49198	29.6873
567.5-572.5		27.4258	23.9249	27.339	21.6832	3.90E-07	29.1887
572.5-577.5		26.6489	23.1854	26.4052	19.8346		28.5508
577.5-582.5		25.0741	24.0151	25.3589	17.2077		28.2294
582.5-587.5		23.595	23.3074	24.1774	7.7922		26.6481
587.5-592.5		23.6982	22.2953	23.2408	8.17889		26.2341
592.5-597.5		24.8433	20.5223	23.2727	1.51E-06		24.7005
597.5-602.5		24.6947	20.2942	20.5142			23.5091
602.5-607.5		24.7661	18.5698	17.4219			21.548
607.5-612.5		23.5646	16.2229	11.4805			19.0632
612.5-617.5		22.9534	13.6966	5.22E-09			15.5532
617.5-622.5		22.9203	14.5255	3.97E-08			5.2426
622.5-627.5		21.6953	10.2715				1.24672
627.5-632.5		21.5698					1.01E-11
632.5-637.5		22.3165					
637.5-642.5		22.1064					
642.5-647.5		21.342					
647.5-652.5		20.4072					
652.5-657.5		17.5867					
657.5-662.5		10.5045					
662.5-667.5		4.48304					
667.5-672.5		7.678					
672.5-677.5		13.348					

Table S2: Coordinates and lenghts of the oligo-FISH probes (named according to birds) adjacent to the 5HL subtelomere based on the barley cv. Morex v2 genome assembly.

Probe	No. oligos	Start (Mb)	End (Mb)	Length (Mb)	Average Turn size (Mb)	Number of turns*
Stork	33987	442.1	459.9	17.7	30.1±0.4	0.6
Eagle	35062	459.9	477.5	17.6	29.2±0.2	0.6
Ostrich	91061	477.4	511.8	34.4	24.8±1.8	1.4
Rhea	105984	511.8	545.3	33.5	21.3±0.5	1.58
Moa	108831	545.3	580.2	34.9	21.6±2.1	1.62
Flamingo	62181	580.1	599.0	18.8	8.3±6.1	2.3

* Length of the probe divided by the average turn size in its region.

Table S3: Volumes of the barley satellite chromosomes 5H and 6H (identified based on their secondary constriction and centromere position) and NOR-free (1H-4H, 7H) chromosomes. The measurements were done on polyacrylamide embedded spatially preserved chromosomes.

Chromosome	n	Mean±SD (µm³)
5H	2	49.5±2.3
6H	3	55.0±12.8
1H-4H, 7H	10	56.1±9.8
1H-7H	15	55.0±10.1

Table S4: Statistics of the metaphase Hi-C datasets. Seven libraries were analyzed: three replicates from interphase libraries, three replicates from metaphase libraries and one more metaphase library generated with an alternative protocol, which yields less unspecific contacts, for comparison with polymer modelling. For each library we computed: total number of contact reads (all reads), percentage of PCR duplicated reads (duplicated), number of non-duplicated reads with a mapping quality (MAPQ) of at least 10 (high-quality reads), number of intra-chromosome contacts separated by more than 1 kb (1 kb separation), intra-chromosome contacts separated by more than 1 Mb (1 Mb separation), and number of inter-chromosome contacts (inter-chromosome). * percentage of all reads: ** percentage relative to number high-quality reads; *** percentage of the reads separated by more than 1 kb.

LIBRARY	ALL READS	DUPLICATED (%*)	HIGH-QUALITY READS (%*)	1KB SEPARATION (%**)	1MB SEPARATION (%***)	INTER-CHROMOSOME (%***)
INTERPHASE_1	260,968,878	13.21	39,558,947 (15.16)	16,036,382 (40.54)	7,110,811 (44.34)	4,138,138 (25.8)
INTERPHASE_2	204,856,338	1.19	31,097,110 (15.18)	18,557,444 (59.68)	8,604,498 (46.37)	4,567,769 (24.61)
INTERPHASE_3	219,294,615	1.49	36,292,924 (16.55)	35,634,600 (98.19)	12,389,518 (34.77)	18,915,266 (53.08)
METAPHASE_1	509,196,403	6.06	91,401,051 (17.95)	62,357,229 (68.22)	12,764,657 (20.47)	48,635,089 (77.99)
METAPHASE_2	735,344,585	8.28	92,941,157 (12.64)	69,241,898 (74.5)	23,853,444 (34.45)	41,427,153 (59.83)
METAPHASE_3	579,559,917	7.09	80,301,755 (13.86)	60,884,103 (75.82)	17,350,884 (28.5)	40,922,614 (67.21)
METAPHASE_AGAR	122,636,722	50.74	12,194,950 (9.94)	9,809,014 (80.43)	4,771,893 (48.65)	3,254,155 (33.17)